TECHNISCHE UNIVERSITÄT DARMSTADT

Direct effects of radon exposure on the neural system - a possible target for pain relief

Vom Fachbereich Biologie

der Technischen Universität Darmstadt

zur Erlangung des akademischen Grades eines

Doctor rerum naturalium

genehmigte Dissertation

von

M.Sc. Juliane Joswig

geboren am 13.10.1994

in Mannheim

Erstgutachter: Prof. Dr. Bodo Laube

Zweitgutachter: Prof. Dr. Gerhard Thiel

Tag der Einreichung: 17.01.2022

Tag der mündlichen Prüfung: 14.02.2022

Darmstadt 2022

Joswig, Juliane: Direct effects of radon exposure on the neural system - a possible target for pain relief
Darmstadt, Technische Universität Darmstadt,
Jahr der Veröffentlichung der Dissertation auf TUprints: 2022
URN: urn:nbn:de:tuda-tuprints-202717
Tag der mündlichen Prüfung: 14.02.2022

„Alle Dinge sind Gift, und nichts ist ohne Gift; Allein die Dosis machts, daß ein Ding kein Gift sei“

Paracelsus 1538

Ehrenwörtliche Erklärung

Ich erkläre hiermit ehrenwörtlich, dass ich die vorliegende Arbeit entsprechend den Regeln guter wissenschaftlicher Praxis selbständig und ohne unzulässige Hilfe Dritter angefertigt habe.

Sämtliche aus fremden Quellen direkt oder indirekt übernommenen Gedanken sowie sämtliche von Anderen direkt oder indirekt übernommenen Daten, Techniken und Materialien sind als solche kenntlich gemacht. Die Arbeit wurde bisher keiner anderen Hochschule zu Prüfungszwecken eingereicht.

Darmstadt den,

……..

Contents

1. Summary

About 1 % of the worldwide population suffers from rheumatoid arthritis, which causes systemic inflammation and leaves patients suffering from chronic pain even after resolution of clinical signs. Patients often decide to undergo radon therapy to relief their pain despite the fact that radon has been declared the second most common cause of developing lung cancer. Although radon therapy has been used for over 100 years in some countries, the molecular mechanism underlying its pain relieving effect is still unknown. However, the identification of the molecular working mechanism of radon therapy is of high interest so that alternative therapies can be developed to achieve comparable pain alleviation without patients having to endure risking the development of lung cancer. Although the experience of pain in general is an important warning device to invoke reflex withdrawal, pain can also take on a disease character. This phenomenon is defined as chronic pain, which presents with pain lasting several weeks or longer and serves no obvious beneficial function. Traditionally, the spinal dorsal horn and periphery were the main targets for pain therapy. However, it has been suggested that when central changes occur in the brain following chronic pain, it may be too late to interfere at the periphery and the brain becomes an essential target to alleviate pain. In case of RA patients, synaptic changes in the brain could present a point of action for radon therapy.

In order to identify a potential molecular working mechanism of radon exposure, this thesis started to investigate the effect radon inhalation exhibits on the neurosensory system. Firstly, due to radon's similar physical characteristics to xenon, the hypothesis arose that radon, like xenon, may bind to N-Methyl-D-aspartate-receptors (NMDARs) thereby inhibiting pathological pain transmission. Molecular dynamic simulations showed that radon indeed hijacks four of the same binding sites as xenon on NMDARs with some binding energies even exceeding those of xenon. Additionally, an in vitro radon binding assay showed an increased amount of DNA double strand breaks (DSBs) in cells expressing NMDARs compared to cells lacking NMDARs. Interpolating from a linear regression correlation between DNA DSB induction and deposited radiation dose, it was calculated that cells expressing NMDARs obtain a 47 % higher dosage from radon exposure. This led to the assumption that especially NMDAR-rich environments could present a target for radon therapy. Therefore, it was validated that radon reaches the brain, which represents a NMDAR-rich environment. Immunofluorescent staining of radon induced DNA DSBs showed that radon damages brain tissue to the same degree as other tissues such as heart or liver. A linear regression from the correlation of DNA DSBs to deposited radiation dose yielded an estimated radiation dose of 2.3 mGy per cell. Lastly, the effect of radon inhalation on K/BxN

serum transfer mice brain indicates a dual function of radon in pain alleviation. While the maintenance of long-term potentiation (LTP) could be impaired after radon exposure caused by a significant reduction of NMDAR GluN2B phosphorylation of Y1472, there is evidence for a restored long-term depression (LTD) expression through significant increase in active protein kinase C-α (PKC-α). All in all, the results presented in this work postulate a novel molecular working mechanism for radon therapy by directly affecting the neurosensory system.

2. Zusammenfassung

Etwa 1 % der Weltbevölkerung leidet an Rheumatoider Arthritis, welche eine systemische Entzündung hervorruft. Patienten klagen über chronischen Schmerzen, selbst nachdem die klinischen Merkmale verschwunden sind. Patienten unterziehen sich oftmals einer Radontherapie zur Schmerzlinderung, obwohl Radon als zweithäufigste Ursache für Lungenkrebs deklariert wurde. Die Radontherapie wird in manchen Ländern schon seit über 100 Jahren angewandt, jedoch ist der zugrundeliegende molekulare Mechanismus der Schmerzlinderung noch nicht erforscht. Die Identifizierung des molekularen Mechanismus der Radontherapie ist von hohem Interesse, da dadurch eine alternative Schmerztherapie entwickelt werden könnte, sodass Patienten nicht länger dem Risiko der Lungenkrebsentstehung ausgesetzt werden müssten. Obwohl die Wahrnehmung von Schmerz ein wichtiges Warnsystem darstellt, das einen reflexartigen Rückzug als Reaktion hervorruft, kann Schmerz zu einer Krankheit werden. Dieses Phänomen wird als chronischer Schmerz bezeichnet und zeigt sich durch Schmerzen, die mehrere Wochen oder länger anhalten und keinen offensichtlichen Nutzen haben. Traditionell werden in der Schmerztherapie das dorsale Horn oder seine Umgebung gezielt behandelt. Es wird jedoch vermutet, dass sich als Folge von chronischen Schmerzen zentrale Änderungen im Gehirn einstellen und es daher bereits zu spät ist, die Schmerzen in der Peripherie zu behandeln, weshalb das Gehirn zum essentiellen Angriffsziel wird. Im Falle von Patienten, die an rheumatoider Arthritis leiden, könnten synaptische Veränderungen im Gehirn ein potenzielles Ziel der Radontherapie darstellen.

Um einen möglichen Wirkmechanismus zu identifizieren wurde in dieser Thesis der Effekt einer Radoninhalation auf das neurosensorische System untersucht. Als erstes wurde durch die ähnlichen physikalischen Eigenschaften von Radon zu Xenon die Hypothese aufgestellt, dass Radon wie Xenon an N-Methyl-D-Aspartat Rezeptoren (NMDARs) binden könnte und somit die Weiterleitung von pathologischen Schmerzen gehemmt wird. Molekulardynamik-Simulationen zeigen, dass Radon in der Tat an vier Bindestellen bindet, an welchen auch Xenon binden kann. Teilweise weist Radon sogar höhere Bindeenergien auf. Zusätzlich zeigt die *in vitro* Radon Bindeuntersuchung eine erhöhte Menge an DNS Doppelstrangbrüchen (DSBs) in Zellen, welche NMDARs exprimieren im Gegensatz zu Zellen, in denen der NMDAR fehlt. Bei der Interpolation einer linearen Regressionsgeraden der Korrelation von induzierten DNS DSBs und der deponierten Strahlungsdosis konnte berechnet werden, dass Zellen die NMDARs exprimieren eine 47 % höhere Strahlungsdosis durch eine Radonexposition erhalten. Dies führte zu der Vermutung, dass vor allem NMDAR-reiche Regionen ein Ziel der Radontherapie darstellen könnten. Deshalb wurde darauffolgend

validiert, dass Radon das Gehirn erreicht, welches eine NMDAR-reiche Umgebung darstellt. Die Immunfluoreszenzfärbungen von Radon-induzierten DNS DSBs zeigen, dass Radonbestrahlung dem Gehirn im selben Maße schadet wie anderen Geweben wie z.B. Herz oder Leber. Eine lineare Regressionsgerade der Korrelation zwischen DNS DSBs und deponierter Strahlendosis ergab eine errechnete Dosis von 2.3 mGy pro Zelle im Gehirn. Zuletzt deutet der Effekt einer Radoninhalation auf das Gehirn von K/BxN Serumtransfer Mäusen auf eine duale Funktion einer Radontherapie zur Schmerzlinderung hin. Während die Aufrechterhaltung von einer Langzeitpotenzierung (LTP) nach einer Radonbehandlung beeinträchtigt sein könnte, was durch die signifikante Reduktion der Phosphorylierung der GluN2B an Y1472 bedingt ist, gibt es Hinweise auf eine Wiederherstellung der Langzeitdepression (LTD) durch die signifikante Erhöhung der aktiven Proteinkinase C-α (PKC-α). Zusammengefasst postulieren die Ergebnisse dieser Arbeit einen neuartigen Mechanismus für die Radontherapie durch einen direkten Effekt auf das neurosensorische System.

3. Introduction

3.1. Rheumatoid Arthritis

Rheumatoid arthritis (RA) is a heterogeneous autoimmune disease that causes systemic inflammation and constitutes a prevalence of 0.5 to 1 % in worldwide population [1]. RA mainly affects the joints causing synovitis and joint destruction and patients present symptoms such as swollen joints, morning stiffness, fatigue and severe pain. Currently, therapies either treat symptoms or reduce disease progression by suppressing immune players and inflammatory mediators but are neither curative nor preventive yet [2]. About 70 % of patients report pain as the preferred area of improvement, making pain management a high priority treatment domain [3]. However, despite the control or resolution of clinical signs of arthritis, RA patients frequently continue to report pain [4]. This leads to the thought that the pain that is initially mediated by inflammation or tissue damage is followed by peripheral and central sensitization [5]. Patients develop a chronic pain state that is caused by maladaptive processes triggered by the initial inflammation. In both, inflammatory and neuropathic pain, an activity dependent structural remodeling of spinal dendritic spines and supraspinal areas seem to have a crucial role in maintaining nociceptive hypersensitivity [6].

3.2. Radon therapy to treat rheumatic diseases

Radon is a naturally occurring radioactive noble gas that has been declared as human carcinogen by the International Agency for Research and Cancer (IARC) and by the United States Environmental Protection Agency (USEPA) [7]. Indoor radon exposure is the second most common cause of lung cancer right after smoking, where the worldwide contribution of radon exposure to lung cancer deaths is estimated at 3-20 % [8]. Remarkably, despite these severe health risks, radon exposure is used for therapeutic purposes for the treatment of rheumatic diseases for many patients in Central Europe and Russia [9]. This therapy is most commonly applied by baths (20 min in radon water; concentration (0.3-3 kBq/L) or inhalation (1 h in caves or galleries with natural radon; concentration 30-160 kBq/m^3) [9]. In several clinical trials starting from the year 2000 patients report significant pain reduction, enhanced mobility and consequently increased quality of life for up to 9 months after receiving radon therapy [10]–[15]. While this underlines the beneficial effect of radon treatment, the molecular working mechanism of radon therapy is still unknown. Since most incorporated radon is discharged by exhalation, the remainder is thought to be effective through radioactive decay and emission of alpha particles and following decay products [16].

3.3. Radon's radiation effects

Radon has three naturally occurring radioactive isotopes that are produced by decay chains of uranium and thorium [17]: ^{222}Rn with a half-life of 3.8 days, ^{220}Rn with a half-life of 55.6 s and ^{219}Rn with a half-life of 3.96 s [18]. Both ^{222}Rn and ^{220}Rn are significant contributors to human radon exposure from natural sources [19]. In **Table 1** the radioactive decay series of both isotopes is depicted, showing that they decay into several unstable daughter nuclides before resulting in stable Pb isotopes.

Table 1: Radioactive decay series of radon [20]

^{222}Rn			^{220}Rn		
Nuclide	**Half-Life**	**Decay-Mode**	**Nuclide**	**Half-Life**	**Decay-Mode**
^{222}Rn	3.825 d	α	^{220}Rn	55 s	α,γ
^{218}Po	3.05 min	α	^{216}Po	0.15 s	α
^{214}Pb	26.8 min	β, γ	^{212}Pb	10.64 h	β, γ
^{214}Bi	19.9 min	β, γ	^{212}Bi	60.6 min	β, γ
^{214}Po	164 µs	α	^{212}Po	304 ns	α
^{210}Pb	22.3 a	β, γ	^{208}Ti	3.05 min	β, γ
^{210}Bi	5 d	β, γ	^{208}Pb	stable	
^{210}Po	138.4 d	α			
^{206}Pb	stable				

Alpha-particle irradiation has a short range (40-90 µm in water) [21] and once radon decays, all subsequent daughter nuclides are solid and will deposit locally, where they will eventually decay thereby emitting all three forms of radioactive radiation [22]. Thus, when discussing the effect of radon exposure, all subsequent decay products should be considered to contribute to its action profile. Ionizing radiation (IR) including α, β, γ-rays as well as x-rays, is associated with a wide spectrum of cellular effects. The most prominent effect of IR is the elevation of free radicals and reactive oxygen species (ROS) leading to DNA damage and persistent modifications of DNA, proteins and lipids [23]. Several studies show radiation induced alterations in the synaptic plasticity including reduced cognition and inhibition of long-term potentiation (LTP), as well as diminished phosphorylation of tyrosine, and removal

of N-methyl-D-aspartate receptors (NMDARs) [24]–[27], that are presumably in correlation with oxidative stress. While high doses of ionizing radiation are associated with tumor development and cognitive impairment, uncertainty prevails concerning the effect of low radiation doses (<100 mGy). Thus, it is possible that the low radiation dose of radon therapy intervenes with synaptic plasticity caused by chronic inflammation, resulting in pain alleviation.

3.3.1. Xenon's similarities to radon

Xenon is the second rarest naturally occurring noble gas at a concentration of max. 0.086 ppm in the atmosphere. Xenon does not undergo metabolism and is not teratogenic [28]. Despite its poor chemical reactivity, xenon has a tendency to interact with living matter [29]–[31]. Under feasible clinical conditions, xenon is the only noble gas with anesthetic potency, where radon falls out due to its radioactive properties. Notably, when using the Meyer-Overton correlation for inert gases, radon is predicted to achieve anesthesia at even lower concentrations than xenon due to its higher oil/gas coefficient (**Figure 1**).

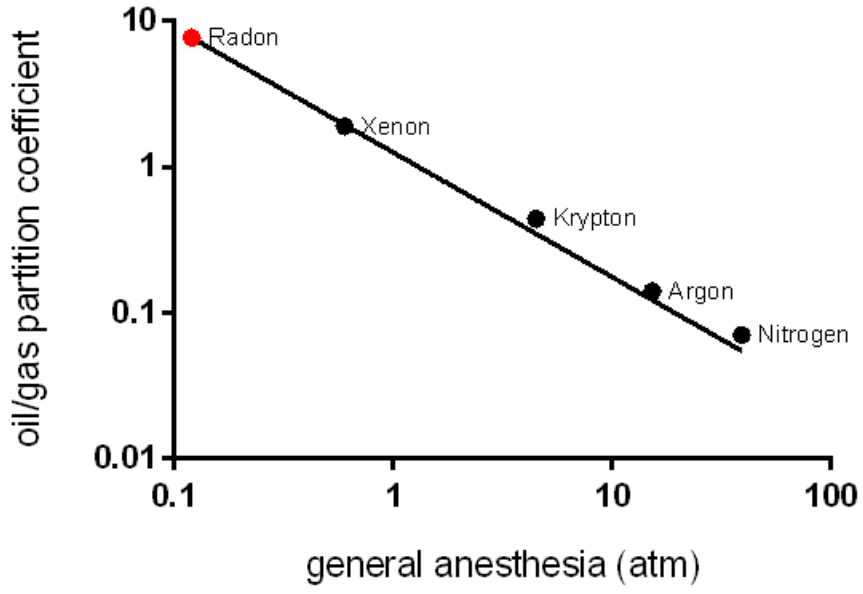

Figure 1: Meyer-Overton correlation for inert gases and nitrogen. The line shows a least-square regression. The black points show general anesthesia (atm) in correlation to their oil/gas partition coefficient at 25 °C. The red point shows theoretical prediction for radon based on its oil/gas partition coefficient. Modified from: [32].

Table 2: Physical properties of nitrogen, argon, krypton, xenon and radon

Physical property	Nitrogen	Krypton	Xenon	Radon
Atomic number	7	36	54	86
Atomic mass (g/mol)	14.0	83.8	131.3	222*
Diameter (Å)	3.64	3.69	4.10	4.17
Density (g/l)(0°C)	1.251	3.736	5.887	9.37
Water/gas partition coefficient at 25 °C	0.015	0.053	0.095	0.23[a]
Oil/gas partition coefficient at 25 °C	0.07	0.44	1.9	7.7 (olive oil)[b]
General anesthesia (atm)	39	4.5	0.6	0.12[c]

Data compiled from the following sources : [32],[a][33], [b][34], [c] theoretical prediction based on Meyer-Overton correlation, * unstable

Xenon's general anesthetic effect is attributed to an interference with post-synaptic signaling by inhibition of NMDARs on cortical, subcortical and spinal level, while an effect on α-amino-3-hydroxy-5-methyl-4-isoxazolepropionic acid receptor (AMPAR) or (GABA)ergic synapses is controversial [35], [36]. Since there is no effect on N-type voltage-gated calcium channels it also does not interfere with neurotransmitter release at neuronal synapses, which further emphasizes xenon's postsynaptic effect [37]. Xenon exhibits a competitive inhibition on NMDARs by weakening the glutamate binding, as well a noncompetitive inhibition by rearrangement of the channel toward a closed or desensitized channel [38], [39]. Additionally to general anesthesia, xenon has analgesic properties [40], [41] and enhanced responsiveness to painful stimulation (central sensitization) can be suppressed by xenon at sub-anesthetic doses, suggesting an involvement of NMDAR evoked LTP-related synaptic plasticity in the human brain [42]. Low-dose xenon also reduces post-operative pain, providing further evidence of an involvement of central sensitization [43]. Due to its rarity, high purity xenon sells for more than \$5000 kg^{-1} and thus separation of molecules of similar size and shape to receive pure xenon poses an important technological challenge. The attempt to selectively adsorb xenon in a crystalline cage resulted in the adsorption of both xenon (4.1 Å) and radon (4.17 Å) in molecular simulations while the separation of krypton (3.69 Å) was possible [44]. This implies that xenon and radon may occupy the same molecular cavities. The similarities of physical properties of xenon and radon (**Table 2**) make the hypothesis of a possible binding of radon to NMDARs conceivable. This could mean that the pain relieving effect of radon therapy may arise through similar mechanisms as xenon's

analgesic effect or be rendered possible through an accumulation of radon at NMDAR-rich sites that are essential for pain processing.

3.4. Structure and function of the N-Methyl-D-aspartate-receptor

Ionotropic glutamate receptors (iGluRs) convert glutamate release from the presynapse into postsynaptic excitation. There are three major families of iGluRs: NMDA, AMPA and kainate receptors. NMDARs play a key role in neuronal plasticity and neuronal exitotoxicity and are highly expressed throughout the brain. Many neuropsychiatric disorders like chronic pain, schizophrenia, Alzheimer's disease or autism spectrum disorders are linked to NMDAR dysfunction concomitant with either altered subunit expression, trafficking, localization or activity [45]. Functional NMDARs are heterotetramers that contain two obligatory GluN1 subunits in combination with two GluN2A-D and/or GluN3A-B subunits [46], [47]. However, the adult brain predominantly expresses NMDARs that are composed of GluN1/GluN2A or GluN1/GluN2B, giving those subunits central roles in synaptic plasticity and function [48], [49]. All NMDARs have a conserved domain organization (**Figure 2 A**): an extracellular amino-terminal domain (ATD) which is important for receptor assembly [50]; an extracellular ligand binding domain (LBD) [51]; a transmembrane domain (TMD) consisting of three transmembrane helices (M1,M3 and M4) and the reentrance loop (M2) which forms the ion channel pore [52]–[54]; an intracellular carboxyl-terminal domain (CTD) which binds scaffold and signaling proteins such as calmodulin as well as phosphatases [55], [56]. When activated, the NDMAR is cation-selective with a high permeability for Ca^{2+} and a lower permeability for Na^{+} and K^{+}. In contrast to other glutamate receptors, the NMDAR acquires the binding of two different ligands for channel opening [57].(**Figure 2 B**) The GluN1 subunit binds glycine (Gly) or D-serine while the GluN2 subunit binds glutamate (Glu)[47]. Since the extracellular glycine concentration is constantly high enough to activate NMDARs, the receptor activity is mainly regulated by presynaptic glutamate release [58]. Additionally, extracellular Mg^{2+} blocks the channel and is highly dependent on the membrane potential [59]. In order to overcome this ion-block, a pre-depolarization of the membrane is required in order to remove the Mg^{2+} from the NMDAR channel pore and enable cation influx. Therefore, NMDARs are usually expressed together with AMPARs which enable the required pre-depolarization [60].

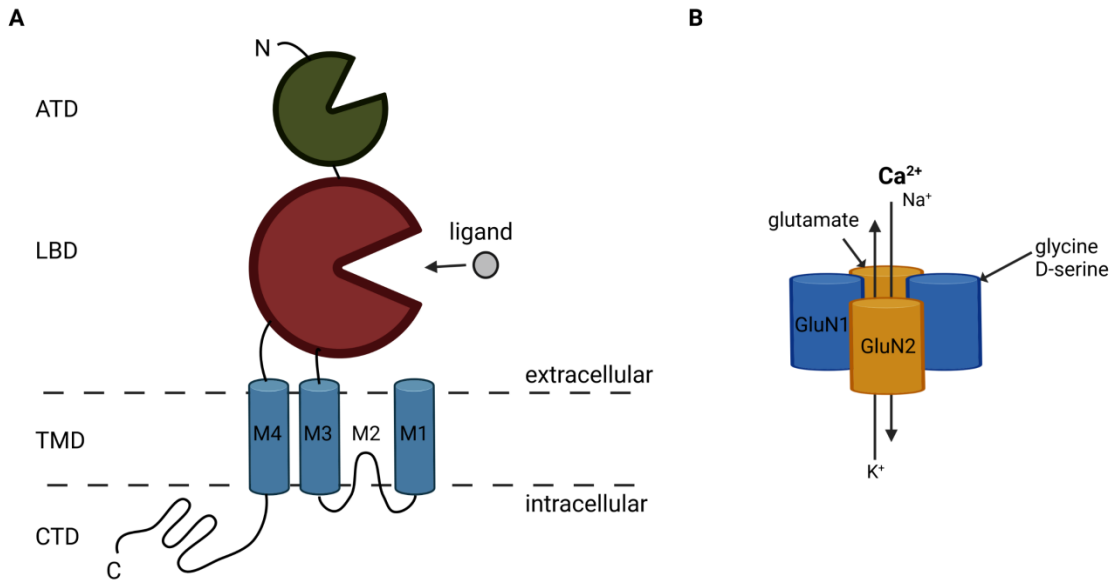

Figure 2: Structure of NMDARs. (**A**) NMDAR subunits have four conserved domains: The amino-terminal domain (ATD) (green), the ligand binding domain (LBD) (red), the transmembrane domain (TMD) (blue) and the carboxyl-terminal domain (CTD). (**B**) Functional NMDARs are heterotetramers with two obligatory GluN1 subunits (blue) which bind glycine or D-serine and in the adult brain predominantly two GluN2 subunits (orange) that bind glutamate. When both ligands bind to the receptor, the conformational change allows the channel pore to open conducting Ca^{2+}, Na^{+} and K^{+}. Modified from: [61]. Figure was created with BioRender.com.

3.5. Physiological pain and its conversion to chronic pain

The experience of pain serves as an important warning device, as not engaging in appropriate protective behaviors against for instance the heat of an open flame or a sharp object can be life-threatening. Physiological pain is sensed by two major specialized nerve fibers: C-fibers and thin myelinated Aδ-fibers. While C-fibers are slower conducting and responsible for prolonged burning sensations, Aδ-fibers are faster and transmit sharp or intense sensations [62]. The Aδ-fibers and C-fibers have a wide range of receptors on their terminals that are responsible for translating noxious stimuli (e.g. thermal, chemical and mechanical) into electrical activity by transient receptor potential. These signals are then amplified by voltage-gated sodium channels to create action potentials [63], [64]. The peripheral inputs are subsequently transmitted from glutamatergic synapses onto second-order neurons in the spinal horn by nociceptive afferents. The net output from the spinal network is carried to distinct projection sites in the brain. The eventual experience of pain is perceived in the cortex, where the information is sent to the spinal cord to invoke the appropriate behavior, such as withdrawal from the noxious stimuli. (**Figure 3 A)**

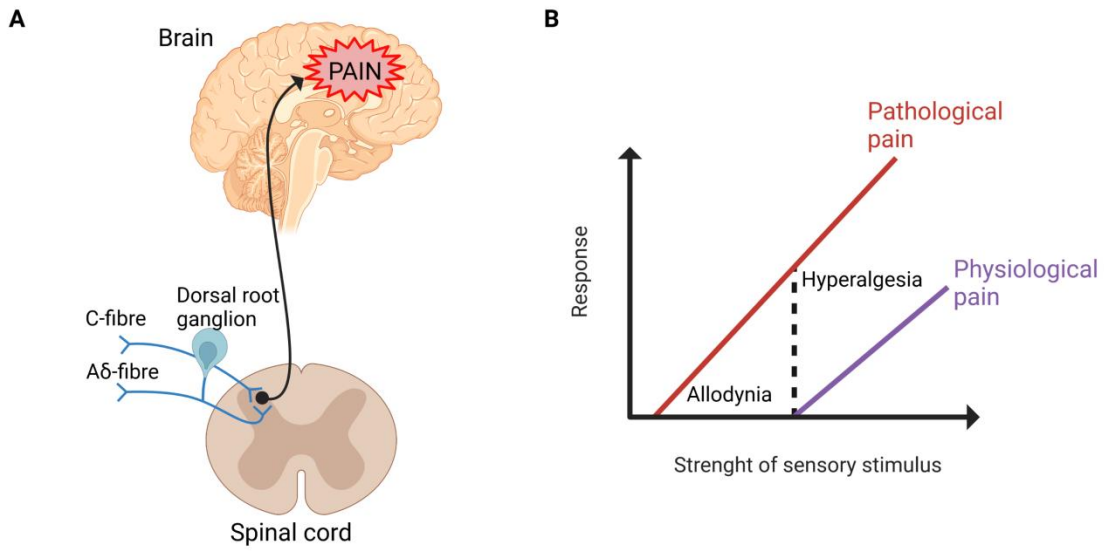

Figure 3: Pain circuits. A Schematic overview of the main circuits mediating physiological pain **(A)** and the manifestations of chronic pain in allodynia (response to innocuous stimuli) and hyperalgesia (enhanced responsiveness to stimuli) **(B)**. Modified from: [65]. Figure was created with BioRender.com.

However, in states of chronic pain nociceptive and non-nociceptive afferents are permanently sensitized and therefore pain takes on a disease character. For instance, when a painful stimulus manifests in an increased response this is described as hyperalgesia while withdrawal behavior in response to innocuous stimuli is categorized as tactile allodynia [66] (**Figure 3 B)**.

3.5.1. Spinal pre- and postsynaptic changes

Chronic pain, that is defined as any pain that lasts for several weeks or longer and serves no obvious beneficial function [67], arises from mechanisms underlying evoked physiological pain. The reduction of threshold (allodynia) and/or increase in magnitude of responsiveness (hyperalgesia) occurs in response to chemical mediators, for example prostaglandins (PGE_2,PGI_2), neuropeptides (bradykinin) and growth factors (NGFs) [68]–[70] that are released by nociceptors and non-neuronal cells such as mast cells, neutrophils or macrophages at the site of tissue injury or inflammation [71]. In response to the signals from chemical mediator, the excitability of nociceptor terminals is modulated by phosphorylation of receptors, ion channels or associated regulatory proteins which alters the expression and intrinsic functional properties of channels in the primary sensory and dorsal horn neurons [72] (**Figure 4**). For example, sensitizing stimuli initiate the activation of the cAMP signaling pathway, activating protein kinase A (PKA) and protein kinase C (PKC) [70], [73], [74] leading to the phosphorylation of the tetrodotoxin (TTX)-resistant voltage-gated sodium channel SNS [75]. Phosphorylation of SNS leads to alteration of the activation threshold and

increases the magnitude of the sodium current to depolarization, leading to an acute as well as long-term increase in the excitability of nociceptors [76], [77]. These changes in peripheral nerves are also referred to as peripheral sensitization and constitute a key element in neural plasticity, which accounts for many clinical manifestations of chronic pain [78], [72].

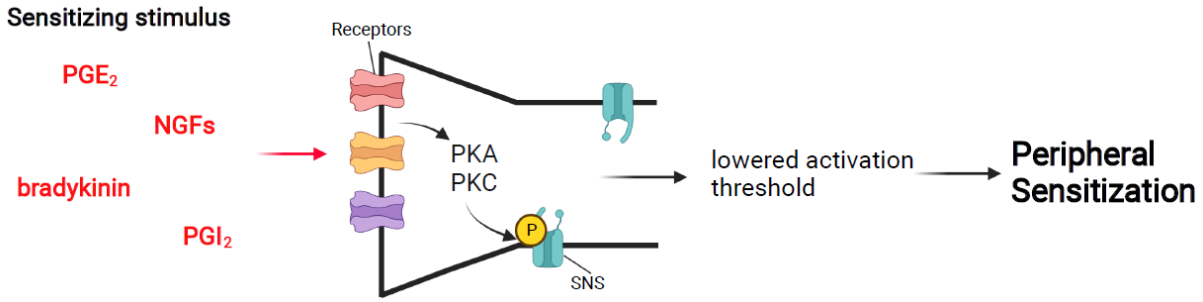

Figure 4: Modulation of peripheral terminals: Peripheral Sensitization. Inflammatory sensitizing agents released during tissue damage activate PKA and PKC through cAMP signaling pathway. PKA and PKC phosphorylate SNS which enables discharge of action potentials with a lowered threshold as the excitability of the nociceptor terminal can be achieved with a reduced amount of depolarization. Modified from : [72]. Figure was created with BioRender.com.

From the central terminals of nociceptors, pain is signaled by release of glutamate generating excitatory post-synaptic currents (EPSCs) in second order dorsal horn neurons [79]. Summation of sub-threshold EPSCs will eventually result in action potential and transmission of pain to higher order neurons. Under normal physiological conditions, this occurs through activation of AMPA and kainate receptors alone without participation of NMDARs. But in the setting of injury or inflammation, the increased amount of neurotransmitter release conditioned through peripheral sensitization will sufficiently depolarize postsynaptic neurons to activate NMDARs. Consequently, the increase of calcium influx strengthens synaptic connections between nociceptors and dorsal horn leading to enhanced responsiveness of pain transmitting neurons and ultimately hyperalgesia. This enhanced processing of pain by postsynaptic alterations is referred to as central sensitization [80] (**Figure 5**). Activation of intracellular signaling cascades and messenger systems, notably kinases (PKA, PKC, SRC) further increase excitability of these neurons [81]. Ionotropic NMDA and AMPA glutamate receptors get phosphorylated on several key residues, which changes their activity and trafficking to or from the membrane [82]–[85]. This leads to facilitated excitatory synaptic responses by recognizing subthreshold inputs that are normally ineffective [86] and spreads hypersensitivity beyond the injured tissue [87].

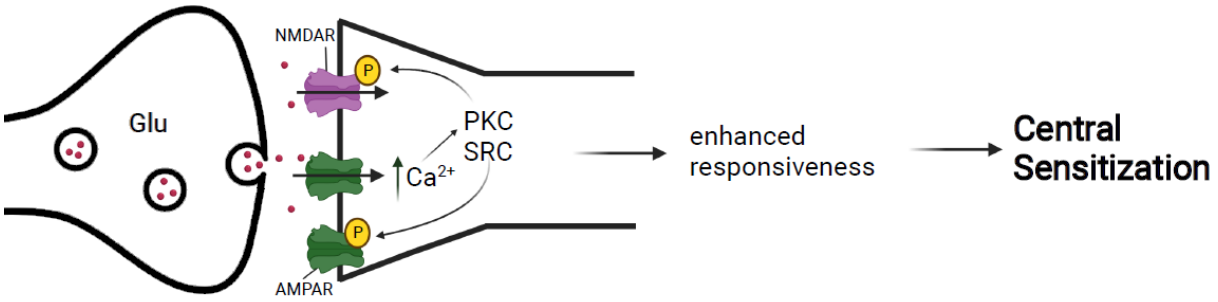

Figure 5: Modulation of nociceptive synaptic transmission: Central sensitization. The increased signaling following peripheral sensitization leads to intracellular changes that subsequently increase responsiveness. Upregulation of NMDARs through phosphorylation and increased AMPA channel insertion lead to the recognition of normally ineffective inputs and thus constituting to central sensitization. Figure was created with BioRender.com.

Finally, long-lasting alterations in the expression or structure of receptors and ion channels are responsible for distorting the normal stimulus-response characteristic and lead to long-term modification of primary sensory neurons [72] completing the chronification of pain (**Figure 6**). The preceding increased signaling caused by peripheral and central sensitization, leads to alterations in the expression of transmitters, synaptic neuromodulators, ion channels, G-protein-coupled receptors and growth associated structural proteins [72], [88]–[91]. Additionally, a subpopulation of Aδ-fiber neurons undergo a phenotype shift towards C-fiber neurons as they express substance P and BDNF and thereby enhancing synaptic transmission in the spinal cord and amplifying the central response to innocuous stimuli [92]. Lastly, a reduction of inhibition through cell death of inhibitory interneurons which occurs after nerve injury facilitates pain transmission [93].

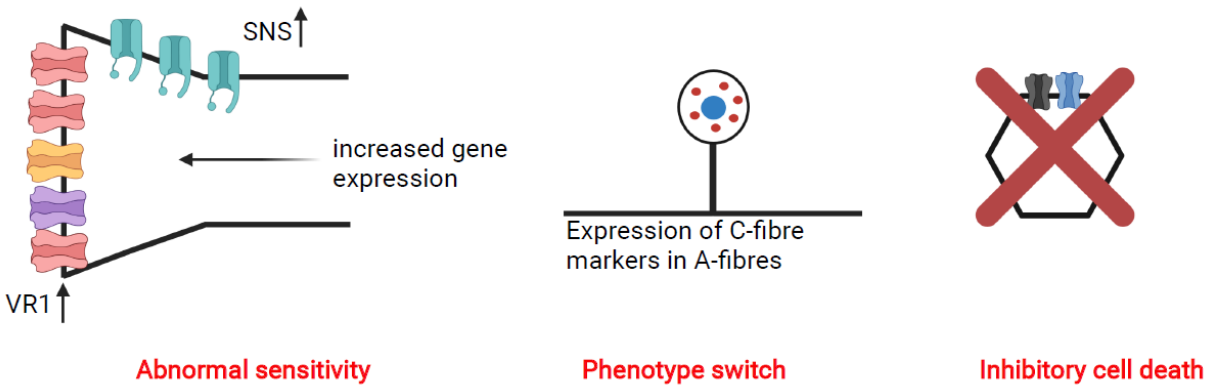

Figure 6: Modification of primary sensory neurons. Abnormal sensitivity through alterations in gene expression as well as a phenotype switch from A-fibers to C-fibers and a reduction of inhibitory interneurons lead to long-lasting changes, distorting the normal stimulus-response characteristic and leading to chronic pain. Modified from:[72]. Figure was created with Biorender.com.

3.5.2. Synaptic changes in cortical neurons

While the spinal dorsal horn and periphery are the traditional targets for treating pain, more and more evidence suggest that central changes occur in the brain after inflammation, making it too late to interfere at the periphery to reduce symptoms [94]. Brain imaging studies in humans have provided crucial evidence that cortical regions of the brain are involved in different types of pain perception [95]–[97]. For instance, nociceptive information from somatic and visceral input is transmitted indirectly to the anterior cingulate cortex (ACC) via the thalamus [98], [99], the amygdala [100] and other pain-related areas of the cortex such as the primary somatosensory cortex (S1)[101]. This widespread connectivity emphasizes the importance of the ACC in the processing of pain. Chronic pain in the ACC is related to a saturated persistent strengthening of synapses, also known as long-term potentiation (LTP), that leads to long-lasting enhanced signaling [67]. Additionally, a suppression of the counter mechanism which reduces the efficacy of signal transmission referred to as long-term depression (LTD) is also linked to chronic pain in the ACC [67].

Taking a closer look at the enhanced signaling, there are four major synaptic mechanisms contributing to the expression of LTP in the ACC: (i) presynaptic enhancement of glutamate release; (ii) structural changes in synapses; (iii) insertion of AMPARs and (iv) post-synaptic enhancement of AMPAR/NMDAR mediated responses [102] (**Figure 7**).

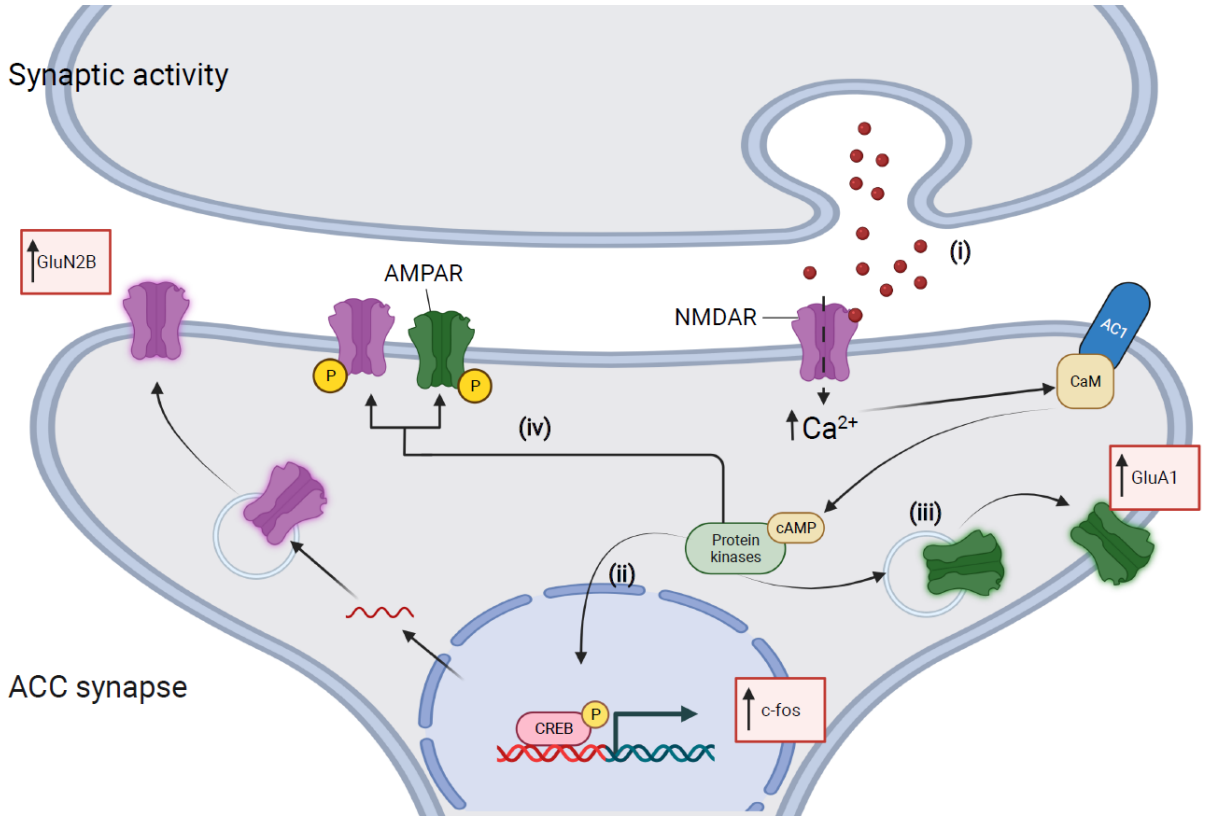

Figure 7: Signaling pathways that upregulate excitatory transmission in the ACC in rodent models of chronic pain. The upregulation of excitatory transmission is achieved through several synaptic mechanisms. **(i)** The release of presynaptic glutamate is increased caused by peripheral and central sensitization; **(ii)** NMDAR dependent LTP induces a NMDAR GluN2B-AC1-cAMP-CREB-GluN2B positive feedback loop, leading to structural changes in the synapse; **(iii)** Insertion of GluR1 homosynaptic AMPAR contributes to the expression of LTP; **(iv)** Post-synaptic enhancement of AMPAR and NMDAR mediated response through phosphorylation alters the activity and trafficking. Modified from: [67], [103]. Figure was created with BioRender.com

Increased presynaptic neurotransmitter release that is caused by central sensitization results in an increase of postsynaptic Ca^{2+} via NMDARs. This triggers the activation of Ca^{2+}-stimulated signaling pathways [104], including the activation of Ca^{2+}/calmodulin-dependent protein kinase II（CaMK II) and adenylyl cyclase 1 (AC1) [105]. Similar to LTP in the hippocampus, it is likely that AC1 generates cAMP, which then activates PKA [67]. Consequently, PKA activates ERK (extracellular signal-regulated kinase) which induces CREB phosphorylation, activating CREB-mediated transcriptional regulation [106] which results in an upregulation of e.g. c-fos [107]. Therefore, Fos protein expression can be used as a marker for neuronal activity after noxious stimulation not only in the dorsal horn of the spinal cord but throughout various regions of the brain including the thalamus, amygdala, hippocampus and anterior cingulate cortex [108]–[111]. Interestingly, the NMDAR GluN2B subunit contains a CREB binding domain and thus the GluN2B subunit may also be regulated by NMDA-calcium-CaM dependent pathway. As peripheral inflammation leads to

an increased expression of NMDAR GluN2B in the ACC [112], this indicates that the NMDAR GluN2B-AC1-cAMP-CREB-GluN2B signaling pathway forms a positive feedback-loop leading to a reinforcement of NMDAR in ACC contributing to chronic pain sensation [103]. Besides the CREB activation, the increased activity of the CaMK II is also responsible for functional recruitment of GluA1 AMPARs which appears to be another key mechanism underlying synaptic plasticity in the ACC [113], [114]. And finally the increased kinase activity leads to increased phosphorylation of AMPARs and NMDARs which enhances the receptor mediated current and is important for the maintenance of LTP leading to ongoing pain perception [115]–[119].

While these changes in the ACC synapse already account for long-lasting changes in pain perception, it is most likely that the combination of enhanced LTP and suppressed LTD are both responsible for the complexity of chronic pain perception. Interestingly, the key to either NMDAR-dependent LTP or LTD induction is the removal of the NMDAR Mg^{2+} block, which is accomplished through pre-depolarization. Maximal Ca^{2+} influx triggers LTP response, while smaller NMDAR-dependent Ca^{2+} leads to LTD induction [120]. Therefore, the distribution of AMPARs in the synapse is crucial for either potentiation or depression. Under normal circumstances, one important regulatory mechanism for LTP/LTD induction is the internalization of AMPARs in the synapse which is associated with the phosphorylation of AMPAR-GluA2 as well as its interactions with the C-terminal PDZ proteins GRIP (glutamate receptor interacting protein), ABP (AMPA receptor binding protein) and PICK 1 (protein interacting with C kinase 1)[121]–[123]. Especially GluA2-PICK1 complexes, which are preferably built upon phosphorylation of GluA2 S880, seem to be important for long-lasting LTD as they show prolonged recycling after internalization [124], [125]. In both NMDAR and metabotropic glutamate receptor (mGluR) dependent LTD the activity of PKC-α, which also binds PICK1, is presumed to be responsible for GluA2 phosphorylation at S880 and thus is required for cerebellar LTD [67], [126] (**Figure 8**).

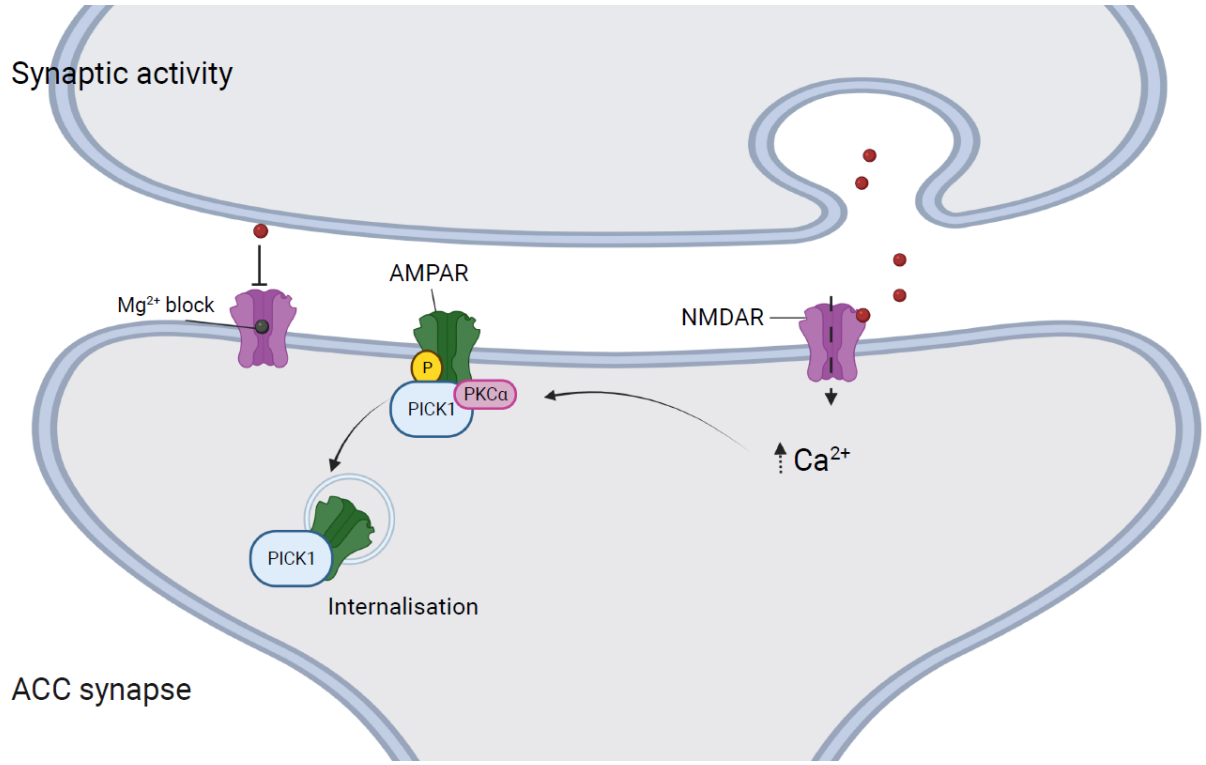

Figure 8: Signaling pathway that leads to long-term depression of excitatory transmission in the ACC. Small NMDAR-dependent Ca^{2+} influx induces internalization of AMPARs. The reduced display of AMPARs leads to insufficient pre-depolarization to remove Mg^{2+} blocks from NMDARs and this subsequently gives rise to long-term depression (LTD). Figure was created with BioRender.com

After nerve injury, however, the AMPAR-GluA2 is downregulated in dorsal horn neurons [127], [128], and in ACC synapses [129]. As the internalization is dependent on GluA2 subunit of AMPAR this means that the internalization of AMPARs cannot take place and thus pre-depolarization to remove Mg^{2+} blocks of NMDARs is still intact. Consequently, the expression of LTD cannot occur and therefore is suppressed. Thus, the downregulation of AMPAR-GluA2 contributes to pathological pain perception in chronic pain models.

3.6. K/BxN serum transfer model as neuropathic pain model

In order to study pain pathways and to find new therapeutic targets for pain relief, different mouse models mimicking human arthritis have been established. The K/BxN mice which express the transgenic T cell receptor KRN and the MHC class II allele A^{g7} develop severe inflammatory arthritis. Serum from these mice can be used to reliably cause arthritis in a wide range of recipient strains (BALB/c; C57BL/6; DBA/1) (K/BxN serum transfer model) which is attributed to high levels of autoantibodies to the glycolytic enzyme glucose-6-phosphate isomerase (G6PI) [130], [131]. However, the induced RA in the serum transfer model is transient and diminishes after 15-30 days unless it is administered repeatedly [132]. The

K/BxN serum transfer model leads to persistent pain resembling a neuropathic condition over time that surprisingly outlasts the inflammation by two weeks [133]. While during the inflammatory state the mice are sensitive to treatment with non-steroidal anti-inflammatory drugs (NSAIDs) e.g. the TNF-blocker etanercept, this is not the case in the post-inflammatory state [133]. In the post-inflammatory state however, the mice are only sensitive to gabapentin [133], which inhibits forward trafficking of α2δ-1-NMDAR complexes and thereby decreasing post-synaptic Ca^{2+} influx [134]. This indicates that there are two mechanisms that drive tactile allodynia in K/BxN serum transfer mice, thus representing a multifaceted model of pain mechanisms of joint inflammation which also occur in human arthritic conditions [133]. Since gabapentin is able to pass the blood-brain barrier [135], it might also exert its effect on brain areas where central changes in the ACC could have contributed to neuropathic pain (see 3.5.2).

3.7. Aim of the study

Radon therapy is carried out in so-called 'healing-caves' for over 100 years for patients suffering from arthritic conditions [136]. Although the therapy with a radioactive gas displays a significant risk of developing lung cancer [7], patients still expose themselves voluntarily to radon as it attenuates their pain, which is the most prominent symptom in RA patients [3], [9].

Since central sensitization is thought to be the cause of the persistent pain in RA patients [4] it is a possible point of action for radon therapy. The aim of this study was to investigate the effect of radon inhalation on the brain, where central changes occur following persistent pain, thus contributing to chronic pain sensation. Firstly, a possible binding to the NMDAR was examined by MD simulation and a self-established radon binding assay. Afterwards, it was investigated whether radon reaches the brain by examining the DNA DSBs in the dentate gyrus of mouse hippocampi. Finally, the effect of radon inhalation on receptors and proteins in the brain were investigated in a neuropathic pain mouse model, in order to elucidate the possible mechanism underlying pain alleviation after radon therapy.

4. Material and Methods

4.1. Antibodies

Table 3: Primary antibodies

Antibody	Host	Manufacturer	Concentration
53BP1 (H-300)	rabbit	Santa Cruz (sc-22760)	1:1500
NMDARζ1 (H-300)	rabbit	Santa Cruz (sc-9058)	1:1250
NMDAR2B	rabbit	Abcam (65783)	1:1000
NMDAR2B (phospho Y1472)	rabbit	Abcam (ab3856)	1:1000
β-actin	mouse	Sigma-Aldrich (A5441)	1:20,000
c-fos	rabbit	Boster Biological (PA1318)	1:10,000
AMPAR GluA1	rabbit	Alomone labs (AGC-004)	1:1000
PKC-α	mouse	Santa Cruz (sc-8393)	1:100

Table 4: Secondary antibodies

Antibody	Host	Manufacturer	Concentration
Anti-rabbit Alexa 594	donkey	Abcam (ab150076)	1:400
Anti-rabbit Alexa 488	donkey	Abcam (150105)	1:400
Anti-rabbit HRP	goat	Thermo Fisher Scientific (32460)	1:10,000
Anti-mouse HRP	goat	Abcam (ab6789)	1:10,000

4.2. Chemicals and Solutions

6-Aminocapric acid	Carl Roth (Karlsruhe, Germany)
Accutase	Sigma-Aldrich (St. Louis, Missouri, USA)
Acrylamide	Carl Roth (Karlsruhe, Germany)
Advanced DMEM/F12	Thermo Fisher Scientific (Waltham, Massachusetts, USA)
APS	Sigma Aldrich (St. Louis, Missouri, USA)
Bromphenol blue	Sigma-Aldrich (St. Louis, Missouri, USA)
BSA	Bio Rad (Feldkirchen,Germany)
Citric acid	Carl Roth (Karlsruhe, Germany)
EDTA	Sigma-Aldrich (St. Louis, Missouri, USA)
Ethanol	Sigma-Aldrich (St. Louis, Missouri, USA)
FCS	Sigma-Aldrich (St. Louis, Missouri, USA)
Gelatin	Merck (Darmstadt, Germany)
Glycerol	VWR (Darmstadt, Germany)
Goat serum	Thermo Fisher Scientific (Waltham, Massachusetts, USA)
HEPES	Carl Roth (Karlsruhe, Germany)
Hoechst 33342	Sigma-Aldrich (St. Louis, Missouri, USA)
KCl	Merck (Darmstadt, Germany)
L-glutamine	Sigma-Aldrich (St. Louis, Missouri, USA)
Mannitol	Sigma-Aldrich (St. Louis, Missouri, USA)
MEM	Thermo Fisher Scientific (Waltham, Massachusetts, USA)
Mercaptoethanol	Sigma Aldrich (St. Louis, Missouri, USA)
Methanol	Carl Roth (Karlsruhe, Germany)
$MgCl_2$	Carl Roth (Karlsruhe, Germany)
Milk	Carl Roth (Karlsruhe, Germany)
MK801	Hello Bio (Bristol, UK)
Na_2HPO_4	Merck (Darmstadt, Germany
NaCl	Carl Roth (Karlsruhe, Germany)3957.1)
NaH_2PO_4	Merck (Darmstadt, Germany)
PBS	Sigma-Aldrich (St. Louis, Missouri, USA)
Penicillin	Sigma-Aldrich (St. Louis, Missouri, USA)
Penicillin/Streptomycin	Sigma-Aldrich (St. Louis, Missouri, USA)
PFA	Sigma Aldrich (St. Louis, Missouri, USA)
Phosphatase inhibitor	Abcam (Cambridge, Massachusetts USA)
Poly-D-Lysine	Sigma-Aldrich (St. Louis, Missouri, USA)
Protease inhibitor	Sigma-Aldrich (St. Louis, Missouri, USA)

Roti®mount FluorCare	Carl Roth (Karlsruhe, Germany)
RPMI	Thermo Fisher Scientific (Waltham, Massachusetts, USA)
SDS	Carl Roth (Karlsruhe, Germany)
Sodium Acetate	Thermo Fisher Scientific (Waltham, Massachusetts, USA)
Sodium citrate	Sigma-Aldrich (St. Louis, Missouri, USA)
Streptomycin	Sigma-Aldrich (St. Louis, Missouri, USA)
Sucrose	Sigma-Aldrich (St. Louis, Missouri, USA)
TEMED	Sigma-Aldrich (St. Louis, Missouri, USA)
Tris	VWR (Darmstadt, Germany)
Triton X-100	Sigma Aldrich (St. Louis, Missouri, USA)
Tween-20	Sigma-Aldrich (St. Louis, Missouri, USA)
Xylol	Carl Roth(Karlsruhe, Germany)

Immunofluorescence staining for cells

PBG	PBS + 0.05 % gelatin
Blocking buffer	PBG + 5 % goat serum + 0.5 % BSA
Antibody buffer	PBG + 5 % goat serum

Protein extraction

Lysis buffer	2 mM EDTA; 50 mM HEPES pH 7.4
Homogenization buffer	2 mM EDTA; 10 mM HEPES pH 7.4; 0.23 M sucrose, protease inhibitor, phosphatase inhibitor

Western Blot

4 x Loading buffer	240 mM Tris/HCl (pH 6.8); 40 % glycerol; 8 % SDS; 0.04 % bromphenol blue
SDS gel	**5 % stacking gel:** 30 % Acrylamide; 10 % APS; 10 % SDS; 1 % TEMED; 0.5 M Tris pH 6.8
	10 % separation gel: 30 % Acrylamide; 10 % APS; 10 % SDS; 1 % TEMED; 1 M Tris pH 8.8
SDS- PAGE running buffer	25 mM Tris; 192 mM glycine; 0.1 % SDS
Anode buffer	60 mM Tris; 40 mM 6-Aminocapric acid; 20 %

	Methanol
Cathode buffer	60 mM Tris; 40 mM 6-Aminocapric acid, 0.1 % SDS
TBS-T	50 mM Tris; 150 mM NaCl; 0.1 % Tween-20
Blocking buffer	5 % milk in TBS-T
Antibody buffer	1 % milk in TBS-T

4.3. Cell culture

Cultivation

Cells were cultivated at 37 °C under humid atmosphere at 5 % CO_2 in T25 flasks (Sarstedt, Nümbrecht, Germany). The cells were cultured until 80 % confluency before passaging. Therefore, the cells were washed with PBS once before they were incubated with Accutase™ until the cells detached from the flasks. The cells were harvested by centrifugation at 1000 rpm for 3 min and then resuspended in 1 ml of the appropriate medium. The cell number was determined using a hemocytometer. Cells were then seeded into new T25 flasks or 6-well chambers (IBIDI, Gräfelfing, Germany) in the needed concentration.

CHO-K1

The immortalized cell line CHO-K1 (Chinese hamster ovary-K1) was cultured in T25 flasks using Advanced DMEM/F12 supplemented with 10 % FCS, 100 U/mL penicillin, 0.1 mg/mL streptomycin and 2 mM L-glutamine. The cells were not used for more than 20 passages.

HEK293

Human embryonic kidney (HEK293) cells were cultivated in T25 flasks using MEM containing 10 % FCS and 2 % penicillin/streptomycin. The cells were not used for more than 20 passages.

Seeding cells on a porous membrane

The porous membrane (Nunc polycarbonate Membrane 3 µm, 6-well format, Thermo Scientific) was coated with Poly-D-Lysine (4 µg/cm^2) by incubating the solution on the membrane overnight at 37 °C. $5 \cdot 10^5$ cells were seeded on top of the membrane.

Transfection

For the transfection of NMDARs 80 % confluent cells were detached with Accutase™ and $1 \cdot 10^7 cells$/ml were resolved in electroporation buffer (5 mM KCl, 15 M $MgCl_2$ 50 mM Mannitol in 1 M Na_2HPO_4/NaH_2PO_4 pH 7.2). Cells were transfected with GluN1/GluN2B/eGFP or RFP (2 µg DNA each) and eGFP or RFP (2 µg DNA) for control cells. Electroporation was performed with Amaxa Nuceleofector II at CHO-K1 high viability program (Lonza, Basel, Switzerland). Before seeding the cells on the porous membrane, the cells were incubated with 100 µL of RPMI Ca^{2+}-free media at 37 °C, 5 % CO_2 for recovery. Then, cells were transferred into fresh culture medium supplemented with 20 µM MK801 to block NMDAR activity in transfected cells and seeded.

4.4. C57Bl/6 mice

C57Bl/6 mice were housed in common type II long cages (2-4 mice/cage, with nesting and hideaway). The mice were provided with free access to food and kept under 12 h light/dark cycle, 22 °C temperature with 50-60 % relative humidity (according to guidelines of the GV-SOLAS).

4.5. Brain tissue

The brains of radon exposed and x-ray irradiated mice was kindly provided by AG Löbrich. The complete protocol of in vivo irradiation, fixation and paraffin embedding is described in [137]. In short, C57Bl/6 mice were exposed to 440 kBq/m^3 in a radon exposure chamber at GSI [138], [139]. For x-ray irradiation, mice were narcotized with isofluorane and then exposed to x-ray irradiation in an isovolt 320 x-ray tube (GE Snensing & Inspection Technologies, Boston, USA). Brain tissues were extracted and divided at the hemispheres for homogeneous fixation. The tissue was fixed in formaldehyde for 16 h at RT and subsequently dehydrated in an ascending ethanol series and concluding xylol incubation at RT. Finally, the mouse brains were embedded in paraffin at 70 °C. The paraffin embedded brain was sliced sagitally with the microtome Hydrax M55 (Zeiss, Oberkochen, Germany). 3 µM hippocampal slices were prepared on glass slides. Slides were then dried at 50 °C overnight and stored at RT until further usage.

Rehydration

The brain tissue samples had to be rehydrated for subsequent immunofluorescent staining. Slides were placed in xylol for 10 min twice before they were placed in a descending sequential ethanol series (100 %, 100 %, 96 %, 80 % 10 %) for 8 min each time. Thereafter, the slides were washed in ddH_2O.

Antigen retrieval

After the slides were rehydrated, the antigens were retrieved by placing the slides in citrate buffer (10 mM (1.8 mM citric acid/8.2 mM sodium citrate), pH 6) for 1 h at 98 °C. After letting the samples cool down for 15 min, they were washed in PBS.

Immunofluorescent staining

The primary antibody was diluted 1:600 in PBS with 0.1 % Triton X-100 and then the samples were stained in a staining chamber at 4 °C overnight. Then the slides were washed trice with PBS. The secondary antibody was diluted 1:600 in PBS with 0.1 % Triton X-100 and samples were stained for 3 h at RT in the dark. The tissue samples were washed with PBS once before they were stained with Hoechst 33342 for 10 min. After staining was complete, the brain tissue samples were washed trice in PBS before they were covered in Roti®mount FluorCare, sealed with nail polish and stored at 4 °C until microscopic investigation.

4.6. Immunofluorescent staining of cells

CHO-K1 cells on porous membrane, 6-well chambers (ibidi, Gräfelfing, Germany) or glass slides were fixed with 4 % PFA for 20 min, permeabilized with 0.1 % Triton X-100 and stained with Hoechst 33342 for 10 min. Then, the cells were blocked with 0.5 % BSA/ 5 % goat serum and incubated overnight at 4 °C. After blocking, the cells were stained with primary antibody overnight at 4 °C. The next day, the samples were washed three times for 10 min with PBG, then incubated with the secondary antinody for 45 min at RT, and finally washed three times with PBG and twice with PBS. Cells in ibidi^{TM} chambers were imaged directly while the membranes or glass slides were mounted on object slides with Roti®mount FluorCare, sealed with nail polish and stored at 4 °C until observation.

4.7. Microscopy

All immunofluorescent stainings were imaged with inverted epifluorescence microscope Axio Observer Z1 (Zeiss, Oberkochen, Germany). Live-cell images were taken with JuLi^{TM} FL microscope (Nano EnTek, Seoul, Korea)

4.8. Analysis of 53BP1 Foci

Single nuclei were detected by the µManager software based on size and shape of the Hoechst 33342 signal. 53BP1 foci were counted manually. The mean of all single cell values of all independent experiments were used for statistical analysis. For absolute foci values,

the Kruskal-Wallis test was used for statistics. For foci number distribution the two-way Anova test was used for statistics. (Graphpad Prism 7.0, GraphPad Software, San Diego, California, USA).

4.9. Molecular Dynamics

The crystal structure of the GluN1/GluN2A ligand binding cores complex with bound glycine and glutamate (PDB: 2A5T) was used for MD simulations. Initial noble gas coordinates were taken over from [39]. Simulations were performed with GROMACS 2019 and the CHARMM36m force field. Xenon and radon parameters were derived from Verlet&Weis and Potoff&Coworkers respectively. The TIPS3P water model was used and each simulation system contained 0.15 mol/L KCl. Temperature and pressure were kept at 298 K and 1 bar using the V-Rescale thermostat and Parrinello-Rahman barostat, respectively. The integration time step was 2 fs. Van der Waals forces were force-switched to zero between 0.8 nm and 1.2 nm. Electrostatics were represented using the PME method and switched to zero between 0.8 nm and 1.2 nm. Bonds including hydrogen atoms were kept constant using LINCS. Each simulation system was energy minimized (steepest descent), equilibrated with position restraints on the protein (Fc = 1000 kJ/mol/nm2) and simulated without restraints for 100 ns. Binding energy differences were estimated using the free energy perturbation (FEP) method. For each binding site, a single xenon atom was gradually transformed to radon with λ increasing from 0 (= Xe) to 1 (= Rn) with a λ-step size of 0.05 (21 simulations per cycle). The soft-core α and σ parameters were set to 0.5 and 0.34 nm, respectively. As starting point, a single frame taken from the simulation with bound xenon after 20 ns of the equilibrium simulations was used. For each binding site, all non-relevant xenon atoms were removed from the simulation system prior to FEP simulations. For each λ-step, the system was equilibrated for another 1 ns and simulated for 15 ns. To prevent the atom from leaving its binding site, a flat-bottomed position restraint of 1000 kJ/mol/nm2 was used to keep it within 0.3 nm of its initial position using the PLUMED2 plugin. The last 10 ns of each step were then used for FEP calculation using the TI method. The same transformation was performed for a single xenon atom in a box of water. Finally, $\Delta\Delta G_{Xe \rightarrow Rn}$ was calculated as the difference between the free energies of transformation in the bound state and in water.

4.10. Radon exposure

CHO-K1 cells

12 h after transfection the cells were moved to fresh 6-well-plates containing 200 µl of fresh media supplemented with 20 µM MK801 which is only enough media to supply the bottom of the cells with medium while the top is exposed to the surrounding atmosphere (porous membrane) or were covered with minimal amount of media supplemented with 20 µM MK801 (glass slides). The plates were either placed into the radon chamber at GSI [138], [139] or inside a cell culture incubator (sham) with 37 °C under humid atmosphere at 5 % CO_2. The radon chamber was held at constant conditions (**Table 5**) for 1 h. Thereafter, the radon chamber was washed to remove all radon residues. The cells were treated a total of 82 min before they were supplied with 2 ml of fresh media supplemented with 20 µM MK801. The cells were incubated for an additional 30 min at 37 °C and 5 % CO_2 before immunofluorescent staining was performed.

Table 5: Exposure conditions for radon exposed cells

Exposure conditions	**glass slide**	**porous membrane**
Temperature (°C)	35.9 ± 0.2	36.8 ± 0.1
Relative humidity (%)	75.1 ± 0.2	73.1 ± 0.6
Barometric pressure (mbar)	1002 ± 3	984 ± 3
CO_2 concentration	~5 (defect detector)	5.82 ± 0.05
^{222}Rn concentration (kBq/m^3)	378.6 ± 9.7	547 ± 6

K/BxN serum transfer mice

The K/BxN serum was injected into recipient C57BL/6 mice 3 days before radon exposure. (Serum and mice were kindly provided from AG Strahlen-Immunbiologie, FAU Erlangen). For radon exposure, the mice were placed into the radon chamber at GSI [138], [139]. Exposure conditions are summarized in **Table 6**.

Table 6: Exposure conditions for sham and radon exposed K/BxN serum transfer mice

Exposure conditions	Sham		Radon	
	Trial 1	Trial 2	Trial 1	Trial 2
Temperature (°C)	23.2 ± 0.2	22.0 ± 0.1	23.4 ± 0.1	22.3 ± 0.1
Relative humidity (%)	68.7 ± 1.4	60.1 ± 3.2	71.6 ± 2.7	67.1 ± 4.7
Barometric pressure (mbar)	1011 ± 3	1017 ± 3	1011 ± 3	1017 ± 3
^{222}Rn concentration	4.5 ± 13.9 Bq/m^3	8.0 ± 4.6 Bq/m^3	466 ± 5 kBq/m^3	489.3 ± 12.5 kBq/m^3

Organ extraction was performed seven days after radon exposure. Immediately after death, the mouse was decapitated and the brain was removed from the skull and washed in PBS. The weight of the mouse brain was determined before it was directly shock frozen in liquid nitrogen. The brain was then stored at -80 °C until further usage.

4.11. Preparation of brain membrane fraction

The whole-brain was submerged into 10 volumes of ice-cold homogenization buffer. Homogenization was performed on ice with polytron homogenizator (Johann Bachhofer, Reutlingen, Germany) by carefully using 5-10 strokes. The resulting suspension was centrifuged at 1000 g for 15 min and the pelleted nuclear fraction was removed. The supernatant was spun at 200,000 g (70.1 Ti rotor, ultracentrifuge, Beckman Coulter, California, USA) for 30 min to yield the crude membrane pellet. This pellet was resuspended in homogenization buffer and then again spun at 200,000 g for 30 min to obtain the washed crude membrane pellet. The final pellet was resuspended in HEPES-lysis buffer and the total protein concentration was determined using a photometric absorption of 280 nm (Nanodrop 200c, Thermo Fisher Scientific, Massachusetts, USA). The crude membrane fraction was then solubilized by adding 0.25 % SDS / 0.25 % sodium deoxycholate and incubating the solution for 15 min on ice while vortexing every 5 min. The solubilized brain membrane fraction was then stored at -80 °C until further analysis by western blotting.

4.12. Western blot

For the analysis of the relative amount of specific proteins of mice brains, western blotting was performed. For this purpose ~100 µg of protein of solubilized brain membrane fractions were mixed with 4 x SDS loading buffer and then denatured at 56 °C for 20 min. The samples were the separated by size using an SDS-PAGE. The samples were loaded on 10 % gel and the protein ladder with size 11-245 kDa (Blueeye-proteinladder, Sigma-Aldrich) was used as a marker. The proteins were separated in SDS-PAGE running buffer at 80 V until the samples run into the stacking gel. Thereafter, the voltage was held constant at 120 V until the proteins of interest were separated. Afterwards, the protein samples were transferred to a PVDF membrane using an electric field perpendicular to the gel. The PVDF membrane was activated in methanol for 15 s, washed in water for 2 min and then transferred into anode buffer. Blotting was performed with TransBlot®Turbo^{TM}Blotting system (Bio-Rad, California, USA) for 35 min at 15 V and max. 0.8 mA. Thereafter, the membrane was blocked in 5 % milkpowder in TBS-T for 1 h at RT. After blocking, the membrane was incubated in 1 % milkpowder in TBS-T containing the primary antibody on a rolling field at 4 °C overnight. Incubation of primary antibody was followed by three washing steps on TBS-T for 15 min each to remove unspecifically and unbound primary antibody. Then incubation with secondary antibody in 1 % milkpowder in TBS-T for 1 h on a rolling field at RT followed. Subsequently, the membrane was washed three times in TBS-T for 15 min each time before the bound secondary antibody was visualized using PierceTM ECL Western Blotting Substrate (Thermo Fisher Scientific), which is converted by the peroxidase coupled to the secondary antibody. The chemiluminescence was detected using the ChemiDoc MP Imaging System (BioRad, California, USA). The relative protein amount was then determined using Image Lab Software (BioRad, California, USA). For statistical analysis Mann-Whitney Test was used (Graphpad Prism 7.0, GraphPad Software, San Diego, California, USA).

5. Results

5.1. Radon lingers at NMDARs

As radon and xenon have similar physical properties and radon was shown to occupy the same molecular structures as xenon [44], the hypothesis of radon occupying the same binding sites as xenon on the NMDAR was initially investigated.

5.1.1. Radon remains at the NMDA ligand binding complex in MD simulations

To further investigate the hypothesis whether radon binds to the NMDA LBD, molecular dynamics (MD) simulations were performed. Firstly, MD simulations starting with several xenon and radon atoms located within the GluN1/GluN2A LBD (PDB: 2A5T) were performed where the initial noble gas positions for xenon were kindly provided by [39] (**Figure 9**).

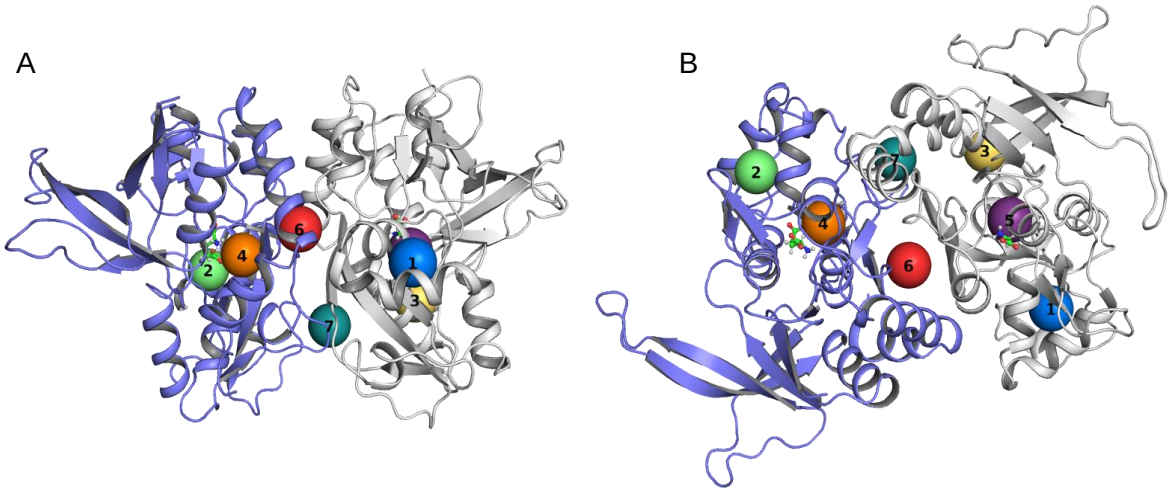

Figure 9: Noble gas binding sites in the GluN1 and GluN2A. The MD simulations were performed by Dr. Daniel Bauer. The binding complex is shown with GluN2A (blue) and GluN1 (grey) in side (A) and top (B) view cartoon with bound glycine and glutamic acid as colored sticks. Suggested xenon binding sites [39] are shown as colored spheres and labeled (1-7).

In **Figure 10 A,** most of the findings regarding xenon binding were qualitative reproduced: four out of seven xenon atoms remained in their corresponding binding pocket for over more than 20 ns of simulation, with Xe-1 and Xe-2 never leaving their initial position. In this simulation, however, Xe-5 dissociated very early, although it was found to stay bound in previous study (data not shown). Surprisingly, the opposite was the case for Xe-2, which never dissociated from the GluN2A subunit in this simulation while it did not stay bound in previous work. Interestingly, no significant difference between the binding of xenon and

radon were found from comparative MD simulations, despite radon's natural behavior to occupy a larger space due to its larger Van der Waals radius. In over 100 ns, the same 4 binding pockets stayed occupied for an extended period of time by radon: Xe/Rn-1 located within a helix-turn-helix motif of the GluN1 subunit, Xe/Rn-2 located within the corresponding motif of the GluN2A subunit, Xe/Rn-4 located next to the glutamate binding site and Xe/Rn-6 located at the GluN1/GluN2 interface **(Figure 10 B**).

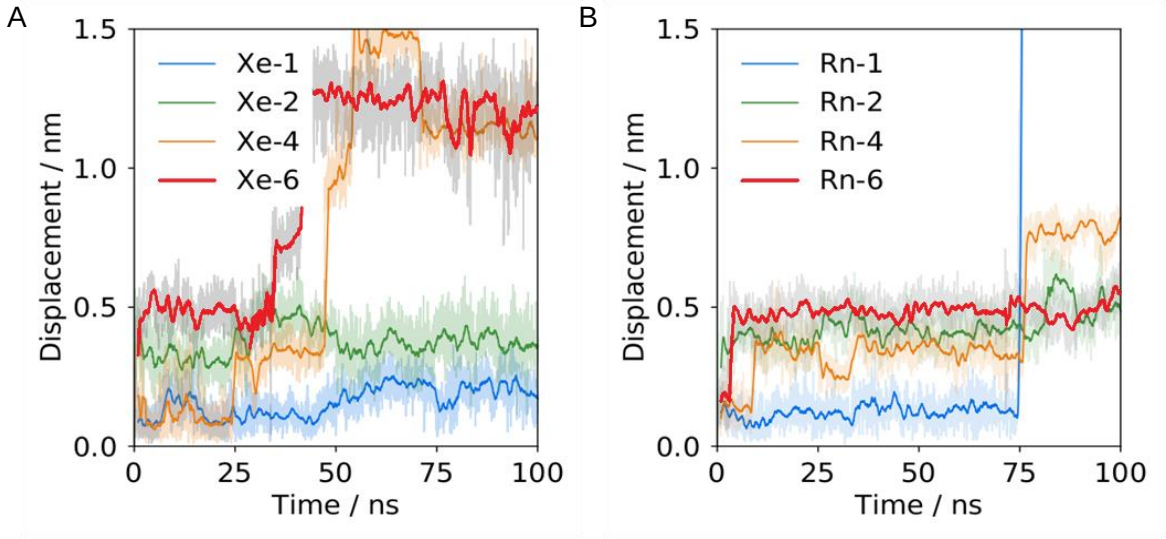

Figure 10: Displacement of relevant xenon (A) and radon (B) atoms from their initial binding site in the NMDAR LBD over a 100 ns MD simulation. The MD simulations were performed by Dr. Daniel Bauer. Four binding sites (labeled 1, 2, 4, and 6) hold on a xenon or radon atom for extended periods of time.

Encouraged by these findings, the differences in binding energies $\Delta\Delta G_{bind}$ (Xe→Rn) were calculated using the free energy perturbation method (FEP) (**Table 7**). Interestingly the binding sites Xe/Rn-2; Xe/Rn-4 and Xe/Rn-6 show a higher binding affinity to radon than to xenon with a difference in free energy of up to -2.4 kJ/mol for Xe/Rn-4. Xenon only showed a better binding affinity than radon at Xe/Rn-1 in these simulations. In comparison with absolute free binding energies of Xe, which range from -10.96 kJ/mol up to -22.26 kJ/mol [39], the small differences in binding energies between the two noble gas species were considered as not significant. All in all, this simulation could show that xenon and radon do indeed show similar binding properties to the NMDAR LBD, giving first supporting data to the hypothesis that radon is able to accumulate at NMDAR-rich areas.

Table 7: Calculated binding energies and differences in binding energy for xenon and radon. The calculations of binding energies were performed by Dr. Daniel Bauer. Xenon binding energies are derived from [39] and absolute radon binding energies are estimated by the difference in binding energies between xenon and radon.

	ΔG_{bind}(Xe) (kJ/mol)	$\Delta\Delta G_{bind}$(Xe→ Rn) (kJ/mol)	ΔG_{bind}(Rn) (kJ/mol) (est.)
Xe/Rn-1	-10.96	+0.59	-10.37
Xe/Rn-2	-	-1.18	-1.18
Xe/Rn-4	-22.26	-2.40	-24.66
Xe/Rn-6	-12.26	-1.586	-13.85

5.1.2. Establishment of an in vitro radon binding assay

Following the *in silico* MD simulation indication that radon binds to the NMDAR LBD, it was the next goal to find evidence that radon does bind to the NMDAR *in vitro* as well. Therefore, the following assay schematically shown in **Figure 11** was designed. This assay's idea is to exploit the low radiation range of α-particles. As radon decays it emits α-radiation which has a range of a few centimeters in air but has only a range of 20-100 µm in water [21]. This means that when radon decays, only a few atoms are close enough to the cell to reach the cell nucleus and generate DNA damage. This DNA damage can then be detected with immunofluorescent staining of the DNA DSB marker 53BP1. However, if radon binds to NMDARs and thus accumulates near the cell, more atoms decay in close proximity to the cell, leading to a higher number of DNA DSBs. This assay investigates the DNA damage induced by radon in cells that do not express NMDARs and compare the amount of damage with the same cells that are transiently transfected with NMDARs, which will subsequently assess a possible radon binding at NMDARs.

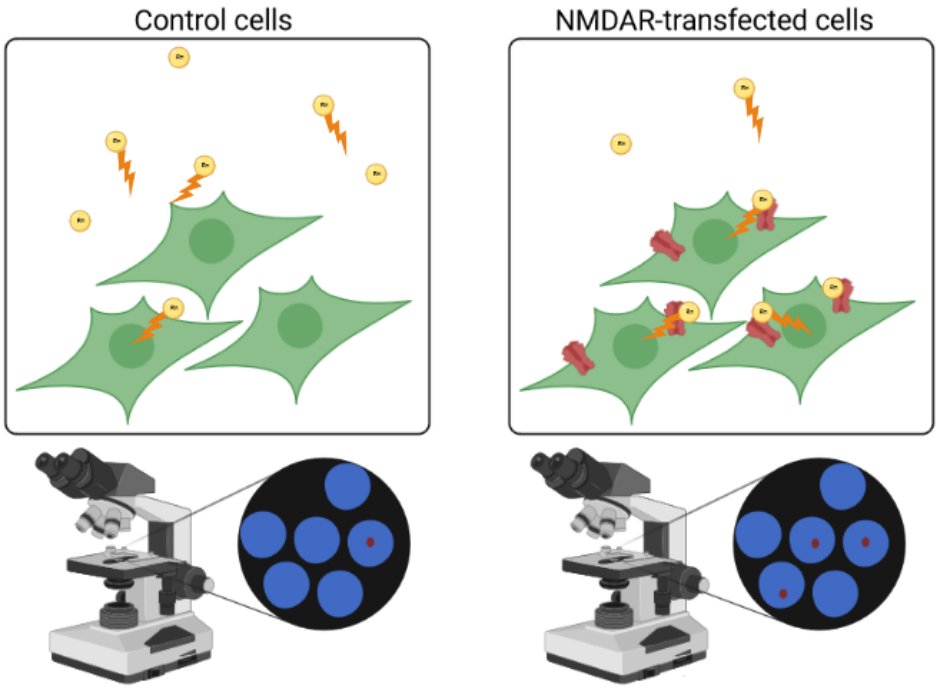

Figure 11: Schema of assay design for investigation of a radon-NMDAR binding. The control cells (left) do not express NMDARs and therefore radon decays randomly throughout the whole exposure system. Due to the low range of α-radiation the chance of hitting the cell nucleus and inducing DNA damage is low. The NMDAR-transfected cells (right) express NMDARs transiently. If radon binds to NMDARs there are more radon atoms in close proximity to the cell nucleus and thus the chance of DNA damage induction is increased. Schema was created with BioRender.com

For this assay, firstly it was important to choose a cell system that suits the requirements; no expression of NMDARs and a low foci number in non-exposed cells. Therefore, HEK293 and CHO-K1 cells were stained with 53BP1 under normal cell culture conditions which is depicted in **Figure 12 A**. Here, it is clearly visible that HEK293 cells show a high number of 53BP1 foci in several cells. With an average number of 7.9 ± 0.4 foci/cell, HEK293 cells were excluded as suitable cell line for the radon binding assay. In comparison to HEK239 cells, CHO-K1 cells showed an average number of 1.13 ± 0.1 53BP1 foci/cell under normal cell culture conditions. Thus, CHO-K1 cells were chosen as cell line for the radon binding assay.

While on the one hand it is possible to exploit the low range of alpha emitters, this also presents another problem due to radon's poor solubility in aqueous solution. However, for the radon binding assay to function properly a close proximity of radon to the cell is inevitable. In order to circumvent this problem, an air-liquid interface cultivation system (**Figure 12 B**) was tested. In an air-liquid interface cultivation system, the medium on top of the cells can be ablated for the time of radon exposure. This enables the radon atoms to diffuse freely on top of the cells without having to dissolve in aqueous solution first. **Figure 12 B** emphasizes the benefit of using the air-liquid interface when comparing the exposure of glass slides with an

air-liquid interface system. The cells cultivated on glass slides which are surrounding by media show no significant difference in the amount of 53BP1 foci between sham (0.93 ± 0.14) and radon (0.72 ± 0.1) exposed cells. In contrast, the cultivation on a porous membrane and exposure in the air-liquid interface shows a significant increase (p = <0.0001) from a mean number of 1.06 ± 0.09 foci/cell to 2.34 ± 0.15 foci/cell for radon exposed cells. Taken together, the results show that the liquid air interface radon exposure system shows a clear difference between sham and radon exposed cells, meaning that the radon atoms can reach the cells where they induce DNA DSBs as they decay. This makes it a suitable exposure condition in order to perform the described radon binding assay.

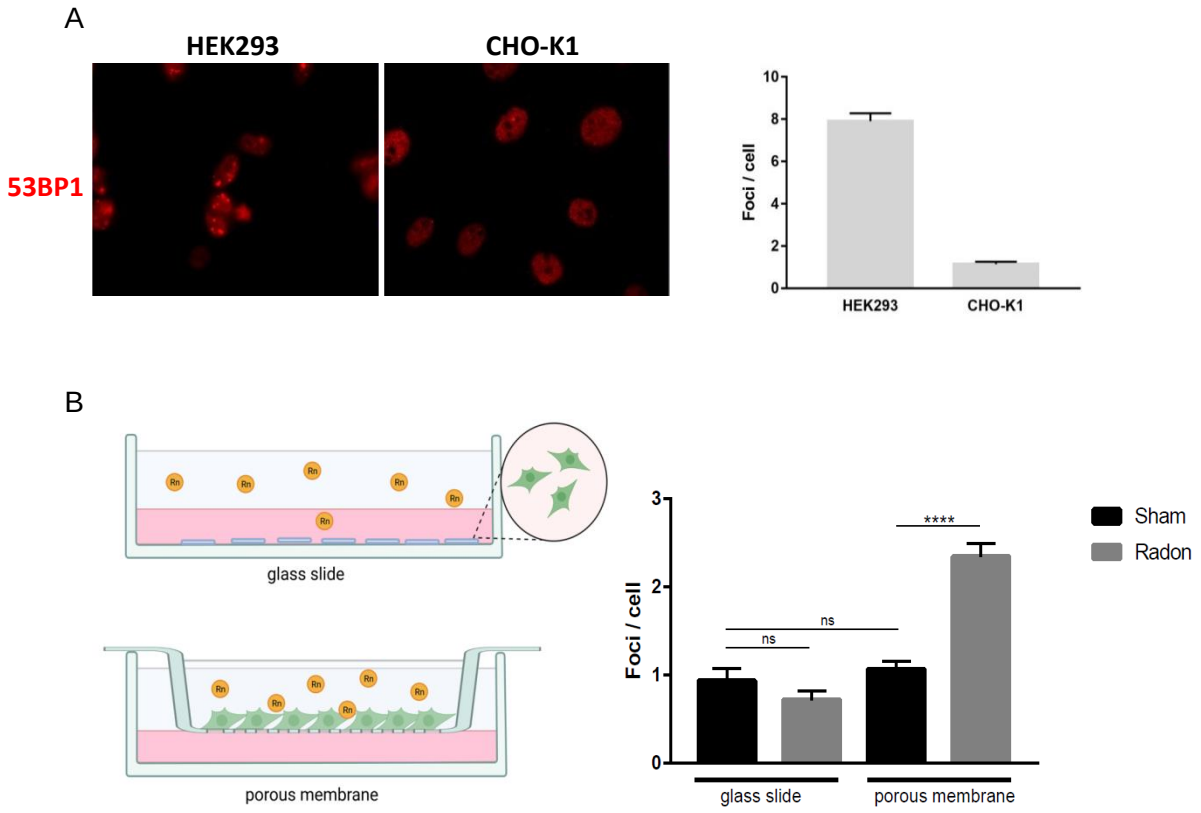

Figure 12: The cell line CHO-K1 and its cultivation on a porous membrane are suited for the radon binding assay. (A) Comparison between 53BP1 foci in HEK293 and CHO-K1 cells. Exemplary immunofluorescent stainings of 53BP1 foci in HEK293 and CHO-K1 under normal culture conditions. Scale bar 10 µm. The average number of 53BP1 foci/cell for HEK293 and CHO-K1 cells. (All error bars show SEM.) **(B)** Comparison between glass slide and porous membrane cultivation during radon exposure. The schema of the different exposure conditions (left) was made with BioRender.com. CHO-K1 cells were exposed to radon on either glass slides (378 kBq/m^3) or a porous membrane (547 kBq/m^3) and the DNA damage was investigated through 53BP1 foci analysis. While there is no difference in the number of foci between sham and radon exposed cells cultivated on glass slides and exposed in medium, there is a significant ($p \leq 0.0001$) difference between cells that were exposed to radon and the sham treated cells grown an a porous membrane, where radon gas was able to freely diffuse on top of the cells. (All error bars show SEM; Kruskal-Wallis Test for statistics; $p > 0.05$ (ns), $p \leq 0.05$ (*), $p \leq 0.01$ (**), $p \leq 0.001$ (***), $p \leq 0.0001$ (****))

Three out of the four crucial possible binding sites of radon on the NMDAR identified in 5.1.1 were found on the GluN2A subunit and in the channel pore. Both, GluN2A and GluN2B subunits are predominantly expressed in the adult brain [48], [49] and therefore both subunits present possible binding sites. The LBD of both GluN2A and GluN2B subunits are identical for 85.1 %, showing similar residues for 92.3 % of the protein sequence. **Figure 13** shows that the structures forming the binding pockets are conserved in both GluN2 subunits and therefore are interchangeable. Since especially the GluN2B shows increased expression in chronic pain models in the brain [112], the GluN2B subunit was chosen for the radon binding assay.

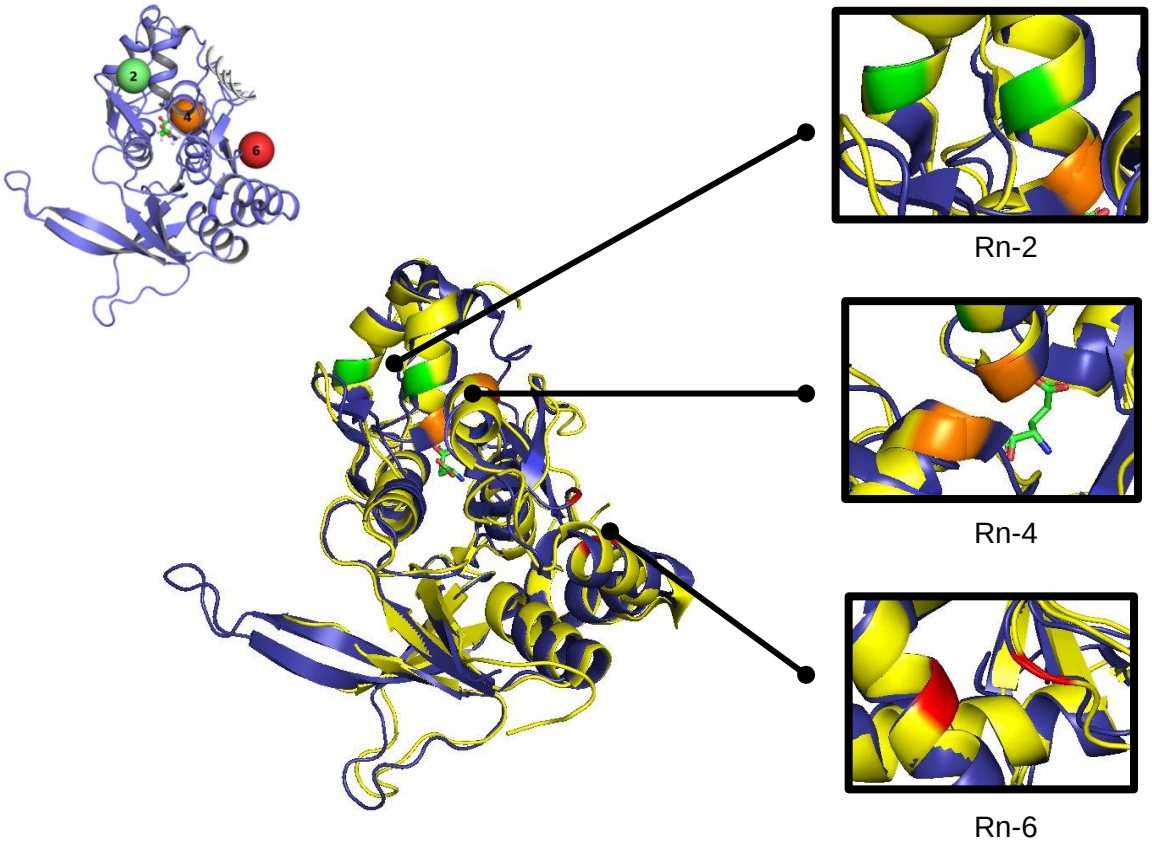

Figure 13: Alignment of NMDAR GluN2A and GluN2B. The alignment of the LBD (top view) of NMDAR GluN2A subunit (blue) (PBD: 2A5T) and the GluN2B subunit (yellow) (PBD: 5IPR) show that the three relevant structures (Rn-2 in green, Rn-4 in orange, Rn-6 in red) to form the binding sites are conserved in both subunits. The top left corner shows the initial noble gas positions as reference (see **Figure 9 B**). The right side shows the magnified sections of the GluN2A and GluN2B aligned structures. (Alignment was created with PyMOL Molecular Graphics System, Version 2.0 Schrödinger, LLC).

In order to find a suitable radon exposure time after the cells were transfected with NMDARs, immunofluorescent stainings were performed. Here, the permeabilization step of the protocol was omitted and instead an extracellular GluN1 antibody was used to investigate whether the NMDARs are located at the surface of the cells, as this is essential for a possible binding of

radon to the NMDAR LBD. In **Figure 14** exemplary immunofluorescent stainings are depicted for four different time points. Surprisingly, as soon as 12 h after transfection, the GluN1 subunit could be detected on the surface of the CHO-K1 cells. Additionally, later time points (24 h, 30 h and 40 h) after transfection were stained. While 24 h and 30 h after transfection the GluN1 subunit was clearly detectable on the surface of the CHO-K1 cells, 40 h of transfection no more intact cells were found expressing the GluN1 subunit on the surface.

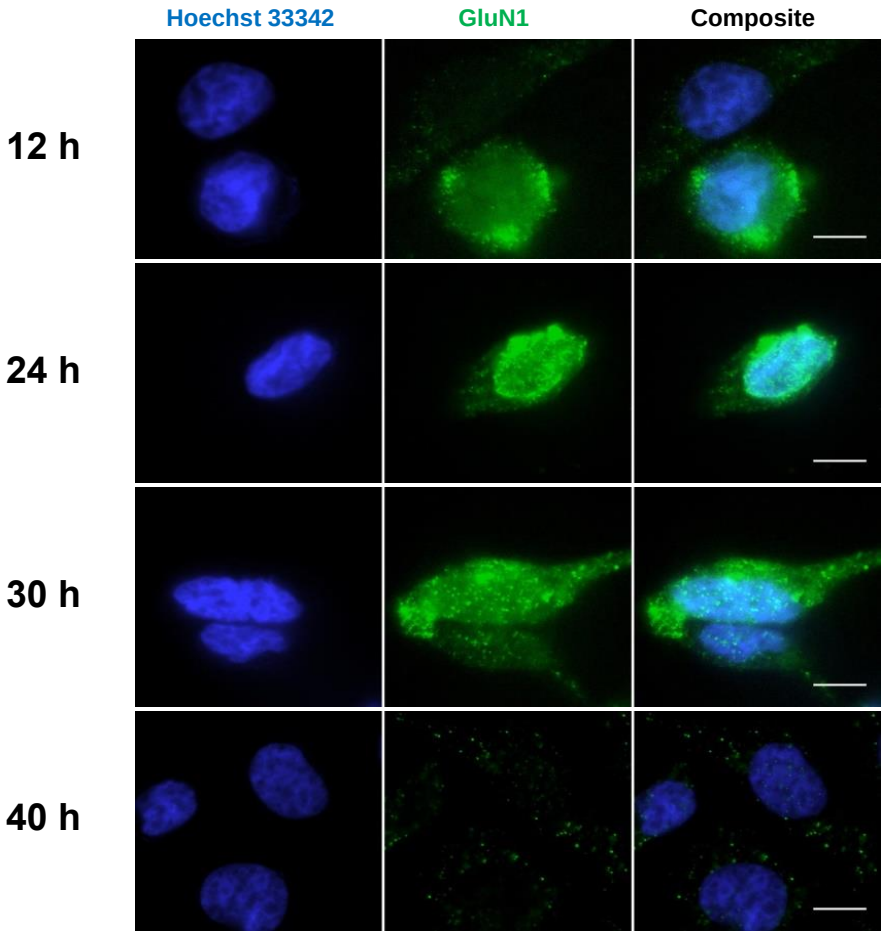

Figure 14: CHO-K1 cells show extracellular NMDAR from 12-30 h after transfection. Cells were stained without permeabilization to exclusively visualize NMDARs that are present on the surface. Blue = Hoechst 33342; Green = GLuN1; Scale bar = 10 µm

Using live-cell microscopy, the amount of transfected cells were observed over a period of 16 h. While the percentage of cells expressing eGFP initially rises from 37 % to 48 %, the cell percentage expressing eGFP decreases after 12 h of cultivation (**Figure 15**). Taken together the results of the NMDAR surface expression and the transfection efficiency, the

12 h time point after transfection was chosen to be a suitable starting point for the radon exposure for the *in vitro* radon binding assay.

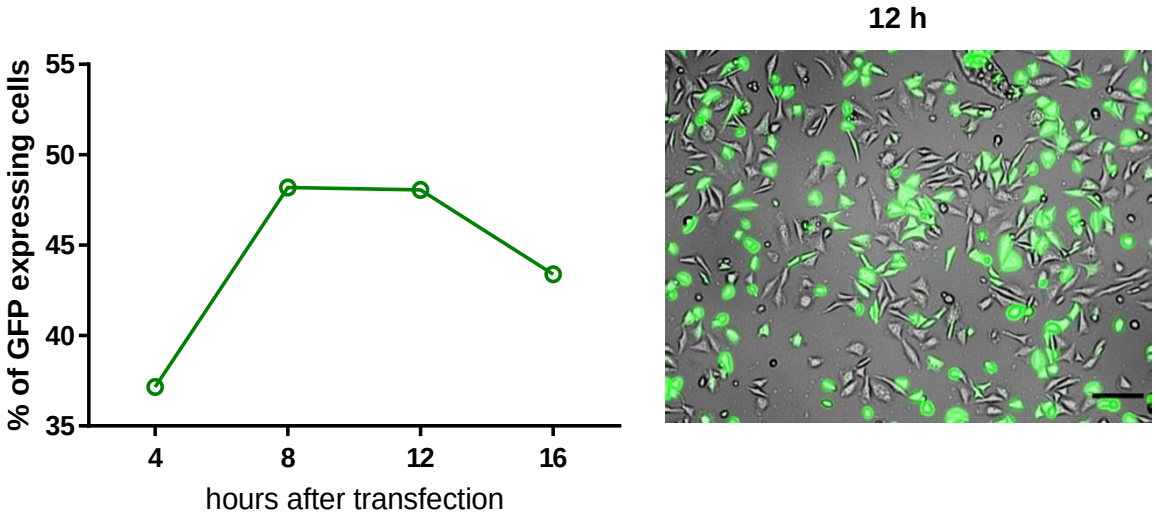

Figure 15: Transfection efficiency decreases 12 h after transfection. The expression of eGFP of transfected cells (eGFP; GluN1; GluN2B) was observed with the JuLi^{TM} Stage Real Time History Recorder. The percentage of eGFP expressing cells was calculated by manual cell counting in the recorded area. Scale bar = 50 µM.

5.1.3. Radon exposure leads to an elevated amount of DSB in cells expressing NMDARs

In order to analyze whether the NMDARs harbor potential radon binding sites, the number of 53BP1 foci in CHO-K1 cells transiently expressing NMDAR in contrast to CHO-K1 cells without NMDARs were investigated. As described above it was hypothesized that, upon binding, more radon atoms will decay in close proximity to the cell, while in contrast to non-binding events the radioactive decay occurs randomly in the whole exposure system. Due to the low range of alpha emitters, radon atoms that decay in close range to the cell will have a higher probability to damage the cell nucleus than radon atoms that randomly decay anywhere in the exposed system. Using this general approach, the DNA damage was quantified through immunofluorescent staining of 53BP1 foci after sham or radon exposure (**Figure 16 A**). The 53BP1 foci in CHO-K1 cells that were sham exposed without NMDARs show a mean number of 1.2 ± 0.13 foci/cell. CHO-K1 cells that were transfected with the NMDAR and sham exposed show a mean foci number of 1.06 ± 0.09 foci/cell. This result shows that there is no difference between the initial number of foci in CHO-K1 cells with or without NMDARs ($p = 0.719$). CHO-K1 cells without NMDARs that were exposed to 547 kBq/m^3 of radon for 1 h show a mean number of 2.07 ± 0.18 foci/cell, while cells with transiently transfected NMDARs have an increased mean foci number of 2.34 ± 0.14 foci/cell ($p < 0.0001$). This result shows that CHO-K1 cells that express NMDARs indeed obtain more

DNA damage from radon exposure than CHO-K1 cells without NMDARs. Thus, these results indicate that there is a higher probability of radon atoms decaying in close proximity to the cell, suggesting a radon binding to NMDARs. In order to further analyze the difference between the cells containing NMDARs and those not containing NMDARs the distribution of cells with no DNA DSBs in comparison to cells with a small amount of DSBs (1-3 foci/cell) and many DSBs (>3 foci/cell) was examined. In **Figure 16 B** a decrease from 60 % to 44 % of cells without DNA DSBs in CHO-K1 cells transfected with eGFP compared to CHO-K1 cells transfected with NMDARs can be observed. In contrast, the percentage of cells showing 1-3 foci/cell is elevated in cells expressing NMDARs (~30 %) in comparison to cells without NMDARs (17 %). The percentage of cells containing >3 foci/cell increases scarcely from 23 to 26 % in eGFP and NMDAR transfected cells respectively. This result shows that while there is only a scarce difference in the number of cells containing more than 3 foci, the overall number of cells with at least one DNA DSB increases and there are fewer cells without DNA damage.

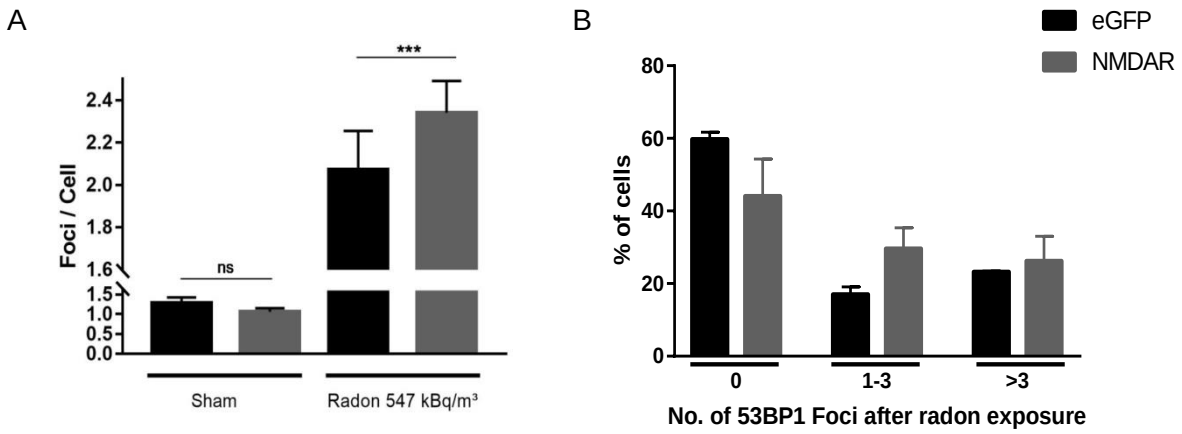

Figure 16: Radon induces more DSBs in CHO-K1 cells containing NMDARs. (A) CHO-K1 cells that were transfected with eGFP or NMDARs 12 h before exposure show no significant difference in the sham exposure (n = 2; 200 cells/n; bar graphs show the mean of all single values), while an increase after radon exposure can be detected when the cells contain NMDARs (n = 3; 200 cells/n; bar graphs show the mean of all single values) (All error bars show SEM; Kruskal-Wallis Test for statistics: $p > 0.05$ (ns), $p \leq 0.05$ (*), $p \leq 0.01$ (**), $p \leq 0.001$ (***), $p \leq 0.0001$ (****)). **(B)** Distribution of 53BP1 foci in CHO-K1 cells exposed to radon for 1 h. About 60 % of cells have no 53BP1 foci when exposed to radon and no NMDARs are expressed, while this decreases to ~45 % in cells containing NMDARs. In addition, the low number (1-3) of foci/ cell is increased in cells that contain NMDARs in comparison to cells without NMDARs (200 cells/n). (All error bars show SEM; Two-way Anova-test for statistics: $p > 0.05$ (ns), $p \leq 0.05$ (*), $p \leq 0.01$ (**), $p \leq 0.001$ (***), $p \leq 0.0001$ (****))

Assuming a linear correlation between DSB induction and physical dose of ionizing radiation, a linear regression using known x-ray doses (**Figure 17)** to estimate the delivered dose to the cells was created. Herein, the calculated average number of DSBs induced by radon exposure is equivalent to 59 mGy for CHO-K1 cells without NMDARs, while the CHO-K1 cells transiently expressing NMDARs received an equivalent dose of 88 mGy. This result

shows that cells with NMDARs receive a 47 % higher dose than CHO-K1 cells without NMDARs.

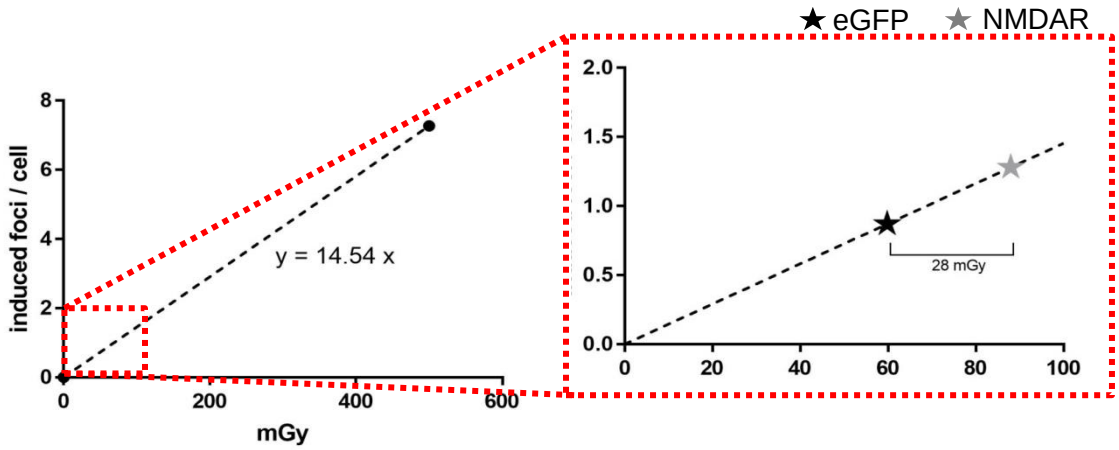

Figure 17: The dosage of radon exposed cells containing NMDARs is increased. DNA DSB induction of x-ray irradiation in CHO-K1 cells was used to define a linear regression correlation between induction of DSBs (foci/cell) and deposited dosage (mGy). The mean average number of foci/cell in eGFP transfected cells (black star) was calculated to correspond to a dose of 59 mGy while NMDAR transfected cells (grey star) yielded a 47 % higher dosage of 88 mGy (enlarged area in red rectangle).

All in all, the in vitro and in situ experimental data support the theory that radon hijacks the xenon bindings sites on the NMDAR LBD, suggesting that NMDAR-rich domains e.g. the brain could be highly affected by radon exposure.

5.2. Radon exposure leads to increased DNA double strand breaks in the dentate gyrus of mouse hippocampi

Radon exposure leads to DNA DSBs in mouse organs such as the heart and liver [137], however the induction of DNA DSBs in the mouse brain has not been investigated yet. Since radon was shown to have a higher impact on cells expressing NMDARs, radon's impact on NMDAR-rich environment like the brain is especially interesting. Therefore, brain tissue of radon and sham exposed mice was stained with the DNA DSBs marker 53BP1 in order to find out whether radon reaches the brain and hence estimate the radiation dosage of such an exposure. **Figure 18** shows representative immunofluorescent stainings of the hippocampal dentate gyrus of the exposed mice. The sham irradiated mice do not show any 53BP1 foci and thus no DNA DSBs in the depicted area, while the radon exposed sample shows one 53BP1 focus (**Figure 18 red arrow**).

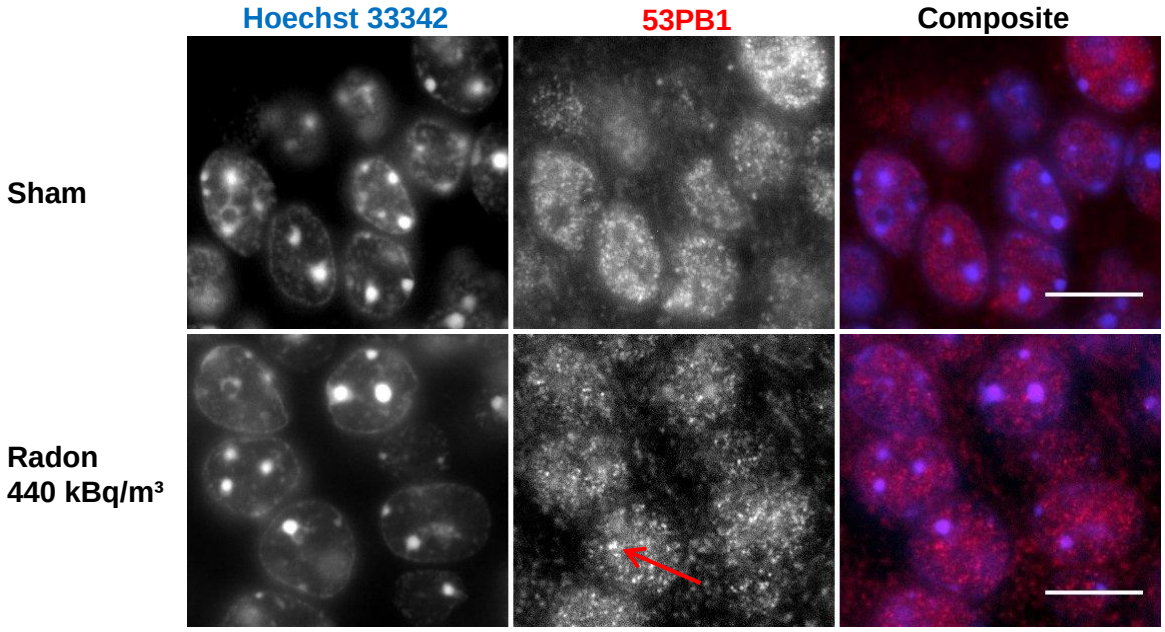

Figure 18: Representative immunofluorescent staining of hippocampal dentate gyrus tissue of radon and sham exposed mice. The cell nucleus was stained with Hoechst 33342, while DNA DSBs were visualized with the repair protein 53BP1. The red arrow indicates 53BP1 foci (Scale bar: 10 µm).

The total number of 53BP1 foci in the hippocampal dentate gyrus was manually counted for all conditions for three mice each. **Figure 19 A** shows the mean average number of 53BP1 foci/cell. The mice that were sham irradiated show a mean foci number of 0.012 ± 0.002. With a mean number of 0.023 ± 0.002 foci/cell, the tissue of radon exposed mice show a significant ($p = 0.039$) twofold increase in DNA DSBs in comparison to the sham irradiated mice. When analyzing the distribution of foci number per cell (**Figure 19 B**), it becomes apparent that the number of cells without any detected DNA DSB decreases significantly ($p=0.027$) by 1 % from 98.9 ± 0.16 % to 97.9 ± 0.35 % from sham exposed mice to radon

exposed mice respectively. The percentage of cells showing one 53BP1 foci/ cell however, increases significantly (p=0.025) by that same percentage from 0.96 ± 0.12 % to 1.95 ± 0.37 %. The percentage of cells with two foci/cell does not differ in the sham and radon exposed mice. This result indicates that the difference in foci number arises as more cells are damaged when mice are exposed to radon, rather than the same cell being hit multiple times.

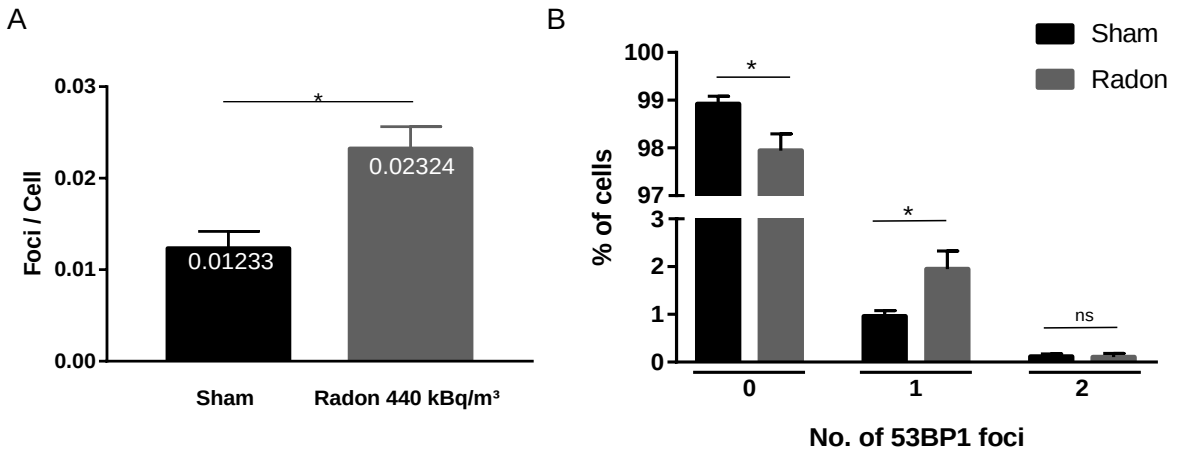

Figure 19: 53BP1 foci in mouse brain tissue after radon exposure are increased. (**A)** The mean average number of 53BP1 foci/cell in the hippocampal dentate gyrus is significantly increased after radon exposure (0.02324 foci/cell) relative to sham (0.01233 foci/cell) (> 500 cells/n; n=3). (All error bars show SEM; Kruskal-Wallis Test was used for statistics: p > 0.05 (ns), p ≤ 0.05 (*), p ≤ 0.01 (**), p ≤ 0.001 (***), p ≤ 0.0001 (****)). **(B)** The distribution of foci number in percentage shows a significant decrease in cells without DNA DSBs after radon exposure, while the percentage of cells with one foci/cell is significantly increased. (). (All error bars show SEM; Two-way Anova test was used for statistics; p > 0.05 (ns), p ≤ 0.05 (*), p ≤ 0.01 (**), p ≤ 0.001 (***), p ≤ 0.0001 (****).

Assuming a linear correlation between the number of 53BP1 foci and the radiation dosage applied, a calculation of the radiation dose emitted in the hippocampal dentate gyrus of the mouse brain was made. In **Figure 20** the linear regression graph used for this calculation is depicted. For radon exposed mice with a mean average number of 0.02324 foci/cell, the corresponding dosage yielded 2.3 mGy.

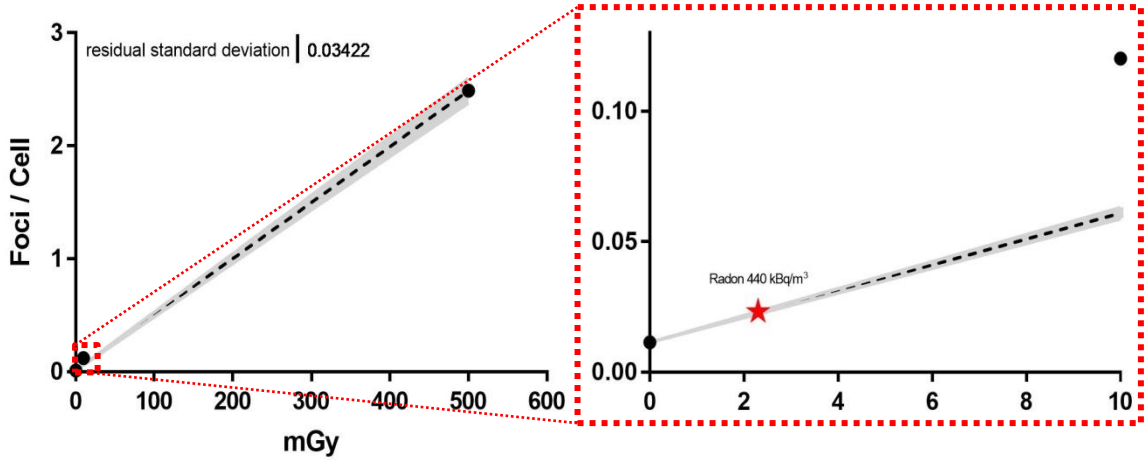

Figure 20: Radon exposure in the mouse hippocampal dentate gyrus corresponds to a dose of 2.3 mGy. DNA DSB induction by x-rays (0 mGy; 10 mGy; 500 mGy) in dentate gyrus of the hippocampus was used to define a linear regression correlation between foci induction and physical dose (mGy). The average number of DNA DSBs induced by radon exposure in dentate gyrus was interpreted as a dose of 2.3 mGy (red star in the enlarged area in the red rectangle).

In summary, the investigation of the mouse brain shows that radon exposed mice indeed show DNA damage corresponding to a calculated dose of 2.3 mGy, which corresponds to an effective low-dose of ionizing radiation that might be capable of inducing changes in the brains dynamic.

5.3. Radon exposure leads to changes in receptor distribution and protein expression

After gathering evidence that radon does have a higher impact on cells expressing NMDARs and is indeed able to directly affect the brain of mice, the next assumption was that this might affect the receptors and proteins responsible for pain sensitization in the brain. For this purpose the K/BxN serum transfer mouse model was used in further radon exposure experiments. The brain membrane fractions of radon and sham exposed K/BxN serum transfer mice were analyzed to investigate changes in the receptor distribution and protein expression.

5.3.1. Radon exposure and its effect on NMDAR GluN2B

Cortical neurons in chronic pain undergo synaptic plasticity to enhance LTP signaling [6]. This leads to postsynaptic receptor re-distribution, including the enhanced expression of NMDAR GluN2B [112]. Here, it was investigated whether radon exposure had any effect on the NMDAR GluN2B receptor subunit by analyzing the relative amount of protein in the brain. **Figure 21** shows western blots depicting NMDAR GluN2B for sham and radon exposed mice as well as a C57Bl/6 mouse internal control. The analysis of the blots show, that the mean amount of GluN2B in correlation to β-actin is 3.84 ± 1.94 AU in sham, whereas the radon exposed mice show a higher value of 6.85 ± 5.37 AU. However, this difference between the sham and radon exposed mice is not significant ($p = 0.68$) due to the high standard deviation of the data. This indicates that at least in the brain of the mice no change in the relative amount of NMDAR GluN2B can be observed.

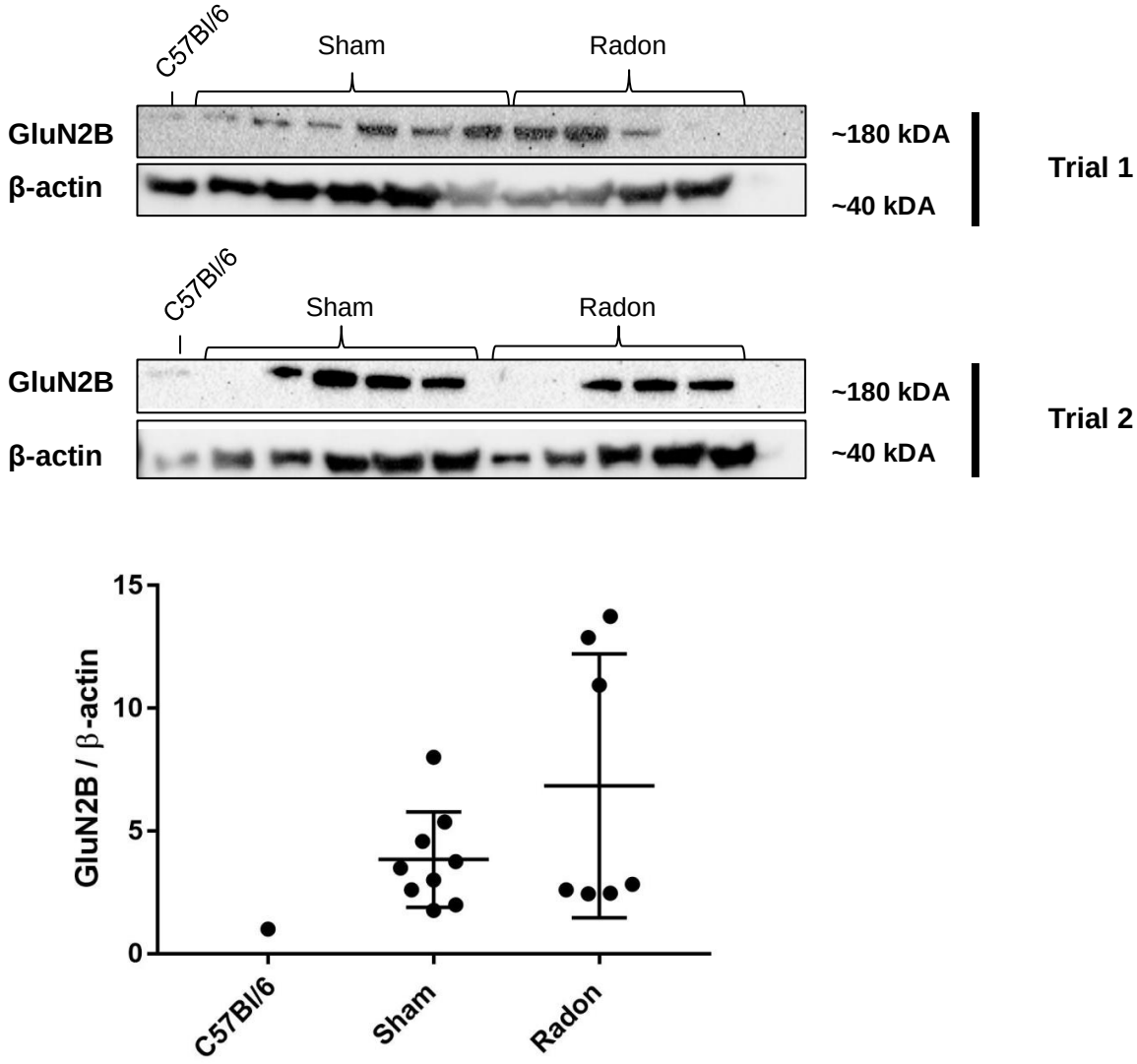

Figure 21: NMDAR GluN2B shows no difference in sham and radon exposed mice. Western blotting was performed by Dr. Bastian Roth. NMDAR GluN2B content was determined in the membrane fraction of brain homogenate. β-actin was used as a loading control. C57Bl/6 mouse was used as internal control between western blots and data was normalized to this control. Blots are shown for both Trials separately, while the graph shows all data collectively. (All error bars show SD. Mann-Whitney Test for statistics: $p > 0.05$ (ns), $p \leq 0.05$ (*)).

The phosphorylation of tyrosine (Y) 1472 of NMDAR GluN2B is associated with an enhanced activity of NMDARs and was reported in post-synaptic synapses of chronic pain mice [115]–[118]. Therefore, the phosphorylation status was also investigated in the K/BxN serum transfer mouse brain. The results in **Figure 22** show no difference in the relative amount of phosphorylated Y1472 NMDAR GluN2B ($p = 0.54$) between sham and radon treated mice. The mean value of GluN2B-pY1472 in sham treated mice is 1.93 ± 1.45 AU, while the radon exposed mice have a mean value of 1.58 ± 1.25 AU. While the relative amounts of GluN2B

and GluN2B-pY1472 do not differ for sham or radon exposed mice, this might be due to different distributions in the group of mice.

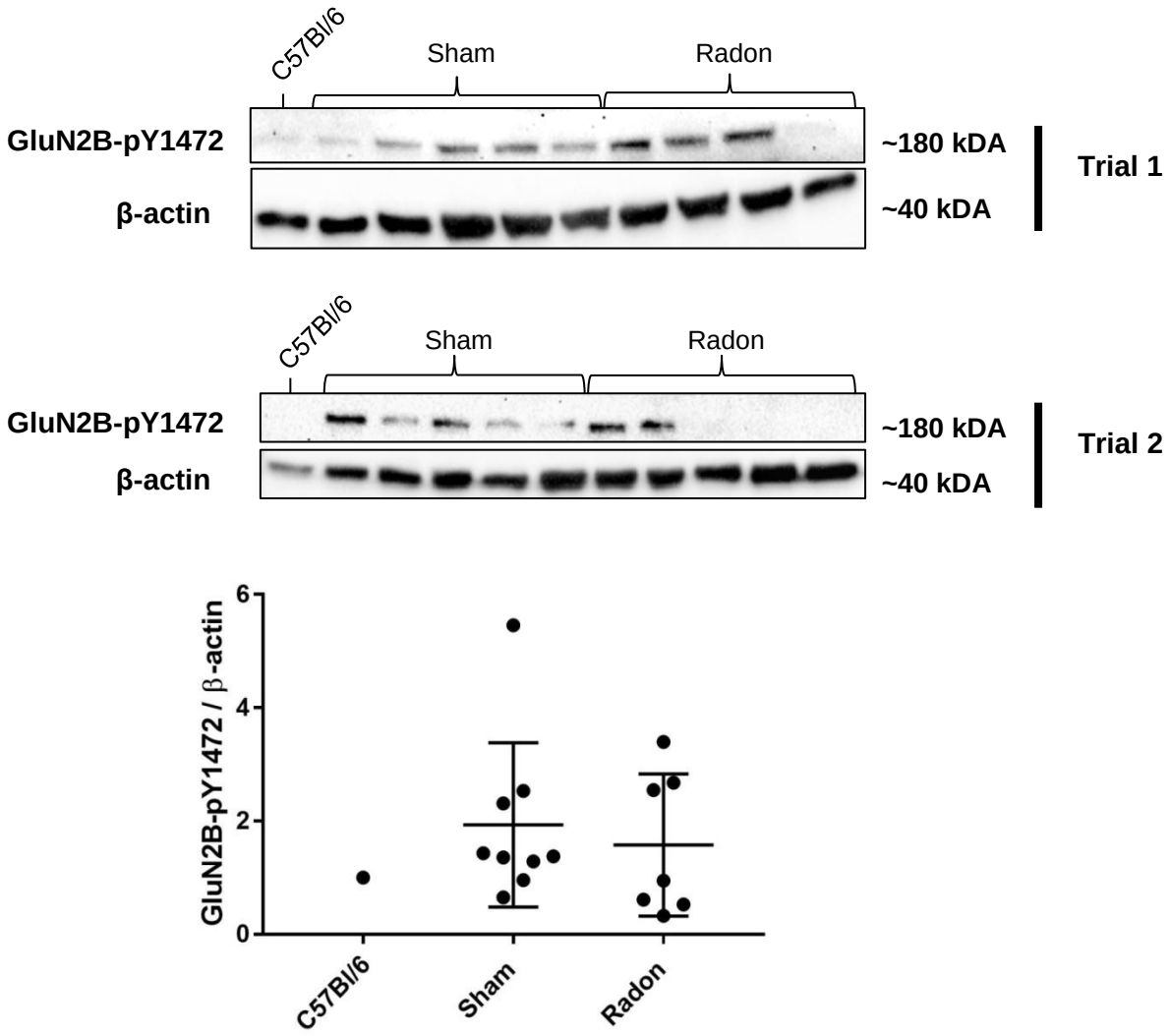

Figure 22: NMDAR GluN2B-pY1472 shows no difference in sham and radon exposed mice. Western blotting was performed by Dr. Bastian Roth. NMDAR GluN2B-pY1471 content was determined in the membrane fraction of brain homogenate. β-actin was used as a loading control. C57Bl/6 mouse was used as internal control between western blots and data was normalized to this control. Blots are shown for both Trials separately, while the graph shows all data collectively. (All error bars show SD; Mann-Whitney Test for statistics: $p > 0.05$ (ns), $p \leq 0.05$ (*)).

During pain sensitization however, the ratio of GluN2B-pY1472 to total GluN2B is enhanced. Thus, it was of particular interest to examine the relative ratio of phosphorylated Y1472 GluN2B to total GluN2B for each mouse individually in order to investigate if radon exposure alters this ratio. Interestingly, **Figure 23** shows that the ratio of NMDAR GluN2B-pY1472 to total NMDAR GluN2B does decrease from 0.53 ± 0.27 AU in sham exposed mice to 0.23 ±0.08 AU in radon exposed mice. Statistical analysis of this data shows that this decrease is

significant with p = 0.016. This result reveals that the percentage of phosphorylated Y1472 GluN2B to total GluN2B is indeed affected by radon exposure.

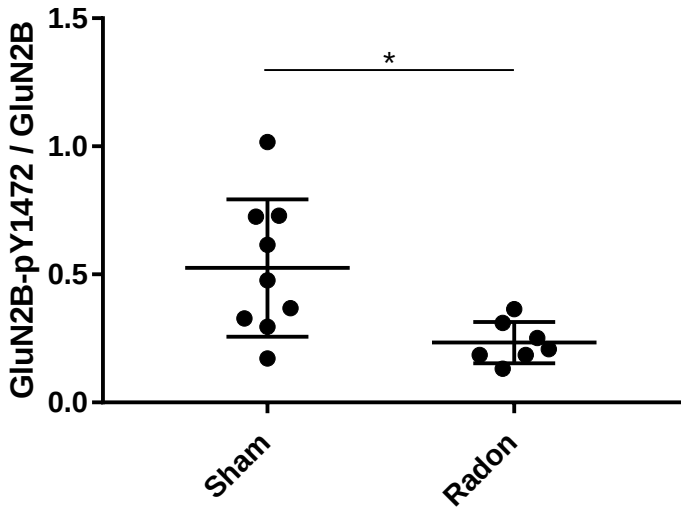

Figure 23: The ratio of GluN2B-pY1472 to GluN2B decreases significantly after radon exposure. Western blotting was performed by Dr. Bastian Roth. NMDAR GluN2B-pY1471 in ratio to total NMDAR GluN2B content for each mouse individually was determined in the membrane fraction of brain homogenate. β-actin was used as a loading control. C57Bl/6 mouse was used as internal control between western blots and data was normalized to this control. (All error bars show SD; Mann-Whitney Test for statistics: $p > 0.05$ (ns), $p \leq 0.05$ (*)).

5.3.2. Radon exposure and its effect on proteins downstream Ca^{2+} signaling

NMDAR-dependent LTP is associated with downstream incorporation of AMPAR GluA1 as well as an up-regulated expression of the immediate early gene c-fos [109], [111], [114]. Hence, it was investigated whether the relative amount of AMPAR GluA1 and the relative amount of Fos protein were altered after radon exposure. The results for the amount of AMPAR GluA1 depicted in **Figure 24** show a minimal decrease from 1.28 ± 0.69 AU in sham treated mice to 1.08 ± 0.44 AU in radon treated mice. However, this decrease is not statistically significant with p = 0.92.

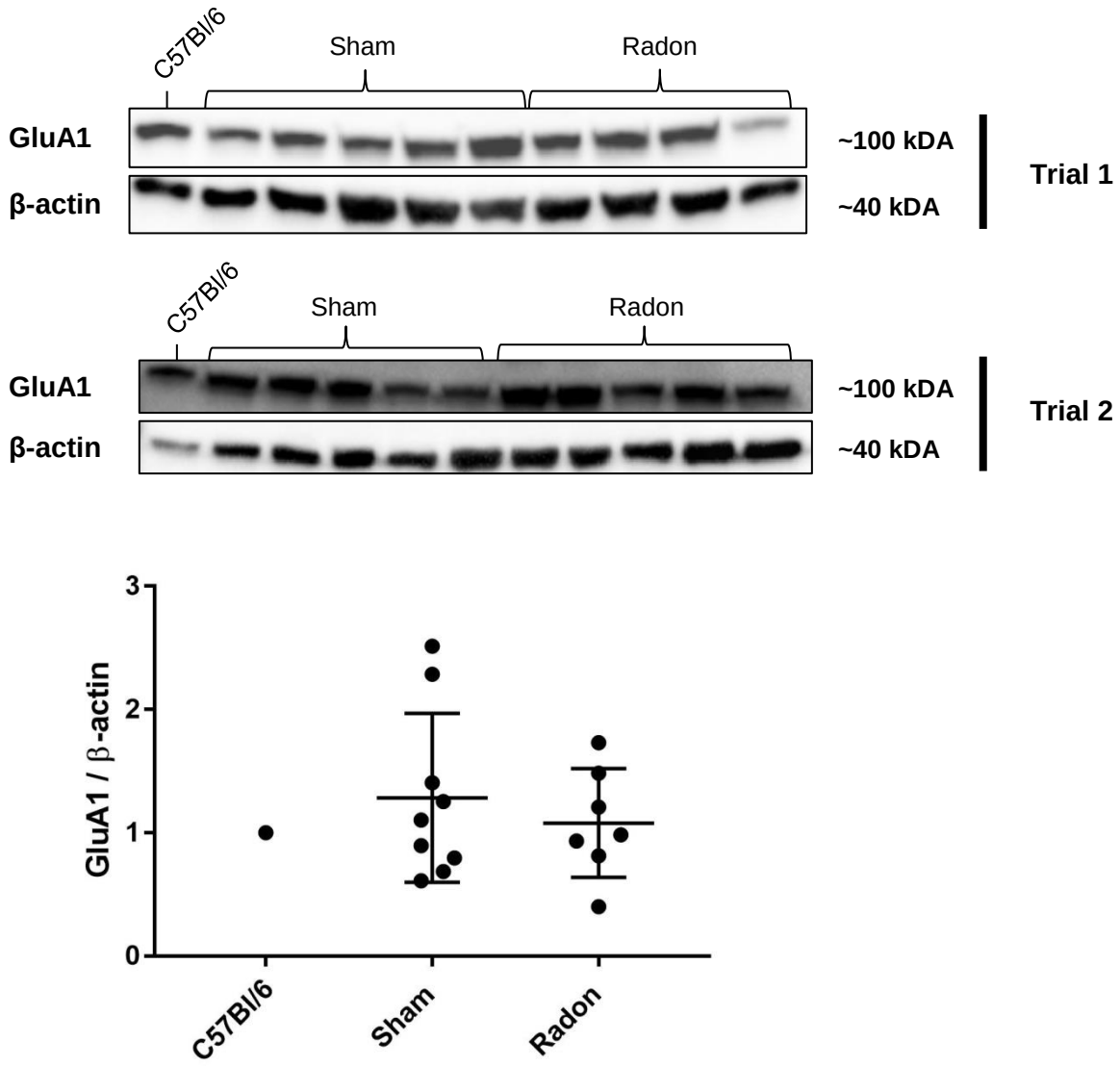

Figure 24: AMPAR GluA1 shows no difference in sham and radon exposed mice. Western blotting was performed by Dr. Bastian Roth. AMPAR GluA1 content was determined in the membrane fraction of brain homogenate. β-actin was used as a loading control. C57Bl/6 mouse was used as internal control between western blots and data was normalized to this control. Blots are shown for both Trials separately, while the graph shows all data collectively. (All error bars show SD; Mann-Whitney Test for statistics: $p > 0.05$ (ns), $p \leq 0.05$ (*)).

Next, the amount of Fos after radon exposure was examined (**Figure 25**). Here, the amount of Fos increases slightly from 0.75 ± 0.17 AU to 0.88 ± 0.22 AU from sham exposed mice to radon exposed mice. The statistical analysis reveals that this increase in the relative amount of Fos is not significant ($p = 0.25$) and thus cannot be interpreted as altered after radon exposure.

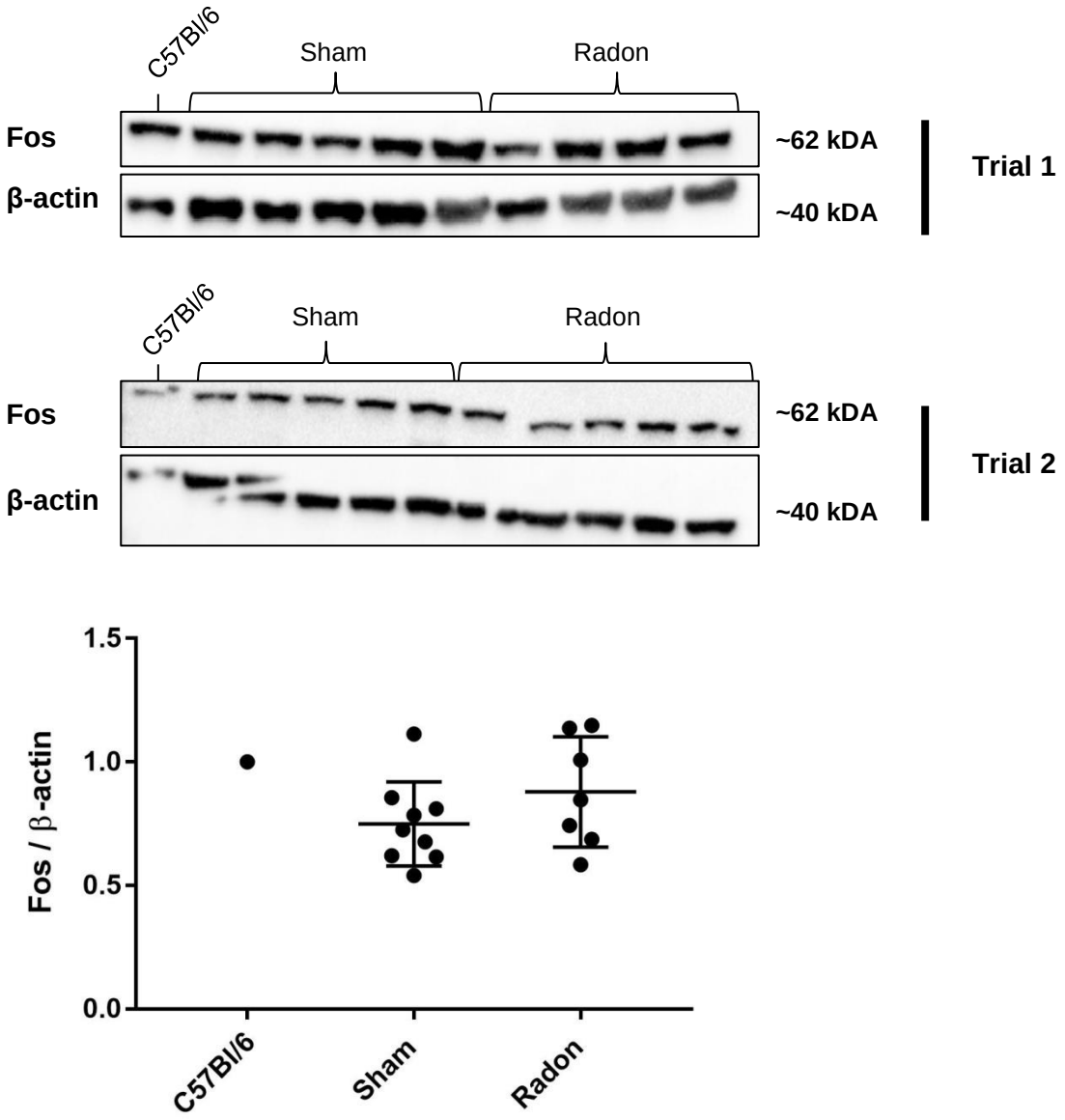

Figure 25: Fos shows no difference in sham and radon exposed mice. Western blotting was performed by Dr. Bastian Roth. Fos content was determined by in the membrane fraction of brain homogenate. β-actin was used as a loading control. C57Bl/6 mouse was used as internal control between western blots and data was normalized to this control. Blots are shown for both Trials separately, while the graph shows all data collectively. (All error bars show SD; Mann-Whitney Test for statistics: $p > 0.05$ (ns), $p \leq 0.05$ (*)).

5.3.3. Effect of radon on PKC-α

While the pain relief after radon exposure might rely on weakened LTP signaling, it is also possible that it affects LTD. In the ACC, LTD is reported to be NMDAR-dependent, which relies on the internalization of AMPAR to prevent pre-depolarization and the removal of the Mg^{2+} blockade of NMDARs. This internalization of AMPAR is achieved by phosphorylation of the AMPAR GluA2 subunit. The PKC-α has been reported to phosphorylate the GluA2, thereby enhancing LTD signaling in the brain [125], [126]. Thus, the amount of PKC-α in the

membrane fraction of mouse brains was examined after radon exposure. The result, depicted in **Figure 26**, shows that the amount of PKC-α in the membrane increases significantly ($p = 0.016$) from 1.37 ± 0.86 AU in sham exposed mice to 2.11 ± 0.4 AU in radon exposed mice.

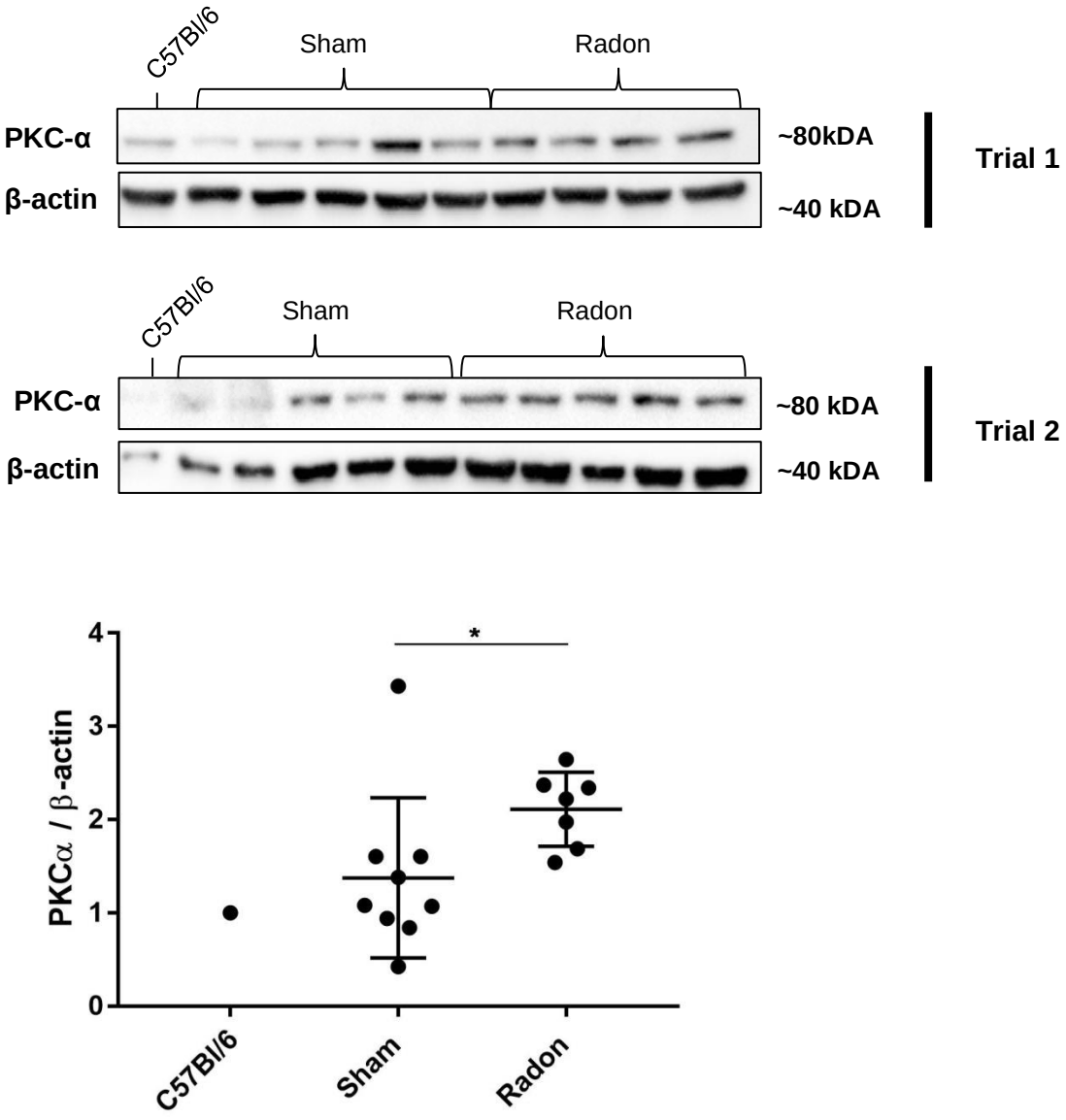

Figure 26: PKC-α is significantly increased after radon exposure. Western blotting was performed by Dr. Bastian Roth. PKC-content was determined by in the membrane fraction of brain homogenate. β-actin was used as a loading control. C57Bl/6 mouse was used as internal control between western blots and data was normalized to this control. Blots are shown for both Trials separately, while the graph shows all data collectively. (All error bars show SD; Mann-Whitney Test for statistics: $p > 0.05$ (ns), $p \leq 0.05$ (*)).

In summary, the investigation of protein re-distribution in mice brain revealed that the ratio of phosphorylated NMDAR GluN2B at Y1472 to total NMDAR GluN2B is significantly decreased in radon exposed mice compared to their sham exposed control. Additionally, the amount of PKC-α in mouse brain is significantly increased after radon exposure.

6. Discussion

Although radon therapy goes along with a significant risk of developing lung cancer [7], many patients voluntarily undergo this form of therapy to reduce their chronic pain [9]. Unfortunately, the molecular working mechanism of pain alleviation after radon therapy remains unknown. Chronic pain does not only affect the periphery, but induces central changes in the brain as well [67]. For instance, post-synaptic LTP is saturated, while LTD is suppressed in the ACC in chronic pain models [67]. In this doctoral thesis, it was hypothesized that radon therapy acts on the neurosensory system by affecting synaptic changes in the brain, thereby exhibiting its pain alleviation effect.

6.1. Radon occupies xenon binding sites at NMDAR LBD

As described in chapter 3.3.1, xenon and radon have similar physical properties and thus are able to occupy the same molecular structures in simulations [44]. As xenon's use as anesthetic is based on binding to NMDARs [38], [39], this mechanism is especially interesting as a possible mode of action for radon as well. Therefore, the potential binding of radon to NMDARs was investigated by molecular dynamics simulations (**Figure 10**). The simulation of the initial noble gas positions for xenon [39], were reproduced with radon for a GluN1/GluN2A ligand binding domain. The results show that three of these binding positions showed an even better binding energy for radon than for xenon (**Table 7**). Interestingly, those positions were located within a helix-turn-helix motif of the GluN2A subunit (Rn-2) next to the glutamate binding site (Rn-4) and located at the GluN1/GluN2A interface (Rn-6). Given that on the one hand xenon binding leads to a weakened glutamate binding which could correspond to the Xe/Rn-4 binding position, it is possible that radon also weakens glutamate binding. On the other hand, binding positions Xe/Rn-2 and Xe/Rn-6 could be responsible for a rearrangement of the channel towards a closed or desensitized state. This result therefore suggests that radon is not only able to bind at the same positions as xenon on the NMDAR LBD but might also exhibit the same anesthetic effect. Taking the Meyer-Overton correlation for inert gases into account (**Figure 1**), radon is theoretically predicted to permit general anesthesia with a lower pressure, given it has the highest oil/gas coefficient of the noble gases. The higher binding energy calculated for radon binding positions 2, 4 and 6 are in good accordance with this prediction. This result is the first evidence that radon might act as an inhibitor on NMDARs in the same way xenon does. The analgesic effect of xenon is attributed to both its competitive and non-competitive inhibition of NMDARs [39], [140], which radon might mimic. Interestingly, the need for post-operative opioids was shown to be reduced by one third over a time period of 72 h after xenon anesthesia, indicating that xenon-related analgesic effect is still active after xenon has been washed out of the body [141].

Furthermore, xenon is able to suppress enhanced responsiveness to pain after repeated painful stimulation at sub-anesthetic doses, indicating that it is able to decrease LTP-related synaptic plasticity in the human brain by inhibition of NMDARs [42] and that xenon thereby enables prolonged analgesia in comparison to sevofluorane. Since radon was shown to bind at the same binding sites, the potency of radon as NMDAR antagonist should not be neglected. It is conceivable that radon induces changes in pain sensitization by inhibiting the NMDAR mediated response, just like xenon, and thus contributes to pain relief after radon inhalation.

Despite this very promising, *in silico* result, it was very important to pursue this hypothesis of a radon binding to NDMARs *in vitro*. The establishment of a suited *in vitro* radon binding assay, however, posed several challenges due to radon being a radioactive gas emitting highly dangerous α-radiation and being poorly soluble in aqueous solutions. Therefore, an indirect binding verification was pursued by utilizing DNA DSBs. Exploiting the low range of α-radiation and assuming that radon binds to NMDARs, its decay would take place in close proximity to the nucleus thereby inducing DNA DSBs, which can be detected by immunofluorescent staining of 53BP1. In a cell system without NMDARs, radon atoms would decay randomly in the whole exposure system, making it less likely that the α-radiation would reach the nucleus (Scheme shown in **Figure 11**). Due to the low number of initial DNA DSBs in healthy cells, CHO-K1 cells were chosen as a suitable cell system. Next, the poor solubility of radon in aqueous solution was approached. Therefore, an air-liquid interface cultivation system was used during radon exposure (**Figure 12 B left)**. Using this cultivation system during radon exposure allowed radon to freely diffuse on top of the cells, thus increasing the radon exposure for the cells. While the cultivation conditions did not have any effect on the number of DNA DSBs in CHO-K1 cells, the number of DNA DSBs after radon exposure greatly increased using air-liquid interface cultivation compared to the cultivation of cells on glass slides (**Figure 12 B right)**. This difference in 53BP1 foci can be explained as radon gas does not diffuse well into the media. However, this diffusion is required for exposure of CHO-K1 cells cultivated on glass slides. In contrast to the glass slides, the air-liquid interface bypasses this problem, as the media required to nourish the cells during radon exposure is delivered from underneath the cell through a porous membrane, while radon can freely diffuse on top of the cells through the air. While the MD simulations were performed with the NMDAR GluN1/GluN2A LBD, for chronic pain models especially the expression of NMDAR GluN2B subunit is increased [112]. Using an alignment of the GluN2A LBD (PBD: 2A5T) and the GluN2B LBD (PBD: 5IPR), the identified molecular structures relevant for the binding positions Rn-2, Rn-4 and Rn-6 were compared (**Figure 13**). Both subunits show identical molecular structures and were therefore deemed as interchangeable. This is further

supported by the fact that 80 % of xenon inhibits NMDAR GluN1/GluN2A and GluN1/GluN2B receptors to the same degree [38]. Consequently, the NMDAR GluN1/GluN2B subunit combination was considered of higher relevance in prospect of the synaptic changes concerning pain perception. The optimal transfection time with NMDARs was determined by immunofluorescent staining (**Figure 14**). Here, it was only of interest at what time point the NMDARs would reach the surface of the cell, as it was assumed that this is enough for a potential binding of radon to the LBD of the receptor. Giving that the cells are proliferating, and thus with time the number of transiently transfected cells decreases in dependence to cell division (**Figure 15**), the earliest time point where NMDARs were detectable on the surface which was 12 h after transfection was determined as optimal for the radon binding assay. In sum, the establishment of a radon binding assay by assessing 53BP1 foci resulted in the following exposure conditions: CHO-K1 cells were cultivated on a porous membrane for 12 h after transfecting NMDARs and were then exposed to radon for 1 h in an air-liquid interface manner before being used for immunofluorescent staining of 53BP1 to assess radon binding by analyzing the induced DNA DSBs.

After determining the best radon exposure conditions for investigating a possible radon binding to NDMARs, the actual experiment revealed a significant difference ($p \leq 0.001$) in induced DNA DSBs between cells transiently transfected with NMDARs (2.34 foci/cell) and cells without transfected NMDARs (2.07 foci/cell) (**Figure 16 A**). As only transfected cells were analyzed in this experiment, it provides strong evidence that the additional NMDARs on the surface of the cells are causing more radon atoms to decay in close proximity inducing DNA DSBs. When analyzing the distribution of 53BP1 foci number per cell, it is instantly noticeable that especially the amount of cells without any focus decrease by 16 %, while the percentage of cells with 1-3 foci per cell increase by about that same percentage. This result shows that a higher percentage of cells are hit by α-radiation emitted by radon atoms than before, providing more evidence that radon binds to NMDARs on the cell's surface before decaying rather than decaying randomly within the whole exposure system. Lastly, when assuming a linear correlation between 53BP1 induction and deposited radiation dose, an increase in dose deposition of 47 % was calculated in cells containing NMDARs (**Figure 17)**. Taken together, the result of the in vitro radon binding assay provides strong evidence that radon indeed accumulates at NMDAR containing cells and depositing a higher radiation dose at these specific sites. This does not only suggest that radon exhibits its value to pain relief by a mode of action similarly to xenon, but also gives rise to the hypothesis that directly deposited α-radiation at NMDAR rich sites e.g. in the brain could play an important role in the pain relief of radon therapy. This suggests that radon could have a unique double-sided

function in the alleviation of chronic pain: (i) binding to NMDARs thereby inhibiting LTP-related synaptic plasticity and (ii) low-dose radiation at specific target sites.

6.2. Detection of radon induced damage in the brain

After gathering evidence that radon binds to NMDARs, the presence of radon in the brain, which presents a NMDAR rich environment, was indirectly validated by analyzing the amount of DNA DSBs in the hippocampal dentate gyrus of radon exposed mice (**Figure 19**). High-LET (linear-energy transfer) radiation such as α-radiation, which is emitted as radon-222 decays, results in very localized DNA damage [142]–[144]. Compared to low-LET, high-LET induces fewer but larger DNA DSB 53BP1 foci, suggesting multiple DSBs in one focus [145]. In a previous thesis, the amount of DNA DSBs after radon exposure was analyzed in various other organs, such as lung, heart and liver [137]. Here, the amount of DNA DSBs in the dentate gyrus of mouse hippocampi was analyzed as representative for the brain, as the cells can be clearly distinguished and counted accordingly. The dentate gyrus of mouse hippocampus shows a lower number of 53BP1 foci after radon exposure of 0.02 foci/cell (**Figure 19 A**) compared to the lung (0.14 foci/cell) or heart (0.08 foci/cell) [137]. When assuming a linear correlation between foci induction and deposited radiation dose, an average corresponding dosage of 2.3 mGy was calculated after radon exposure (**Figure 20)**. Although, while high-LET is known to induce so-called α-tracks [144], no such tracks could be observed in the dentate gyrus of radon exposed mice. **Figure 19 B** shows that especially the number of cells hit once increases significantly by 1 percentage point while the percentage of undamaged cells decreases significantly by 1 percentage point. It is quite possible that due to the much localized energy deposition and thus close proximity of DNA DSBs, multiple foci were counted as one focus, which is a known source of error when quantifying α-radiation induced DNA DSB foci. Therefore, it should be noted that because it is likely that multiple DNA DSBs were interpreted as one focus the actual amount of DNA DSBs in the dentate gyrus was probably underestimated, suggesting that the actual dosage is even higher than 2.3 mGy in the brain. Nevertheless, the results show that inhaled radon is indeed affecting the brain just like other organs such as heart and liver, which is in good accordance with previous literature [146]–[149]. Additionally, long-term exposure to residential radon is associated to brain cancer [150], [151] and neurodegenerative diseases such as multiple sclerosis and Alzheimer's disease [152], further confirming that radon inhalation directly affects the brain. While high-dose IR is associated with tumor development, the effect of low-dose irradiation is less certain. In human neural progenitor cells, irradiation dosages of 31 mGy over a time period of 72 h showed altered gene expression of inflammatory pathways involving interferon signaling [153]. Also, in female rats

the irradiation dose of 1.15 mGy showed a decreased expression for genes of calcium signaling pathway in the prefrontal cortex amongst others [154]. Both these examples emphasize that low-dose irradiation by radon inhalation may alter gene expression in the brain thereby affecting synaptic plasticity and exhibiting a pain relieving effect.

6.3. Radon inhalation induces changes in synaptic protein distribution that could lead to pain relief

To address the question what effect inhibition of NMDAR and/or deposition of targeted α-radiation has on pain processing, the relative amount of several proteins in the brain of K/BxN serum transfer mice was analyzed. It should be noted that the K/BxN serum transfer mice are a multifaceted model of pain mechanisms as it exerts two different pain states. While during inflammation the K/BxN serum transfer mice respond to NDSAIDs, this sensitivity is lost in a post-inflammatory state where only gabapentin was able to exert a pain-relieving effect [133]. This model therefore matches human arthritic conditions very well and is especially interesting, as patients suffering from rheumatoid arthritis continue to report ongoing pain despite a resolution of clinical signs of arthritis [155] which could correspond to the post-inflammatory state in the K/BxN serum transfer model. Traditionally, the spinal dorsal horn and periphery were the main targets for pain therapy. However, recent data suggests that when central changes occur in the brain after injury or inflammation, it is too late to interfere with the periphery [94]. Synaptic plasticity in the brain thus may be the cause of persisting pain after the acute inflammation, and this is exactly where radon therapy is applied to achieve pain alleviation. Therefore, the changes in protein level in the brain after radon therapy were of particular interest in order to shed some light on a possible mode of action of radon exposure. Since the previous results of this thesis show that radon has a binding affinity for NMDARs, this was also the first protein closely investigated. In chronic pain models, NMDAR GluN2B is upregulated in the brain, thus leading to hypersensitivity through enhanced LTP and blocking NMDAR mediated responses reduces behavioral sensitization [112]. Additionally, in the dorsal horn neurons, the blockade of NMDARs with tramadol significantly reduced GluN2B expression as well as the phosphorylation state of GluN2B at Y1472, achieving pain alleviation [156]. In this study, the relative amount of NMDAR GluN2B and its phosphorylated Y1472 state in the brain was investigated in radon and sham exposed mice (**Figure 21**; **Figure 22**). However, the standard deviation of NMDAR GluN2B level of the K/BxN serum transfer mice was high, especially for the mice exposed with radon. Thus, the amount of GluN2B after radon exposure in the brain could neither be described as increasing nor decreasing. Additionally, the phosphorylated Y1472 GluN2B showed no significant difference between mice that were exposed to sham or radon

exposure. Even though, the average relative amount of GluN2B and GluN2B-pY1472 did not change, the ratio of GluN2B to GluN2B-pY1472 for each mouse individually shows a significant reduction (p=0.016) of phosphorylated Y1472 GluN2B in radon exposed mice compared to sham exposed mice (**Figure 23**). This result indeed suggests that radon might counteract enhanced NMDAR transmission by reducing the phosphorylation of Y1472 of NMDAR GluN2B and thus impeding in LTP maintenance. The phosphorylation of Y1472 GluN2B is mediated by SRC-family kinases such as Fyn [115]–[118] which is again regulated by NMDAR activation [157]. Therefore, the results indicate that inhibition of NMDARs by radon itself could lead to a reduced GluN2B-pY1472 level, which disrupts LTP and contributes to pain alleviation. As described in chapter 3.5.2 a saturated LTP induces c-fos expression as well as recruitment of homomeric AMPA GluA1 receptors downstream of NMDAR mediated Ca^{2+} signaling [107], [114]. In this thesis, however, neither Fos nor AMPAR GluA1 was increased after radon exposure (**Figure 24**, **Figure 25**). C-fos is only transiently expressed after stimulation as its expression is autorepressed by the Fos protein [158] and therefore the level of Fos might have been reduced immediately after radon exposure. However since the brain extraction was performed seven days after radon treatment, this time point might have been simply too late to observe any significant changes in Fos level. Although AMPAR GluA1 is rapidly recruited to the synapse, it is then replaced by GluA2/3 leading to an increase in synaptic LTP [159]. This indicates that a decrease in AMPAR GluA1 would occur in both, sham exposed mice due to AMPAR GluA1 replacement with AMPAR GluA2/3 and radon exposed mice due to inhibition of NMDARs and thus a lower recruitment of AMPAR GluA1 in the first place. As for Fos, an earlier time point might have shown a more distinct result, as the replacement of GluA1 to GluA2/3 in the sham mice might have not been as advanced. Nonetheless, both outcomes (protein level of Fos and AMPAR GluA1) do not discredit the hypothesis of an NMDAR inhibition by radon. Finally, as chronic pain does not only involve saturated LTP, but also suppressed LTD [67], the amount of PKC-α was investigated in the brain after radon exposure. Interestingly, PKC-α was found to be significantly (p=0.016) upregulated after radon exposure compared to sham exposed mice (**Figure 26**). PKC-α has contrary functions in different tissues. While PKC-α inhibition in dorsal horn neurons is responsible for pain relief [160], it is associated with AMPAR GluA2 phosphorylation and consequent AMPAR internalization leading to LTD in the brain [126], [161]. In this thesis, since the level of PKC-α was investigated in the brain, its upregulation suggests a restoration of suppressed LTD, possibly by internalization of AMPARs. In other studies, PKC activation was quite similarly able to rescue LTD in ACC after total loss of LTD, although it should be noted that in this study both PKC-α and/or β could have been responsible for the rescuing effect [162]. Additionally, the restoration of long-term depression is associated with alleviation of pain hypersensitivity [129], [163]. However, it remains unclear

how the inhibition of NMDARs by radon should induce the activation of PKC-α. But, as suggested before, radon might play a dual role by inhibiting the NMDARs on the one hand and by emitting IR among decay at specific target sites on the other hand. Low-dose IR rapidly activates the neuroimmune system and was shown to increase TNF-α expression in the brain [164]. Additionally, the physical induction of TNF-α expression was shown to be induced by NFκB (nuclear factor kappa B) [165], which was shown to be significantly increased in the brain of radon exposed mice (0.5 or 2 kBq/m³ for 24 h) [166]. Therefore, it is conceivable that radon exposure activates NFκB by causing DNA damage and oxidative stress and NFκB in turn induces TNF-α expression. Interestingly, a TNF-α induced signaling pathway has been demonstrated to induce the translocation of PKC-α from the cytosol to the membrane in bystander cells as a consequence of α-radiation [167]. Putting these pieces together, it seems possible that radon exposure emits low-dose irradiation in the brain which induces DNA damage and oxidative stress and subsequently causes the activation of NFκB. NFκB induces TNF-α expression which causes the activation of PKC-α in bystander cells, leading to an increased internalization of AMPAR GluA2, consequently contributing to pain alleviation by restoration of LTD. It should be noted that, excessive bioavailability of TNF-α disrupts the integrity of human blood-brain barrier through excessive activation of PKC-α [168] however, “the dose makes the poison“ and thus the little amount of irradiation caused by radon might be more beneficial than harmful in this case.

7. Conclusion

The results presented in this work show that that radon is indeed capable to hijack NMDAR binding sites similar to xenon in MD simulations and in vitro through an increase of DNA damage caused by radon at NMDAR expressing cells. Additionally, it was shown that radon inhalation reaches the brain and causes tissue damage to a similar degree as heart or liver [137]. Based on the findings that the ratio of NMDAR pY1472 GluN2B to overall NMDAR GluN2B is significantly decreased and the activity of PKC-α is significantly increased in radon exposed mice, the following hypothesis on the molecular mechanism underlying pain alleviation after radon exposure arose (**Figure 27**).

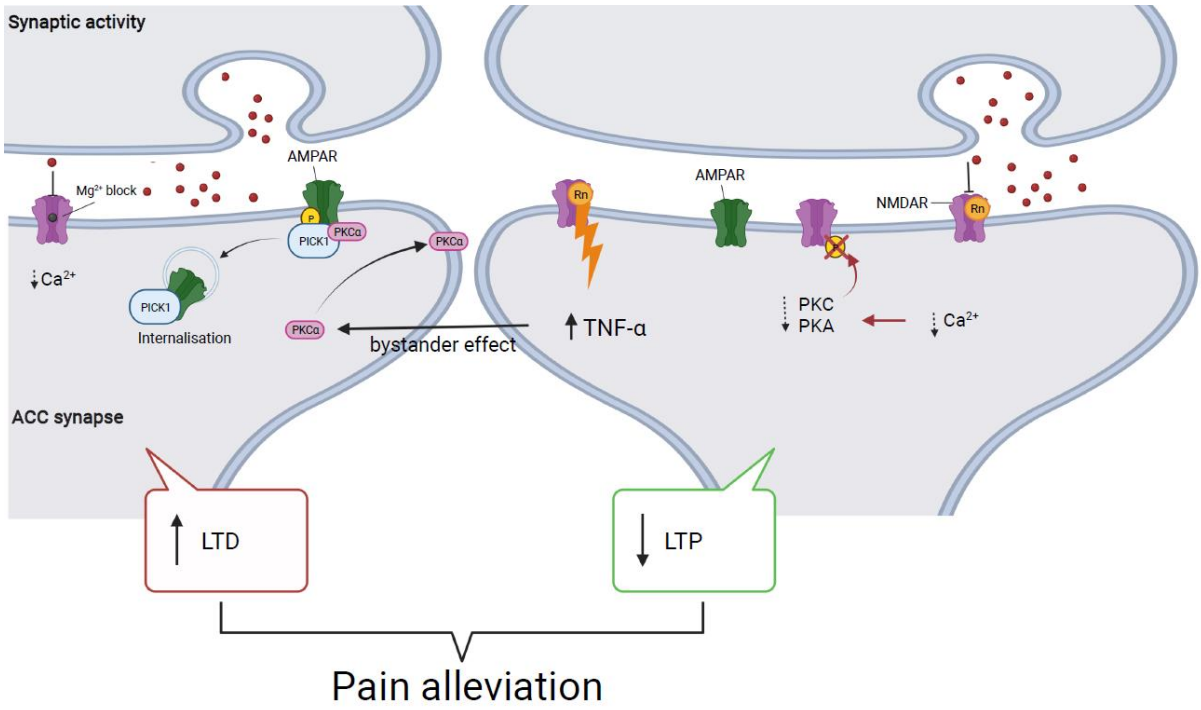

Figure 27: Schematic model of hypothetical molecular mechanism of radon therapy to alleviate chronic pain. Radon binds to NMDARs thereby inhibiting the NMDAR mediated Ca^{2+} influx. Consequently, phosphorylation of NMDAR Y1471 GluN2B is impaired leading to a reduction of LTP. Additionally, radon preferentially decays within close proximity of the post-synapse due to a high level of NMDARs leading to an increase in TNF-α in directly hit cells. This triggers translocation of PKC-α from the cytosol to the membrane in bystander cells. The PKC-α activity leads to the internalization of AMPARs by phosphorylation of S880 and binding of PICK1. The lowered amount of AMPAR in the synapse impairs the removal of Mg^{2+} block from NMDARs and consequently a decrease in Ca^{2+} influx, thereby restoring LTD expression. Figure was created with BioRender.com.

Radon atoms are capable of binding NMDARs at various sites within the receptor, which might inhibit the NMDAR mediated response similarly to xenon [38], [39]. This inhibition leads to a lowered Ca^{2+} influx. Therefore, there is no activating CaM and NOS to phosphorylate Y1472 at NMDA GluN2B receptors and preventing the maintenance of LTP. While the inhibition of NMDARs is preventing the phosphorylation on the one hand, the

decay of radon emits α-particles which induce TNF-α release in directly hit cells. TNF-α then mediates the translocation of PKC-α from the cytosol into the membrane in bystander cells, thereby activating PKC-α [167]. PKC-α is known to interact with PICK1, which then binds to AMPAR GluA2 subunit. The phosphorylation of S880 and the PICK1 association leads to an internalization of AMPAR with an increased retention in the cytosol. By decreasing the amount of AMPARs in a heterosynaptic fashion, even when the radon inhibition of NMDARs wears off, the required pre-depolarization to remove the Mg^{2+} block from all NMDARs is not given anymore and thus LTP expression is suppressed on the one hand and LTD is restored on the other hand. While this mechanism might be less relevant in other tissues, in the brain which undergoes central changes in response to chronic inflammation [67], this dual function of radon may prevent and alleviate hypersensitivity. The effect, however, would only last for a limited amount of time, as the source of the inflammation would still be intact and thus synaptic plasticity following the chronic inflammation would re-occur.

In summary, the results presented in this doctoral thesis give rise to a hypothetical molecular working mechanism for radon to alleviate chronic pain without targeting the immune system itself, but rather by interacting with the neurosensory system. Firstly, the inhibitory potency of radon on NMDARs may lead to a decrease in LTP-related synaptic plasticity and secondly, low-dose ionizing radiation induces a neuroinflammatory response resulting in LTD restoration in the brain.

8. Bibliography

[1] Y. Alamanos, P. V. Voulgari, and A. A. Drosos, “Incidence and Prevalence of Rheumatoid Arthritis, Based on the 1987 American College of Rheumatology Criteria: A Systematic Review,” *Semin. Arthritis Rheum.*, vol. 36, no. 3, pp. 182–188, 2006, doi: 10.1016/j.semarthrit.2006.08.006.

[2] M. Abbasi *et al.*, “Strategies toward rheumatoid arthritis therapy; the old and the new,” *J. Cell. Physiol.*, vol. 234, no. 7, pp. 10018–10031, 2019, doi: 10.1002/jcp.27860.

[3] T. Heiberg and T. K. Kvien, “Preferences for improved health examined in 1,024 patients with rheumatoid arthritis: Pain has highest priority,” *Arthritis Care Res.*, vol. 47, no. 4, pp. 391–397, 2002, doi: 10.1002/art.10515.

[4] K. Biddle and N. Sofat, “Understanding the Mechanisms of Pain in Rheumatoid Arthritis,” *Rheum. Arthritis - Other Perspect. Towar. a Better Pract.*, pp. 1–21, 2020, doi: 10.5772/intechopen.93829.

[5] G. Gonçalves dos Santos *et al.*, “The neuropathic phenotype of the K/BxN transgenic mouse with spontaneous arthritis: pain, nerve sprouting and joint remodeling,” *Sci. Rep.*, vol. 10, no. 1, Dec. 2020, doi: 10.1038/s41598-020-72441-5.

[6] R. Kuner and H. Flor, “Structural plasticity and reorganisation in chronic pain,” *Nat. Rev. Neurosci.*, vol. 18, no. 1, pp. 20–30, 2016, doi: 10.1038/nrn.2016.162.

[7] N. R. Council, *Health Effects of Exposure to Radon: BEIR VI*. Washington, DC: The National Academies Press, 1999.

[8] S. H. Kim, W. J. Hwang, J. S. Cho, and D. R. Kang, “Attributable risk of lung cancer deaths due to indoor radon exposure,” *Ann. Occup. Environ. Med.*, vol. 28, no. 1, pp. 8–11, 2016, doi: 10.1186/s40557-016-0093-4.

[9] A. Falkenbach, J. Kovacs, A. Franke, K. Jörgens, and K. Ammer, “Radon therapy for the treatment of rheumatic diseases - Review and meta-analysis of controlled clinical trials,” *Rheumatol. Int.*, vol. 25, no. 3, pp. 205–210, 2005, doi: 10.1007/s00296-003-0419-8.

[10] A. Franke, L. Reiner, H. G. Pratzel, T. Franke, and K. L. Resch, “Long-term efficacy of radon spa therapy in rheumatoid arthritis--a randomized, sham-controlled study and follow-up.,” *Rheumatology (Oxford).*, vol. 39, no. 8, pp. 894–902, Aug. 2000, doi: 10.1093/rheumatology/39.8.894.

[11] A. Franke, L. Reiner, and K.-L. Resch, “Long-term benefit of radon spa therapy in the rehabilitation of rheumatoid arthritis: a randomised, double-blinded trial.,” *Rheumatol. Int.*, vol. 27, no. 8, pp. 703–713, Jun. 2007, doi: 10.1007/s00296-006-0293-2.

[12] P. F. Rühle *et al.*, “Impact of radon and combinatory radon/carbon dioxide spa on pain and hypertension: Results from the explorative RAD-ON01 study,” *Mod. Rheumatol.*,

vol. 29, no. 1, pp. 165–172, 2019, doi: 10.1080/14397595.2018.1442640.

[13] A. V. A. N. Tubergen *et al.*, “Combined Spa – Exercise Therapy Is Effective in Patients With Ankylosing Spondylitis : A Randomized Controlled Trial,” *Arthritis Care Res.*, pp. 430–438, 2001.

[14] M. Shehata *et al.*, “Effect of combined spa-exercise therapy on circulating TGF-beta1 levels in patients with ankylosing spondylitis.,” *Wien. Klin. Wochenschr.*, vol. 118, no. 9–10, pp. 266–272, May 2006, doi: 10.1007/s00508-006-0560-y.

[15] G. Dischereit, N. Neumann, U. Müller-Ladner, B. Kürten, and U. Lange, “Einfluss einer seriellen niedrig-dosierten Radonstollen-Hyperthermie auf Schmerz, Krankheitsaktivität und zentrale Zytokine des Knochenmetabolismus bei ankylosierender Spondylitis–eine Prospektivstudie,” *Aktuelle Rheumatol.*, vol. 39, no. 05, pp. 304–309, 2014.

[16] W. Pratzel, HG; Schnizer, *Handbuch der medizinischen Bäder: Radon-Bäder*. Haug, Heidelberg, 1992.

[17] S. Lawrence, “The Chemistry of Radon,” *Radiochim. Acta*, vol. 32, no. 1–3, pp. 163–172, 1983, doi: 10.1524/ract.1983.32.13.163.

[18] C. M. Lederer, “COMPUTERIZED PRODUCTION OF A DATA COMPILATION-A TABLE OF ISOTOPES,” 1973.

[19] F. Paquet *et al.*, “ICRP Publication 137: Occupational Intakes of Radionuclides: Part 3.,” *Ann. ICRP*, vol. 46, no. 3–4, pp. 1–486, Dec. 2017, doi: 10.1177/0146645317734963.

[20] O. Sarenio, “Leitfaden zur Messung von Radon, Thoron und ihren Zerfallsprodukten, Veröffentlichungen der Strahlenschutzkommission,” *Bundesministerium für Umwelt, Naturschutz und Reakt.*, 2002.

[21] H. Song, S. Senthamizhchelvan, R. F. Hobbs, and G. Sgouros, “Alpha particle emitter radiolabeled antibody for metastatic cancer: What can we learn from heavy ion beam radiobiology?,” *Antibodies*, vol. 1, no. 2, pp. 124–148, 2012, doi: 10.3390/antib1020124.

[22] J. Porstendörfer and A. Reineking, “Indoor Behaviour and Characteristics of Radon Progeny,” *Radiat. Prot. Dosimetry*, vol. 45, no. 1–4, pp. 303–311, Dec. 1992, doi: 10.1093/rpd/45.1-4.303.

[23] S. Tapio, “Ionizing radiation effects on cells, organelles and tissues on proteome level.,” *Adv. Exp. Med. Biol.*, vol. 990, pp. 37–48, 2013, doi: 10.1007/978-94-007-5896-4_2.

[24] E. R. Elliott, J. A. Van Ziffle, P. Scapini, B. M. Sullivan, R. M. Locksley, and C. A. Lowell, “Deletion of Syk in Neutrophils Prevents Immune Complex Arthritis,” *J. Immunol.*, vol. 187, no. 8, pp. 4319–4330, 2011, doi: 10.4049/jimmunol.1100341.

[25] L. Shi *et al.*, “Spatial learning and memory deficits after whole-brain irradiation are associated with changes in NMDA receptor subunits in the hippocampus.,” *Radiat. Res.*, vol. 166, no. 6, pp. 892–899, Dec. 2006, doi: 10.1667/RR0588.1.

[26] S. J. Kempf *et al.*, “The cognitive defects of neonatally irradiated mice are accompanied by changed synaptic plasticity, adult neurogenesis and neuroinflammation,” *Mol. Neurodegener.*, vol. 9, p. 57, Dec. 2014, doi: 10.1186/1750-1326-9-57.

[27] P. H. Wu *et al.*, “Radiation induces acute alterations in neuronal function.,” *PLoS One*, vol. 7, no. 5, p. e37677, 2012, doi: 10.1371/journal.pone.0037677.

[28] G. A. Lane, M. L. Nahrwold, A. R. Tait, M. Taylor-Busch, P. J. Cohen, and A. R. Beaudoin, “Anesthetics as teratogens: nitrous oxide is fetotoxic, xenon is not.,” *Science*, vol. 210, no. 4472, pp. 899–901, Nov. 1980, doi: 10.1126/science.7434002.

[29] J. R. Trudell, D. D. Koblin, and E. I. Eger, “A molecular description of how noble gases and nitrogen bind to a model site of anesthetic action,” *Anesth. Analg.*, vol. 87, no. 2, pp. 411–418, 1998, doi: 10.1097/00000539-199808000-00034.

[30] M. Schiltz, R. Fourme, I. Broutin, and T. Prangé, “The catalytic site of serine proteinases as a specific binding cavity for xenon,” *Structure*, vol. 3, no. 3, pp. 309–316, 1995, doi: 10.1016/S0969-2126(01)00161-7.

[31] T. Prangé *et al.*, “Exploring hydrophobic sites in proteins with xenon or krypton,” *Proteins Struct. Funct. Genet.*, vol. 30, no. 1, pp. 61–73, 1998, doi: 10.1002/(SICI)1097-0134(19980101)30:1<61::AID-PROT6>3.0.CO;2-N.

[32] R. Dickinson and N. P. Franks, “Bench-to-bedside review: Molecular pharmacology and clinical use of inert gases in anesthesia and neuroprotection,” *Crit. Care*, vol. 14, no. 4, pp. 1–12, 2010, doi: 10.1186/cc9051.

[33] R. F. Weiss, *Krypton, Xenon and Radon gas-solubilities*, vol. 4, no. 3–4. 1980.

[34] E. Nussbaum and J. B. Harsh, “Radon Solubility in Fatty Acids and Triglycerides,” *J. Phys. Chem.*, vol. 62, no. 1, pp. 81–84, Jan. 1958, doi: 10.1021/j150559a021.

[35] N. P. Franks, R. Dickinson, S. L. M. De Sousa, A. C. Hall, and W. R. Lieb, “How does xenon produce anaesthesia? [8],” *Nature*, vol. 396, no. 6709, p. 324, 1998, doi: 10.1038/24525.

[36] R. Haseneder, S. Kratzer, E. Kochs, C. Mattusch, M. Eder, and G. Rammes, “Xenon attenuates excitatory synaptic transmission in the rodent prefrontal cortex and spinal cord dorsal horn,” *Anesthesiology*, vol. 111, no. 6, pp. 1297–1307, 2009, doi: 10.1097/ALN.0b013e3181c14c05.

[37] I. L. White, N. P. Franks, and R. Dickinson, “Effects of isoflurane and xenon on Ba2+-currents mediated by N-type calcium channels.,” *Br. J. Anaesth.*, vol. 94, no. 6, pp. 784–790, Jun. 2005, doi: 10.1093/bja/aei126.

[38] R. Dickinson *et al.*, “Competitive inhibition at the glycine site of the N-methyl-D-aspartate receptor by the anesthetics xenon and isoflurane: Evidence from molecular modeling and electrophysiology,” *Anesthesiology*, vol. 107, no. 5, pp. 756–767, 2007, doi: 10.1097/01.anes.0000287061.77674.71.

[39] L. T. Liu, Y. Xu, and P. Tang, “Mechanistic insights into xenon inhibition of NMDA receptors from MD simulations,” *J. Phys. Chem. B*, vol. 114, no. 27, pp. 9010–9016, 2010, doi: 10.1021/jp101687j.

[40] F. BOOMSMA, J. RUPREHT, A. J. M. I. T. VELD, F. H. D. JONG, M. DZOLJIC, and B. LACHMANN, “Haemodynamic and neurohumoral effects of xenon anaesthesia A comparison with nitrous oxide,” *Anaesthesia*, vol. 45, no. 4, pp. 273–278, 1990, doi: 10.1111/j.1365-2044.1990.tb14731.x.

[41] S. Petersen-Felix, M. Luginbühl, T. W. Schnider, M. Curatolo, L. Arendt-Nielsen, and A. M. Zbinden, “Comparison of the analgesic potency of xenon and nitrous oxide in humans evaluated by experimental pain,” *Br. J. Anaesth.*, vol. 81, no. 5, pp. 742–747, 1998, doi: 10.1093/bja/81.5.742.

[42] O. Adolph *et al.*, “Xenon-induced changes in CNS sensitization to pain,” *Neuroimage*, vol. 49, no. 1, pp. 720–730, 2010, doi: 10.1016/j.neuroimage.2009.08.034.

[43] T. F. Holsträter *et al.*, “Intranasal application of xenon reduces opioid requirement and postoperative pain in patients undergoing major abdominal surgery: A randomized controlled trial,” *Anesthesiology*, vol. 115, no. 2, pp. 398–407, 2011, doi: 10.1097/ALN.0b013e318225cee5.

[44] L. Chen *et al.*, “Separation of rare gases and chiral molecules by selective binding in porous organic cages,” *Nat. Mater.*, vol. 13, no. 10, pp. 954–960, 2014, doi: 10.1038/nmat4035.

[45] P. Paoletti, C. Bellone, and Q. Zhou, “NMDA receptor subunit diversity: Impact on receptor properties, synaptic plasticity and disease,” *Nat. Rev. Neurosci.*, vol. 14, no. 6, pp. 383–400, 2013, doi: 10.1038/nrn3504.

[46] H. Monyer *et al.*, “Heteromeric NMDA receptors: molecular and functional distinction of subtypes.,” *Science*, vol. 256, no. 5060, pp. 1217–1221, May 1992, doi: 10.1126/science.256.5060.1217.

[47] M. H. Ulbrich and E. Y. Isacoff, “Rules of engagement for NMDA receptor subunits,” *Proc. Natl. Acad. Sci. U. S. A.*, vol. 105, no. 37, pp. 14163–14168, 2008, doi: 10.1073/pnas.0802075105.

[48] C. Akazawa, R. Shigemoto, Y. Bessho, S. Nakanishi, and N. Mizuno, “Differential expression of five N-methyl-D-aspartate receptor subunit mRNAs in the cerebellum of developing and adult rats.,” *J. Comp. Neurol.*, vol. 347, no. 1, pp. 150–160, Sep. 1994, doi: 10.1002/cne.903470112.

[49] H. Monyer, N. Burnashev, D. J. Laurie, B. Sakmann, and P. H. Seeburg, “Developmental and regional expression in the rat brain and functional properties of four NMDA receptors.,” *Neuron*, vol. 12, no. 3, pp. 529–540, Mar. 1994, doi: 10.1016/0896-6273(94)90210-0.

[50] M. Gielen, B. S. Retchless, L. Mony, J. W. Johnson, and P. Paoletti, “Mechanism of differential control of NMDA receptor activity by NR2 subunits,” *Nature*, vol. 459, no. 7247, pp. 703–707, 2009, doi: 10.1038/nature07993.

[51] M. Arvola and K. Keinänen, “Characterization of the ligand-binding domains of glutamate receptor (GluR)-B and GluR-D subunits expressed in Escherichia coli as periplasmic proteins,” *J. Biol. Chem.*, vol. 271, no. 26, pp. 15527–15532, 1996, doi: 10.1074/jbc.271.26.15527.

[52] J. J. Krupp, B. Vissel, S. F. Heinemann, and G. L. Westbrook, “N-terminal domains in the NR2 subunit control desensitization of NMDA receptors,” *Neuron*, vol. 20, no. 2, pp. 317–327, 1998, doi: 10.1016/S0896-6273(00)80459-6.

[53] R. Kazi, Q. Gan, I. Talukder, M. Markowitz, C. L. Salussolia, and L. P. Wollmuth, “Asynchronous movements prior to pore opening in NMDA receptors,” *J. Neurosci.*, vol. 33, no. 29, pp. 12052–12066, 2013, doi: 10.1523/JNEUROSCI.5780-12.2013.

[54] I. Talukder, P. Borker, and L. P. Wollmuth, “Specific sites within the ligand-binding domain and ion channel linkers modulate NMDA receptor gating,” *J. Neurosci.*, vol. 30, no. 35, pp. 11792–11804, 2010, doi: 10.1523/JNEUROSCI.5382-09.2010.

[55] W. G. Tingley, K. W. Roche, A. K. Thompson, and R. L. Huganir, “of the C-terminal domain,” vol. 364, no. July, pp. 1991–1994, 1993.

[56] M. D. Ehlers, S. Zhang, J. P. Bernhardt, and R. L. Huganir, “Inactivation of NMDA receptors by direct interaction of calmodulin with the NR1 subunit,” *Cell*, vol. 84, no. 5, pp. 745–755, 1996, doi: 10.1016/S0092-8674(00)81052-1.

[57] N. W. Kleckner and R. Dingledine, “Requirement for glycine in activation of NMDA-receptors expressed in Xenopus oocytes.,” *Science*, vol. 241, no. 4867, pp. 835–837, Aug. 1988, doi: 10.1126/science.2841759.

[58] S. Ahmadi, U. Muth-Selbach, A. Lauterbach, P. Lipfert, W. L. Neuhuber, and H. U. Zeilhofer, “Facilitation of spinal NMDA receptor currents by spillover of synaptically released glycine.,” *Science*, vol. 300, no. 5628, pp. 2094–2097, Jun. 2003, doi: 10.1126/science.1083970.

[59] M. L. Mayer, G. L. Westbrook, and P. B. Guthrie, “Voltage-dependent block by Mg2+ of NMDA responses in spinal cord neurones.,” *Nature*, vol. 309, no. 5965, pp. 261–263, May 1984, doi: 10.1038/309261a0.

[60] P. H. Seeburg, N. Burnashev, G. Köhr, T. Kuner, R. Sprengel, and H. Monyer, “The NMDA receptor channel: molecular design of a coincidence detector.,” *Recent Prog.*

Horm. Res., vol. 50, pp. 19–34, 1995, doi: 10.1016/b978-0-12-571150-0.50006-8.

[61] K. B. Hansen *et al.*, “Structure , function , and allosteric modulation of NMDA receptors,” vol. 150, no. 8, pp. 1081–1105, 2018.

[62] B. W. F. Fenton, E. Shih, and J. Zolton, “The neurobiology of pain perception in normal and persistent pain Bradford W Fenton, Elim Shih and Jessica Zolton,” *Pain Manag.*, vol. 4, no. July 2015, pp. 1–26, 2017, [Online]. Available: http://www.futuremedicine.com/doi/10.2217/pmt.15.27.

[63] M. A. Nassar *et al.*, “Nociceptor-specific gene deletion reveals a major role for Na,” *Pnas*, vol. 101, no. 34, pp. 12706–12711, 2004.

[64] J. N. Wood, J. P. Boorman, K. Okuse, and M. D. Baker, “Voltage-gated sodium channels and pain pathways.,” *J. Neurobiol.*, vol. 61, no. 1, pp. 55–71, Oct. 2004, doi: 10.1002/neu.20094.

[65] R. Kuner, “Central mechanisms of pathological pain,” *Nat. Med.*, vol. 16, no. 11, pp. 1258–1266, 2010, doi: 10.1038/nm.2231.

[66] C. J. Woolf and R. J. Mannion, “Neuropathic pain: aetiology, symptoms, mechanisms, and management.,” *Lancet (London, England)*, vol. 353, no. 9168, pp. 1959–1964, Jun. 1999, doi: 10.1016/S0140-6736(99)01307-0.

[67] T. V. P. Bliss, G. L. Collingridge, B. K. Kaang, and M. Zhuo, “Synaptic plasticity in the anterior cingulate cortex in acute and chronic pain,” *Nat. Rev. Neurosci.*, vol. 17, no. 8, pp. 485–496, 2016, doi: 10.1038/nrn.2016.68.

[68] C. L. Stucky, L. G. Abrahams, and V. S. Seybold, “Bradykinin increases the proportion of neonatal rat dorsal root ganglion neurons that respond to capsaicin and protons,” *Neuroscience*, vol. 84, no. 4, pp. 1257–1265, 1998, doi: https://doi.org/10.1016/S0306-4522(97)00572-1.

[69] S. Pitchford and J. D. Levine, “Prostaglandins sensitize nociceptors in cell culture,” *Neurosci. Lett.*, vol. 132, no. 1, pp. 105–108, 1991, doi: 10.1016/0304-3940(91)90444-X.

[70] X. Shu and L. M. Mendell, “Nerve growth factor acutely sensitizes the response of adult rat sensory neurons to capsaicin,” *Neurosci. Lett.*, vol. 274, no. 3, pp. 159–162, 1999, doi: 10.1016/S0304-3940(99)00701-6.

[71] V. Gangadharan and R. Kuner, “Pain hypersensitivity mechanisms at a glance,” *DMM Dis. Model. Mech.*, vol. 6, no. 4, pp. 889–895, 2013, doi: 10.1242/dmm.011502.

[72] C. J. Woolf and M. W. Salter, “Neuronal plasticity: Increasing the gain in pain,” *Science (80-.).*, vol. 288, no. 5472, pp. 1765–1768, 2000, doi: 10.1126/science.288.5472.1765.

[73] P. Cesare, L. V. Dekker, A. Sardini, P. J. Parker, and P. A. McNaughton, “Specific involvement of PKC-ε in sensitization of the neuronal response to painful heat,”

Neuron, vol. 23, no. 3, pp. 617–624, 1999, doi: 10.1016/S0896-6273(00)80813-2.

[74] S. G. Khasar, G. Mccarter, and J. D. Levine, “Epinephrine produces a β-adrenergic receptor-mediated mechanical hyperalgesia and in vitro sensitization of rat nociceptors,” *J. Neurophysiol.*, vol. 81, no. 3, pp. 1104–1112, 1999, doi: 10.1152/jn.1999.81.3.1104.

[75] E. M. Fitzgerald, K. Okuse, J. N. Wood, A. C. Dolphin, and S. J. Moss, “cAMP-dependent phosphorylation of the tetrodotoxin-resistant voltage-dependent sodium channel SNS,” *J. Physiol.*, vol. 516, no. 2, pp. 433–446, 1999, doi: 10.1111/j.1469-7793.1999.0433v.x.

[76] S. England, S. Bevan, and R. J. Docherty, “PGE2 modulates the tetrodotoxin-resistant sodium current in neonatal rat dorsal root ganglion neurones via the cyclic AMP-protein kinase A cascade,” *J. Physiol.*, vol. 495, no. 2, pp. 429–440, 1996, doi: 10.1113/jphysiol.1996.sp021604.

[77] S. G. Khasar, M. S. Gold, and J. D. Levine, “A tetrodotoxin-resistant sodium current mediates inflammatory pain in the rat,” *Neurosci. Lett.*, vol. 256, no. 1, pp. 17–20, 1998, doi: 10.1016/S0304-3940(98)00738-1.

[78] M. Ronald and W. P. D., “Pain Mechanisms: A New Theory,” *Science (80-.).*, vol. 150, no. 3699, pp. 971–979, Nov. 1965, doi: 10.1126/science.150.3699.971.

[79] A. I. Basbaum, D. M. Bautista, G. Scherrer, and D. Julius, “Cellular and molecular mechanisms of pain.,” *Cell*, vol. 139, no. 2, pp. 267–284, Oct. 2009, doi: 10.1016/j.cell.2009.09.028.

[80] C. J. Woolf, “Evidence for a central component of post-injury pain hypersensitivity,” *Nature*, vol. 306, no. 5944, pp. 686–688, 1983, doi: 10.1038/306686a0.

[81] A. Latremoliere and C. J. Woolf, “Central sensitization: a generator of pain hypersensitivity by central neural plasticity,” *J. pain*, vol. 10, no. 9, pp. 895–926, Sep. 2009, doi: 10.1016/j.jpain.2009.06.012.

[82] B. U. Keller, M. Hollmann, S. Heinemann, and A. Konnerth, “Calcium influx through subunits GluR1/GluR3 of kainate/AMPA receptor channels is regulated by cAMP dependent protein kinase.,” *EMBO J.*, vol. 11, no. 3, pp. 891–896, Mar. 1992.

[83] A. L. Carvalho, C. B. Duarte, C. J. Faro, A. P. Carvalho, and E. V Pires, “Calcium influx through AMPA receptors and through calcium channels is regulated by protein kinase C in cultured retina amacrine-like cells.,” *J. Neurochem.*, vol. 70, no. 5, pp. 2112–2119, May 1998, doi: 10.1046/j.1471-4159.1998.70052112.x.

[84] H. J. Chung, Y. H. Huang, L.-F. Lau, and R. L. Huganir, “Regulation of the NMDA receptor complex and trafficking by activity-dependent phosphorylation of the NR2B subunit PDZ ligand.,” *J. Neurosci.*, vol. 24, no. 45, pp. 10248–10259, Nov. 2004, doi: 10.1523/JNEUROSCI.0546-04.2004.

[85] I. M. Raman, G. Tong, and C. E. Jahr, “Beta-adrenergic regulation of synaptic NMDA receptors by cAMP-dependent protein kinase.,” *Neuron*, vol. 16, no. 2, pp. 415–421, Feb. 1996, doi: 10.1016/s0896-6273(00)80059-8.

[86] C. J. Woolf and A. E. King, “Dynamic alterations in the cutaneous mechanoreceptive fields of dorsal horn neurons in the rat spinal cord,” *J. Neurosci.*, vol. 10, no. 8, pp. 2717 LP – 2726, Aug. 1990, doi: 10.1523/JNEUROSCI.10-08-02717.1990.

[87] Z. Ali, R. A. Meyer, and J. N. Campbell, “Secondary hyperalgesia to mechanical but not heat stimuli following a capsaicin injection in hairy skin.,” *Pain*, vol. 68, no. 2–3, pp. 401–411, Dec. 1996, doi: 10.1016/s0304-3959(96)03199-5.

[88] K. Noguchi, R. Dubner, and M. A. Ruda, “Preproenkephalin mRNA in spinal dorsal horn neurons is induced by peripheral inflammation and is co-localized with Fos and Fos-related proteins.,” *Neuroscience*, vol. 46, no. 3, pp. 561–570, 1992, doi: 10.1016/0306-4522(92)90144-q.

[89] G. J. Michael and J. V Priestley, “Differential Expression of the mRNA for the Vanilloid Receptor Subtype 1 in Cells of the Adult Rat Dorsal Root and Nodose Ganglia and Its Downregulation by Axotomy,” *J. Neurosci.*, vol. 19, no. 5, pp. 1844 LP – 1854, Mar. 1999, doi: 10.1523/JNEUROSCI.19-05-01844.1999.

[90] R. J. Mannion *et al.*, “Neurotrophins: peripherally and centrally acting modulators of tactile stimulus-induced inflammatory pain hypersensitivity.,” *Proc. Natl. Acad. Sci. U. S. A.*, vol. 96, no. 16, pp. 9385–9390, Aug. 1999, doi: 10.1073/pnas.96.16.9385.

[91] A. N. Akopian *et al.*, “The tetrodotoxin-resistant sodium channel SNS has a specialized function in pain pathways,” *Nat. Neurosci.*, vol. 2, no. 6, pp. 541–548, 1999, doi: 10.1038/9195.

[92] S. Neumann, T. P. Doubell, T. Leslie, and C. J. Woolf, “Inflammatory pain hypersensitivity mediated by phenotypic switch in myelinated primary sensory neurons.,” *Nature*, vol. 384, no. 6607, pp. 360–364, Nov. 1996, doi: 10.1038/384360a0.

[93] J. J. Azkue, “Peripheral nerve insult induces NMDA receptor-mediated, delayed degeneration in spinal neurons,” *Eur. J. Neurosci.*, vol. 10, no. 6, pp. 2204–2206, 1998, doi: 10.1046/j.1460-9568.1998.00260.x.

[94] M. Zhuo, “Long-term potentiation in the anterior cingulate cortex and chronic pain,” *Philos. Trans. R. Soc. B Biol. Sci.*, vol. 369, no. 1633, 2014, doi: 10.1098/rstb.2013.0146.

[95] S. W. Derbyshire, “Meta-Analysis of Thirty-Four Independent Samples Studied Using PET Reveals a Significantly Attenuated Central Response to Noxious Stimulation in Clinical Pain Patients.,” *Curr. Rev. Pain*, vol. 3, no. 4, pp. 265–280, 1999, doi: 10.1007/s11916-999-0044-7.

[96] M. L. Phillips *et al.*, “The effect of negative emotional context on neural and behavioural responses to oesophageal stimulation.,” *Brain*, vol. 126, no. Pt 3, pp. 669–684, Mar. 2003, doi: 10.1093/brain/awg065.

[97] J. D. Talbot, S. Marret, A. C. Evans, E. Meyer, M. C. Bushnell, and G. H. Duncan, “Multiple representations of pain in human cerebral cortex,” *Science (80-.).*, vol. 251, no. 4999, pp. 1355–1358, 1991, doi: 10.1126/science.2003220.

[98] J. C. Kung and B. C. Shyu, “Potentiation of local field potentials in the anterior cingulate cortex evoked by the stimulation of the medial thalamic nuclei in rats,” *Brain Res.*, vol. 953, no. 1–2, pp. 37–44, 2002, doi: 10.1016/S0006-8993(02)03265-1.

[99] J.-W. Yang, H.-C. Shih, and B.-C. Shyu, “Intracortical circuits in rat anterior cingulate cortex are activated by nociceptive inputs mediated by medial thalamus.,” *J. Neurophysiol.*, vol. 96, no. 6, pp. 3409–3422, Dec. 2006, doi: 10.1152/jn.00623.2006.

[100] W. Ma and M. Peschanski, “Spinal and trigeminal projections to the parabrachial nucleus in the rat: electron-microscopic evidence of a spino-ponto-amygdalian somatosensory pathway.,” *Somatosens. Res.*, vol. 5, no. 3, pp. 247–257, 1988, doi: 10.3109/07367228809144629.

[101] K. Eto *et al.*, “Inter-regional contribution of enhanced activity of the primary somatosensory cortex to the anterior cingulate cortex accelerates chronic pain behavior,” *J. Neurosci.*, vol. 31, no. 21, pp. 7631–7636, 2011, doi: 10.1523/JNEUROSCI.0946-11.2011.

[102] M. Zhuo, “Cortical excitation and chronic pain,” *Trends Neurosci.*, vol. 31, no. 4, pp. 199–207, 2008, doi: 10.1016/j.tins.2008.01.003.

[103] M. Zhuo, “Plasticity of NMDA receptor NR2B subunit in memory and chronic pain,” *Mol. Brain*, vol. 2, no. 1, pp. 1–11, 2009, doi: 10.1186/1756-6606-2-4.

[104] F. Wei *et al.*, “Calmodulin regulates synaptic plasticity in the anterior cingulate cortex and behavioral responses: A microelectroporation study in adult rodents,” *J. Neurosci.*, vol. 23, no. 23, pp. 8402–8409, 2003, doi: 10.1523/jneurosci.23-23-08402.2003.

[105] Z. Wu, S. T. Wong, and D. R. Storm, “Modification of the calcium and calmodulin sensitivity of the type I adenylyl cyclase by mutagenesis of its calmodulin binding domain,” *J. Biol. Chem.*, vol. 268, no. 32, pp. 23766–23768, 1993, doi: 10.1016/s0021-9258(20)80447-5.

[106] Y. Kawasaki *et al.*, “Ionotropic and metabotropic receptors, protein kinase A, protein kinase C, and Src contribute to C-fiber-induced ERK activation and cAMP response element-binding protein phosphorylation in dorsal horn neurons, leading to central sensitization,” *J. Neurosci.*, vol. 24, no. 38, pp. 8310–8321, 2004, doi: 10.1523/JNEUROSCI.2396-04.2004.

[107] Z. Xia, H. Dudek, C. K. Miranti, and M. E. Greenberg, “Calcium influx via the NMDA

receptor induces immediate early gene transcription by a MAP kinase/ERK-dependent mechanism.," *J. Neurosci.*, vol. 16, no. 17, pp. 5425–5436, Sep. 1996, doi: 10.1523/JNEUROSCI.16-17-05425.1996.

[108] F. bing Shao *et al.*, "Anxiolytic effect of GABAergic neurons in the anterior cingulate cortex in a rat model of chronic inflammatory pain," *Mol. Brain*, vol. 14, no. 1, pp. 1–22, 2021, doi: 10.1186/s13041-021-00849-9.

[109] E. Bullitt, "Expression of C-fos-like protein as a marker for neuronal activity following noxious stimulation in the rat," *J. Comp. Neurol.*, vol. 296, no. 4, pp. 517–530, 1990, doi: 10.1002/cne.902960402.

[110] S. Jarrin, A. Pandit, M. Roche, and D. P. Finn, "Differential Role of Anterior Cingulate Cortical Glutamatergic Neurons in Pain-Related Aversion Learning and Nociceptive Behaviors in Male and Female Rats," *Front. Behav. Neurosci.*, vol. 14, no. August, pp. 1–10, 2020, doi: 10.3389/fnbeh.2020.00139.

[111] L. G. Lei, Y. Q. Zhang, and Z. Q. Zhao, "Pain-related aversion and Fos expression in the central nervous system in rats," *Neuroreport*, vol. 15, no. 1, pp. 67–71, 2004, doi: 10.1097/00001756-200401190-00014.

[112] L. J. Wu *et al.*, "Upregulation of forebrain NMDA NR2B receptors contributes to behavioral sensitization after inflammation," *J. Neurosci.*, vol. 25, no. 48, pp. 11107–11116, 2005, doi: 10.1523/JNEUROSCI.1678-05.2005.

[113] H. Toyoda *et al.*, "Roles of the AMPA receptor subunit GluA1 but not GluA2 in synaptic potentiation and activation of ERK in the anterior cingulate cortex," *Mol. Pain*, vol. 5, pp. 1–15, 2009, doi: 10.1186/1744-8069-5-46.

[114] H. Toyoda, L.-J. Wu, M.-G. Zhao, H. Xu, and M. Zhuo, "Time-dependent postsynaptic AMPA GluR1 receptor recruitment in the cingulate synaptic potentiation.," *Dev. Neurobiol.*, vol. 67, no. 4, pp. 498–509, Mar. 2007, doi: 10.1002/dneu.20380.

[115] T. Nakazawa *et al.*, "Characterization of Fyn-mediated tyrosine phosphorylation sites on GluRε2 (NR2B) subunit of the N-methyl-D-aspartate receptor," *J. Biol. Chem.*, vol. 276, no. 1, pp. 693–699, 2001, doi: 10.1074/jbc.M008085200.

[116] J. A. P. Rostas, V. A. Brent, K. Voss, M. L. Errington, T. V. P. Bliss, and J. W. Gurd, "Enhanced tyrosine phosphorylation of the 2B subunit of the N-methyl-D-aspartate receptor in long-term potentiation," *Proc. Natl. Acad. Sci. U. S. A.*, vol. 93, no. 19, pp. 10452–10456, 1996, doi: 10.1073/pnas.93.19.10452.

[117] Y. T. Wang and M. W. Salter, "Regulation of NMDA receptors by tyrosine kinases and phosphatases," *Nature*, vol. 369, no. 6477, pp. 233–235, 1994, doi: 10.1038/369233a0.

[118] T. Abe *et al.*, "Fyn kinase-mediated phosphorylation of NMDA receptor NR2B subunit at Tyr1472 is essential for maintenance of neuropathic pain," *Eur. J. Neurosci.*, vol. 22,

no. 6, pp. 1445–1454, 2005, doi: 10.1111/j.1460-9568.2005.04340.x.

[119] Q. Song *et al.*, “Selective phosphorylation of AMPA receptor contributes to the network of long-term potentiation in the anterior cingulate cortex,” *J. Neurosci.*, vol. 37, no. 35, pp. 8534–8548, 2017, doi: 10.1523/JNEUROSCI.0925-17.2017.

[120] J. Rochester, “Contemplation,” *IEEE Technol. Soc. Mag.*, vol. 28, no. 1, p. 3, 2009, doi: 10.1109/MTS.2009.931859.

[121] J. Xia, H. J. Chung, C. Wihler, R. L. Huganir, and D. J. Linden, “Cerebellar long-term depression requires PKC-regulated interactions between GluR2/3 and PDZ domain-containing proteins.,” *Neuron*, vol. 28, no. 2, pp. 499–510, Nov. 2000, doi: 10.1016/s0896-6273(00)00128-8.

[122] H. Toyoda, L.-J. Wu, M.-G. Zhao, H. Xu, Z. Jia, and M. Zhuo, “Long-term depression requires postsynaptic AMPA GluR2 receptor in adult mouse cingulate cortex.,” *J. Cell. Physiol.*, vol. 211, no. 2, pp. 336–343, May 2007, doi: 10.1002/jcp.20940.

[123] C. H. Kim, H. J. Chung, H. K. Lee, and R. L. Huganir, “Interaction of the AMPA receptor subunit GluR2/3 with PDZ domains regulates hippocampal long-term depression.,” *Proc. Natl. Acad. Sci. U. S. A.*, vol. 98, no. 20, pp. 11725–11730, Sep. 2001, doi: 10.1073/pnas.211132798.

[124] D. T. Lin and R. L. Huganir, “PICK1 and phosphorylation of the glutamate receptor 2 (GluR2) AMPA receptor subunit regulates GluR2 recycling after NMDA receptor-induced internalization,” *J. Neurosci.*, vol. 27, no. 50, pp. 13903–13908, 2007, doi: 10.1523/JNEUROSCI.1750-07.2007.

[125] G. L. Collingridge, S. Peineau, J. G. Howland, and Y. T. Wang, “Long-term depression in the CNS,” *Nat. Rev. Neurosci.*, vol. 11, no. 7, pp. 459–473, 2010, doi: 10.1038/nrn2867.

[126] M. Leitges, J. Kovac, M. Plomann, and D. J. Linden, “A unique PDZ ligand in PKCα confers induction of cerebellar long-term synaptic depression,” *Neuron*, vol. 44, no. 4, pp. 585–594, 2004, doi: 10.1016/j.neuron.2004.10.024.

[127] Y. Chen, V. A. Derkach, and P. A. Smith, “Loss of Ca(2+)-permeable AMPA receptors in synapses of tonic firing substantia gelatinosa neurons in the chronic constriction injury model of neuropathic pain.,” *Exp. Neurol.*, vol. 279, pp. 168–177, May 2016, doi: 10.1016/j.expneurol.2016.03.001.

[128] D. Z. Lee, J. M. Chung, K. Chung, and M.-G. Kang, “Reactive oxygen species (ROS) modulate AMPA receptor phosphorylation and cell-surface localization in concert with pain-related behavior.,” *Pain*, vol. 153, no. 9, pp. 1905–1915, Sep. 2012, doi: 10.1016/j.pain.2012.06.001.

[129] Y. J. Wang *et al.*, “Restoration of Cingulate Long-Term Depression by Enhancing Non-apoptotic Caspase 3 Alleviates Peripheral Pain Hypersensitivity,” *Cell Rep.*, vol. 33,

no. 6, p. 108369, 2020, doi: 10.1016/j.celrep.2020.108369.

[130] P. A. Monach, C. Benoist, and D. Mathis, “The Role of Antibodies in Mouse Models of Rheumatoid Arthritis, and Relevance to Human Disease,” *Adv. Immunol.*, vol. 82, pp. 217–248, 2004, doi: 10.1016/S0065-2776(04)82005-4.

[131] H. Ji *et al.*, “Genetic influences on the end-stage effector phase of arthritis,” *J. Exp. Med.*, vol. 194, no. 3, pp. 321–330, 2001, doi: 10.1084/jem.194.3.321.

[132] A. S. Korganow *et al.*, “From systemic T cell self-reactivity to organ-specific autoimmune disease via immunoglobulins,” *Immunity*, vol. 10, no. 4, pp. 451–461, 1999, doi: 10.1016/S1074-7613(00)80045-X.

[133] C. A. Christianson, M. Corr, G. S. Firestein, A. Mobargha, T. L. Yaksh, and C. I. Svensson, “Characterization of the acute and persistent pain state present in K/BxN serum transfer arthritis,” *Pain*, vol. 151, no. 2, pp. 394–403, Nov. 2010, doi: 10.1016/j.pain.2010.07.030.

[134] J. Chen *et al.*, “The α2δ-1-NMDA Receptor Complex Is Critically Involved in Neuropathic Pain Development and Gabapentin Therapeutic Actions.,” *Cell Rep.*, vol. 22, no. 9, pp. 2307–2321, Feb. 2018, doi: 10.1016/j.celrep.2018.02.021.

[135] C. P. Robinson, “Gabapentin,” *Drugs of Today*, vol. 30, no. 6, pp. 451–457, 1994, doi: 10.4324/9781315825748-31.

[136] K. Becker, “One century of radon therapy,” *Int. J. Low Radiat.*, vol. 1, no. 3, pp. 333–357, 2004.

[137] J. Mirsch, “Biologischer Nachweis niedriger Dosen ionisierender Strahlung,” 2017.

[138] A. Maier, “Entwicklung einer Radonkammer und Messung der Radonlöslichkeit in Gewebe,” p. 92, 2015.

[139] A. Maier *et al.*, “Experimental setup for radon exposure and first diffusion studies using gamma spectroscopy,” *Nucl. Instruments Methods Phys. Res. Sect. B Beam Interact. with Mater. Atoms*, vol. 362, pp. 187–193, 2015, doi: 10.1016/j.nimb.2015.09.042.

[140] R. Dickinson *et al.*, “Competitive Inhibition at the Glycine Site of the N -Methyl- D -aspartate Receptor by the Anesthetics Xenon and Isoflurane,” no. 5, pp. 756–767, 2016.

[141] A. Abramo, C. Di Salvo, F. Foltran, F. Forfori, M. Anselmino, and F. Giunta, “Xenon anesthesia improves respiratory gas exchanges in morbidly obese patients.,” *J. Obes.*, vol. 2010, 2010, doi: 10.1155/2010/421593.

[142] Y. Hagiwara *et al.*, “3D-structured illumination microscopy reveals clustered DNA double-strand break formation in widespread γH2AX foci after high LET heavy-ion particle radiation,” *Oncotarget; Vol 8, No 65*, 2017, [Online]. Available: https://www.oncotarget.com/article/22679/text/.

[143] A. J. A. *et al.*, “Dynamics of DNA Double-Strand Breaks Revealed by Clustering of

Damaged Chromosome Domains," *Science (80-.).*, vol. 303, no. 5654, pp. 92–95, Jan. 2004, doi: 10.1126/science.1088845.

[144] S. J. Roobol *et al.*, "Comparison of high-and low-let radiation-induced dna double-strand break processing in living cells," *Int. J. Mol. Sci.*, vol. 21, no. 18, pp. 1–19, 2020, doi: 10.3390/ijms21186602.

[145] A. Sollazzo, B. Brzozowska, L. Cheng, L. Lundholm, H. Scherthan, and A. Wojcik, "Live Dynamics of 53BP1 Foci Following Simultaneous Induction of Clustered and Dispersed DNA Damage in U2OS Cells," *International Journal of Molecular Sciences* , vol. 19, no. 2. 2018, doi: 10.3390/ijms19020519.

[146] Y. Ishimori, H. Tanaka, A. Sakoda, T. Kataoka, K. Yamaoka, and F. Mitsunobu, "Measurements of radon activity concentration in mouse tissues and organs," *Radiat. Environ. Biophys.*, vol. 56, no. 2, pp. 161–165, 2017, doi: 10.1007/s00411-017-0682-9.

[147] G. M. Kendall and T. J. Smith, "Doses to organs and tissues from radon and its decay products.," *J. Radiol. Prot. Off. J. Soc. Radiol. Prot.*, vol. 22, no. 4, pp. 389–406, Dec. 2002, doi: 10.1088/0952-4746/22/4/304.

[148] M. Pirmoradi, A. Negarestani, and A. Baghizadeh, "VARIATION SIMULATION OF RADON CONCENTRATION IN THE TISSUES AND ORGANS OF THE BODY BY AN ELECTRICAL CIRCUIT.," *Radiat. Prot. Dosimetry*, vol. 187, no. 3, pp. 390–401, Dec. 2019, doi: 10.1093/rpd/ncz180.

[149] N. E. and H. J. B., "Radon Solubility in Rat Tissues," *Science (80-.).*, vol. 125, no. 3247, pp. 552–553, Mar. 1957, doi: 10.1126/science.125.3247.552.

[150] A. Ruano-Ravina *et al.*, "Residential radon exposure and brain cancer: An ecological study in a radon prone area (Galicia, Spain)," *Sci. Rep.*, vol. 7, no. 1, pp. 1–7, 2017, doi: 10.1038/s41598-017-03938-9.

[151] E. V. Bräuner *et al.*, "Residential Radon and Brain Tumour Incidence in a Danish Cohort," *PLoS One*, vol. 8, no. 9, 2013, doi: 10.1371/journal.pone.0074435.

[152] S. Gómez-Anca and J. M. Barros-Dios, "Radon exposure and neurodegenerative disease," *Int. J. Environ. Res. Public Health*, vol. 17, no. 20, pp. 1–17, 2020, doi: 10.3390/ijerph17207439.

[153] M. Katsura *et al.*, "Effects of Chronic Low-Dose Radiation on Human Neural Progenitor Cells," *Sci. Rep.*, vol. 6, no. January, pp. 1–12, 2016, doi: 10.1038/srep20027.

[154] A. Kovalchuk *et al.*, "Profound and Sexually Dimorphic Effects of Clinically-Relevant Low Dose Scatter Irradiation on the Brain and Behavior ," *Frontiers in Behavioral Neuroscience* , vol. 10. p. 84, 2016, [Online]. Available: https://www.frontiersin.org/article/10.3389/fnbeh.2016.00084.

[155] P. Taylor *et al.*, "Patient perceptions concerning pain management in the treatment of

rheumatoid arthritis," *J. Int. Med. Res.*, vol. 38, no. 4, pp. 1213–1224, 2010, doi: 10.1177/147323001003800402.

[156] Y. Xu *et al.*, "The spinal NR2BR/ERK2 pathway as a target for the central sensitization of collagen-induced arthritis pain," *PLoS One*, vol. 13, no. 7, pp. 1–13, 2018, doi: 10.1371/journal.pone.0201021.

[157] J. Garthwaite, G. Garthwaite, R. M. J. Palmer, and S. Moncada, "NMDA receptor activation induces nitric oxide synthesis from arginine in rat brain slices," *Eur. J. Pharmacol. Mol. Pharmacol.*, vol. 172, no. 4–5, pp. 413–416, 1989, doi: 10.1016/0922-4106(89)90023-0.

[158] J. I. Morgan and T. Curran, "Stimulus-transcription coupling in the nervous system: Involvement of the inducible proto-oncogenes fos and jun," *Annu. Rev. Neurosci.*, vol. 14, pp. 421–451, 1991, doi: 10.1146/annurev.ne.14.030191.002225.

[159] S. Shi, Y. Hayashi, J. A. Esteban, and R. Malinow, "Subunit-specific rules governing AMPA receptor trafficking to synapses in hippocampal pyramidal neurons.," *Cell*, vol. 105, no. 3, pp. 331–343, May 2001, doi: 10.1016/s0092-8674(01)00321-x.

[160] O. Kopach *et al.*, "Spinal PKCα inhibition and gene-silencing for pain relief: AMPAR trafficking at the synapses between primary afferents and sensory interneurons," *Sci. Rep.*, vol. 8, no. 1, pp. 1–14, 2018, doi: 10.1038/s41598-018-28512-9.

[161] J. L. Perez, L. Khatri, C. Chang, S. Srivastava, P. Osten, and E. B. Ziff, "PICK1 targets activated protein kinase Cα to AMPA receptor clusters in spines of hippocampal neurons and reduces surface levels of the AMPA-type glutamate receptor subunit 2," *J. Neurosci.*, vol. 21, no. 15, pp. 5417–5428, 2001, doi: 10.1523/jneurosci.21-15-05417.2001.

[162] S. J. Kang *et al.*, "Plasticity of metabotropic glutamate receptor-dependent long-term depression in the anterior cingulate cortex after amputation," *J. Neurosci.*, vol. 32, no. 33, pp. 11318–11329, 2012, doi: 10.1523/JNEUROSCI.0146-12.2012.

[163] M. Aymanns, S. S. Yekta, and J. Ellrich, "Homotopic long-term depression of trigeminal pain and blink reflex within one side of the human face.," *Clin. Neurophysiol. Off. J. Int. Fed. Clin. Neurophysiol.*, vol. 120, no. 12, pp. 2093–2099, Dec. 2009, doi: 10.1016/j.clinph.2009.08.027.

[164] J. M. York *et al.*, "The biobehavioral and neuroimmune impact of low-dose ionizing radiation.," *Brain. Behav. Immun.*, vol. 26, no. 2, pp. 218–227, Feb. 2012, doi: 10.1016/j.bbi.2011.09.006.

[165] J. Veeraraghavan, M. Natarajan, S. Aravindan, T. S. Herman, and N. Aravindan, "Radiation-triggered Tumor Necrosis Factor (TNF) α-NFκB cross-signaling favors survival advantage in human neuroblastoma cells," *J. Biol. Chem.*, vol. 286, no. 24, pp. 21588–21600, 2011, doi: 10.1074/jbc.M110.193755.

[166] T. Kataoka *et al.*, “Radon inhalation induces manganese-superoxide dismutase in mouse brain via nuclear factor-κB activation,” *J. Radiat. Res.*, vol. 58, no. 6, pp. 887–893, 2017, doi: 10.1093/jrr/rrx048.

[167] Z. Fang, A. Xu, L. Wu, T. K. Hei, and M. Hong, “The role of protein kinase C alpha translocation in radiation-induced bystander effect,” *Sci. Rep.*, vol. 6, pp. 1–9, 2016, doi: 10.1038/srep25817.

[168] Z. Abdullah and U. Bayraktutan, “Suppression of PKC-α attenuates TNF-α-evoked cerebral barrier breakdown via regulations of MMP-2 and plasminogen-plasmin system,” *Biochim. Biophys. Acta - Mol. Basis Dis.*, vol. 1862, no. 7, pp. 1354–1366, 2016, doi: 10.1016/j.bbadis.2016.03.014.

9. Figure and Table directory

10. List of Abbreviations

(+)-MK801	5R,10S)-(+)-5-methy-10,11-dihydro-5H-dibenzo[a,d]cyclohepten-5,10-imine
ABP	AMPA receptor Binding Protein
AC1	Adenylyl cyclase 1
ACC	Anterior cingulate cortex
AMPA	α-Amino3-hydroxy-5-methyl-4-isoxazole-propionic acid
AMPAR	AMPA receptor
APS	Ammoniumpersulfate
atm	Standard atmosphere
AU	Arbitrary Unit
BDNF	Brain-derived neurotrophic factor
BSA	Bovine Serum Albumin
Ca^{2+}	Calcium
CaM	Calmodulin
CaMK II	Ca^{2+}/calmodulin protein kinase II
cAMP	Cyclic AMP
CHO	Chinese Hamster Ovary
CNS	Central nervous system
CREB	cAMP response element-binding protein
DMEM	Dulbecco's Modified Eagle Medium
DMEM	Dulbecco's Modified Eagle Medium
DMSO	Dimethyl sulfoxide
DNA	Deoxyribonucleic acid
DSB	Double strand break
EDTA	Ethylenedieminetetraacetic acid
eGFP	enhanced Green Fluorescent Protein
ERK	Extracellular signal-regulated kinase
FCS	Fetal Calf Serum
FEP	Free Energy Perturbation
G6PI	Glucose -6-phosphate isomerase
GABA	*gamma*-Aminobutyric acid
GRIP	Glutamate Receptor Interacting Protein
GSI	Gesellschaft für Schwerionenforschung
HEK	Human Embryonic Kidney
HEPES	(4-(2-hydroxyethyl)-1-piperazineethanesulfonic acid

IARC	International Agency for Research and Cancer
IC	Immune complex
LTD	Long-term depression
LTP	Long-term potentiation
MD	Molecular Dynamics
MEM	Minimal Essential Media
mGluR	Metabotropic Glutamate receptor
MHC	Major histocompatibility complex
NGF	Neurotrophic factor
NMDA	N-Methyl-D-aspartate
NMDAR	N-Methyl-D-aspartate-receptor
NSAID	Non-steroidal anti-inflammatory drug
PAGE	Polyacrylamide Gelelectrophoresis
PBS	Phosphate Buffered Saline
PDB	Protein Data Bank
PDZ	Postsynaptic density-95/Discs large/zona occludens-1
PFA	Paraformaldehyde
PFA	Paraformaldehyde
PG	Prostaglandin
PICK	Protein Interacting with C Kinase
PKA	Protein Kinase A
PKC	Protein Kinase C
PME	Particle Mesh Ewald
ppm	Parts per million
RA	Rheumatoid arthritis
rpm	rounds per minute
RPMI	Roswell Park Memorial Institute Medium
RT	Room Temperature
S	Serine
SD	Standard deviation
SDS	Sodium Dodecyl Sulfate
SEM	Standard Error of Mean
SNS	Sensory-neuron-specific
SRC	Sarcoma
TEMED	Tetramethylethylenediamine
TNF	Tumor Necrosis Factor

Tris	Tris(hydroxymethyl)aminomethane
TTX	Tetrodotoxin
USEPA	United States Environmental Protection Agency
Y	Tyrosine

11. Curriculum vitae

Personal Data

Name	Juliane Joswig
Date of Birth	13.10.1994
Place of Birth	Mannheim

Education

10/2015-07/2017	Master of Science Technical Biology, Technische Universität Darmstadt
10/2012-08/2015	Bachelor of Science Biology, Technische Universität Darmstadt
2012	Allgemeine Hochschulreife, Internationales Abitur Baden-Württemberg, Bergstraßengymnasium Hemsbach

Professional background

07/2020-today	parental leave
10/2017-07/2020	Scientific Assistant at Department of Neurophysiology and Neurosensory Systems, Technische Universität Darmstadt
2015	Assistant scientist, Tutor for “Mathematics for Biology”, Technische Universität Darmstadt

Conferences

09/2019	DeGBS, Mannheim, Poster Presentation, Title: “Accumulation of radon at nociceptors”
05/2019	BMBF-NUK, Karlsruhe, Project Presentation, Title: “Gastransmitter- Eine mögliche Rolle für Radon“
09/2018	GBS, Frankfurt, Poster Presentation, Title: “Effects of radon on nociceptors”

Publications

Lutz H, Nguyen TA, Joswig J, Rau K, Laube B. NMDA Receptor Signaling Mediates cFos Expression via Top2β-Induced DSBs in Glioblastoma Cells. Cancers (Basel). 2019;11(3):306.

Leeder WM, Giehler F, Joswig J, Göringer HU. Bioinspired Design of Lysolytic Triterpenoid-Peptide Conjugates that Kill African Trypanosomes. *Chembiochem*. 2019;20(10):1251-1255.

12. Danksagung

Zuallererst möchte ich Prof. Dr. Bodo Laube dafür danken, dass er mir die Möglichkeit gegeben hat, an einem so interessanten Thema zu forschen und mir jederzeit mit konstruktiven Vorschlägen zur Seite stand und mir das Vertrauen zum selbständigen Entwickeln dieser Arbeit geschenkt hat. Außerdem möchte ich mich bedanken, dass er mich trotz anderer Umstände jederzeit unterstützt hat.

Ich danke Prof. Dr. Gerhard Thiel dafür, dass er sich als Zweitgutachter für meine Dissertation zu Verfügung gestellt hat.

Ich danke Dr. Daniel Bauer, für die Zusammenarbeit und die Bereitstellung der MD Simulationsdaten. Ich danke außerdem Dr. Andreas Maier, der die Radonbehandlung von Zellen und Tieren möglich gemacht hat.

Besonders danken möchte ich zudem Dr. Bastian Roth, der mir freundlicherweise seine experimentellen Daten der Western Blots zur Verfügung gestellt hat. Ein großer Dank auch dafür, dass er immer einen Lösungsvorschlag parat hatte, wenn man sich augenscheinlich in einer Sackgasse befand und für seinen unermüdlichen Arbeitseinsatz für die AG.

Außerdem danken möchte ich Kirsten, die mit mir die Betreuung der Derma-Übung gemeistert hat und immer ein offenes Ohr für mich hatte.

Ein Riesendank geht an die AG Laube, die maßgeblich dafür verantwortlich war, dass mir die Zeit der Dissertation stets Freude bereitet hat. Besonders meinen Bürokolleginnen Katja und Selina möchte ich für die Gespräche, Aufmunterungen und die Zeit, die wir miteinander verbracht haben, danken. Danke auch an Nina, Gabi, Michi, Kai, Axel, Raj, Max, Kiki und Henk für die schöne Arbeitsatmosphäre.

Ein besonderer Dank geht an meine Familie. Meine Eltern, die immer für mich da sind und mich stets unterstützen. Außerdem danke ich meinen Freunden Katharina, Julia und Sophia, für die schönen Momente bei Kaffee und Kuchen und die mentale Unterstützung.

Vielen Dank liebe Nora, dass es dich gibt und du mir jeden Tag so viel Freude schenkst. Danke auch an Baby#2, du bist meine größte Motivationshilfe.

Zuletzt möchte ich meinem Mann danken. Danke für den Rückhalt, die Motivation und Liebe, die du mir stets entgegenbringst. Ohne dich wäre ich nicht so weit gekommen. Danke für dein offenes Ohr bei den doch eher einseitigen Diskussionen über diese Arbeit. Vielen Dank, dass du mich stets aufmunterst und für die unzähligen (fr)Esspakete, die mir neue Kraft geben.